People's Democratic Republic of Algeria

Ministry of Higher Education and Scientific Research

University of El Oued

Faculty of Exact Sciences

LEVRES Laboratory, University of El Oued.

A Doctoral Thesis

Submitted in fulfillment of the requirements for the/ Doctorate degree in the third cycle of Science

Field: Physics

Specialization: Physics of Materials

ELABORATION AND CHARACTERISATION OF THIN FILMS OF COBALT OXIDE

Presented by: Bali Khadidja

Supervised by: Beggas Azzeddine

Defended in the presence of the Examination Committee:

Name	Rank	Affiliation	Role
Zeroual Soria	Pr	University of El-Oued	Chair
Beggas Azzeddine	Pr	University of El-Oued	Supervisor
Gahtar Abdelouahab	MCA	University of El-Oued	Examiner
Bentouilla Omar	Pr	University of Ouargla	Examiner
Benramache said	Pr	University of Biskra	Examiner
Lakel Abdelghani	Pr	University of Biskra	Examiner

Academic Year: 1447-1448 AH / 2025-2026

Acknowledgements

I thank ALLAH the Almighty for giving me the courage, the will and the patience to complete this present work.

First of all, I would like to express my sincere gratitude and all my thanks to my thesis Director **Pr .Beggas Azzeddine**, professor at Elchahid Hamma Lakhder University. El Oued, for his help, guidance and the time he spent witnessing the elaboration of this work. I thank him for his availability, his kindness, his support, his ideas and advices. May Allah protect you.

I am also grateful to **Pr. Zeroual Soria**, professor at Elchahid Hamma Lakhder University. El Oued, for having given me the honor of chairing the jury for the defense of this thesis.

My warm thanks go also to **Pr. Lakel Abdelghani**, professor at University of Biskra

, who kindly agreed to be part of the jury and to examine my work.

I would like to thank **Pr. Benramache said** from the University of Biskra for his welcome in his laboratory and his conduct of the electrical properties, and for all his comments on my manuscript and for his generous help.

Last, I would especially like to thank Professor **Gahtar Abdelouahab** for his help in preparing this thesis.

Dedications

I dedicate this work to my mother and father in remembrance and gratitude for their love and compassion…..

God bless them

To my brothers: Nadir, Hichem, Ahmed, Cherif, Aymen

To my sisters: Fatima, Meriem and Yamina.

My husband: Laid

To my children: Tassnim, Retedj, and Imed

To all my friends

To my colleagues

Finally, to everyone who contributed to the completion of this work.

Khadidja Bali

TABLE OF CONTENTS

Acknowledgements…….....……..…II
Dedications... III
Table of contents …….....IV
List of figures.....VII
List of tables.....XI
General introduction..... 2

CHAPTER I
Bibliographic Study of Cobalt Oxides Thin Films.

I.1. Introduction…….....……..7
I.2.Transparent CONDUCTIVE OXIDES (TCO_s)……...……7
I.3.Properties of transparent conducting oxides (TCO_s) ……...…8
I.4.Types of (TCO_s) …….....……..12
I.5. Cobalt…….....……14
I.6. Cobalt oxides…….....……16
I.7.Applications of Cobalt OXIDE CO_3O_4 thin film…..……23
I.8. Conclusion…….....……28
References……..……29

CHAPTER II
Elaboration and Characterizations Techniques

II.1.Introduction ……...……36
II.2.Whati is the film? ……..……36
II.3.Classification of Deposition Technologies…….……37
II.3.1.Physical vapor deposition (PVD) …….....…..…… 38
II.3.2. Chemical vapor deposition…….....…… 42
II.3.3. Spray Paralysis……42
II.3.4. Adventages of Spray Paralysis Deposition…….....……43
II.3.5.Specific Aspects of Chemically Sprayed Thin Films to Consider……....44

II.4. Characterization methods…….....…….……46
II.4. 1. X rays diffraction (XRD) …….....……..……46
II.4. 2.FT-IR spectroscopy…….....…….……48
II.4. 3.Scanning Electron Microscopy (SEM) …….....……..…49
II.4. 4.Energy dispersive X-ray spectroscopy (EDS) ……..……50
II.4. 5. Optical spectrophotometry……...……51
II.4. 6.Four-point probe resistivity measurements……..……52
II.5. Conclusion…….....……..……54
References……...……55

Chapter III

THE EFFECT OF SUBSTRATE TEMPERATURE ON the PROPERTIES OF CO3O4 THIN FILMS.

III.1. Introduction..……59
III.2. Experimental details…….....……59
III.2.1. Films Preparation…….....……..……59
III.2.2. Characterization techniques…….....……60
III.3. Results and discussion…….....……..……60
III.3.1. X-Ray Diffraction…….....……60
III.3.2.SEM & EDS analysis…….....……..…75
III.3.3. FTIR analysis…….....…….……78
III.3.4. Optical properties…….....……..……79
III.3.5. Electrical properties…….....……..……82
III.4. Conclusion…….....…….……84
References…….....……...……85

Chapter IV

EFFECT OF CONCENTRATION ON THE PROPERTIES OF Co_3O_4THIN FILMS

IV.1.Introduction…….....……89
IV.2. .Results and discussion…….....…….……89
IV.2.1. Film thickness…….....……..……89
IV.2.2. X-Ray Diffraction…….....……89
IV.2.3.Morphological and elemental analysis……..……96
IV.2.4. FTIR analysis…….……99
IV.2.5. Optical properties…….....……..……...101
IV.2.6.Electrical characteristics…….....……...104
IV.3. . Conclusion…….....……...……..106
References…….....……108
General conclusion and suggestions for future work…….....……114
Abstract…….....…….……117
Appendix…….....……..……119

CHAPTER I
Bibliographic Study of Cobalt Oxides Thin Films.

Figure I.1. Band gap engineering of TCO material. …….....……...…9
Figure I.2. Transmittance spectrum of TCO material……..……..11
Figure I.3. Crystal structures of typical n-type TCOs……..……..13
Figure I.4. Crystal structures of typical p-type TCOs.…… ……..…....14
Figure I. 5.Axis of easy magnetization: a) α-Co and b) β-Co …….....…15
Figure I. 6.CoO cell, where O and Co atoms are face-centered cubic (fcc)…….….17
Figure I.7.Unit cell (on the left) and primitive cell (on the right) of Co3O4…...…..…20
Figure I.8. Optical transmittance of Co3O4 thin films as a function of substrate temperatures……..…….....21
Figure I.9. Schematic representations of the band structure of Co3O4……21
Figure I.10. Dependence of electrical conductivity in Co3O4 films on substrate temperature……..…….……22
Figure I.11. Charge /discharge curves of Co3O4 thin film……..…...…23
Figure I. 12. Measurement scheme of (a) Co3O4/TiO2 heterostructures…….…24
Figure I.13.Cobalt oxide as photocatalyst for water splitting ……...…24
Figure I. 14. Scheme of the proposed CO2 hydration process catalyzed by the plasma-deposited Co3O4-based thin film…….…….……25
Figure I. 15. Schematic representation of electrochromic device cell using Co3O4 film……..….25
Figure I. 16. (a) Device schematic showing self-bias ultraviolet photodetection….....26
Figure I. 16. (b) Energy band diagram of the TiO2/Co3O4 UV photodetector..…….26
Figure I.17. The schematic diagram of a sandwiched Pt/Co3O4/Pt structure…….26
Figure I. 18. Mechanism of antibacterial and antifungal activity of CuO,ZnO,Co3O4 nanoparticals and CuO- ZnO-Co3O4 nanocomposite…….……...……27
Figure I.19. Schematic illustration for the fabrication of ZnCo3O4/rGO/CPE modified electrode and its mechanism for amepriometric detection of glucose……...28

CHAPTER II
Elaboration and Characterizations Techniques

Figure. II. 1. Schematic of Thermal evaporation by resistive heating …….……39
Figure II.2. General diagram of Electron Beam Evaporator …….....……39
Figure II.3. Schematics of simplified sputtering systems: (a) DC, (b) RF ……40
Figure II. 4. General diagram of PLD …….....…… 41
Figure II. 5. The MBE growth chamber design, the sample is fixed in the chamber center on a rotating holder ……...41
Figure II.6.Sequence of gas transport and reaction processes contributing to CVD film growth ……..…42
Figure II.7.Schematic representation of a spray pyrolysis deposition ……..…43
Figure II.8: Formation Stages of Thin Film …….....44
Figure II. 9.Schematic representation of the three known film growth modes……....46
Figure II.10.Schematic diagram of Bragg diffraction …….....……...…47
Figure II.11.Illustrate the peak widths FWHM ($\Delta\theta=\beta$)…….....…… ……. …48
Figure II.12.Fourier Transform Infra-Red spectroscopy…….……..49
Figure II.13.Scanning Electron Microscopy (SEM)…….....……50
Figure II.14.Schematic diagram of an energy dispersive X-ray spectroscopy system……..50
Figure II.15.Schematic representation of constituent elements of a Spectrophotometer UV-VIS-NIR ……...…51
Figure. II.16. Curve represent the function $(\alpha h\upsilon)^2=f(h\upsilon)$…….....……...… …..…52
Figure II.17.Linear four-point probe configuration..…….. … …….54

Chapter III
THE EFFECT OF SUBSTRATE TEMPERATURE ON the PROPERTIES OF CO3O4 THIN FILMS.

Figure III.1. XRD spectra of Cobalt Oxide at various temperatures ……...…61
Figure III.2.TC values of Co_3O_4 layers vs substrate temperatures …….....…74
Figure III.3. SEM of Co_3O_4 thin layers fabricated at: (a): 250°C, (b): 300°C, (c): 350°C, and (d): 400°C ……..….76
Figure III.4. EDS micrographs of Co_3O_4 thin films prepared with various substrate temperature (a):250°C, (b): 300°C, (c):350 °C and (d): 400°C. ……...…77
Figure III.5. Transmittance spectra of Cobalt Oxide at various substrate temperature ..……....78
Figure III.6. Transmittance spectra of Cobalt Oxideat various temperatures: (a): 250°C, (b):300°C, (c):350°Cand (d): 400°C…….....79
Figure III.7 Development of the absorption coefficient (α) of the Cobalt Oxideat a various temperatures…….80
Figure III. 8. Plots of $(ahv)^2$against hv of $Co_3O_4$for temperatures :(a): 250°C, (b):300°C, (c):350°C and(d): 400°C……..……81
Figure III. 9. Variation of the opticalgap (E_g), grain size (D) and conductivity as a function of the various temperature of the Cobalt Oxide films……...…..83

Chapter IV

EFFECT OF CONCENTRATION ON THE PROPERTIES OF Co_3O_4 THIN FILMS

Figure IV.1.DRX spectra *of Cobalt Oxide (a):C=0.025, (b):C=0.075, (c): C=0.05 and (d): C=0.1mol/l*……..…90
Figure IV.2.Crystalline size, Microstrain, and dislocation density of CO_3O_4 layersversus the molar concentration ……..…….....……95
Figure IV.3. SEM of Co_3O_4layers prepared at different concentrations (a): 0.025 M, (b): 0.05M, (c): 0.075 M and (c): 0.1 M.……...……...……97
Figure IV.4. EDS micrographs of Co_3O_4 layers prepared at various concentrations(a): 0.025 M, (b): 0.05 M, , (c): 0.075 M and (c): 0.1 M. ……...……..……98
Figure IV.5. Transmittance spectra of Co_3O_4 for different concentration ……100
Figure IV.6. indicates the transmittance spectra obtained for Co3O4for various molar concentration ……..……..…101
Figure IV.7. The absorption coefficient versus the wavelength…….…..102
Figure IV.8. $(\alpha h\nu)^2$versus energy (hν) for different molar concentration ……..103
Figure IV.9. Optical gap, Grain size, and Conductivity versus the concentration....106

CHAPTER I
Bibliographic Study of Cobalt Oxides Thin Films.

Table I.1.Crystal structure and lattice parameters of Co. …….....15
Table I.2. The different thermal and thermodynamic parameters……..……16
Table I.3.The different potentials of the half-reactions of Cobalt reductions.....16
Table I.4.Summary. of the basic physical and chemical properties of Co3O4 thin films…….....18
Table I.5.optical parameter values of the thin layers of Co3O4 that were deposited..21

CHAPTER II
Elaboration and Characterizations Techniques

Table II. 1. Thin Film Applications. …….....……37
Table II. 2. classification of thin-film deposition techniques 38

Chapter III
THE EFFECT OF SUBSTRATE TEMPERATURE ON the PROPERTIES OF CO3O4 THIN FILMS.

Table III.1. Inter-planar distances (d_{hkl}) of Co_3O_4samples for various temperatures.…….....…71
Table III.2. The parameters (a, b and c) and volume of the unit cell V values comparing to the data listed on JCPDS card #-074-01…….....……71
***Table* III.*3.The crystallites size (Dhkl) of* Co_3O_4 thin films at a variety of temperatures.……...…….....72**
***Table* III.*4.The dislocation density (δ_{hkl})of Co_3O_4 thin films at a variety of substrate temperature*……..73**
Table III. 5. Microstress values (ε_{hkl}) of Co_3O_4 films at various substrate temperature…….73
Table III.6. Texture coefficient (TC_{hkl}) of Co_3O_4 thin films at a variety of substrate temperature……..…74

Table III.7. The average values of D, ε and δ of Co_3O_4 thin films at various substrate temperature……..……..…….75
Table III.8. Resistivity and conductivity of Co_3O_4layers at various substrate temperature……..……...82

Chapter IV

EFFECT OF CONCENTRATION ON THE PROPERTIES OF Co_3O_4THIN FILMS

Table IV.1. Lattice parameters (a, b, c, and d) and unit cell volume V compared to (JCPDS card #01-074-1657) values …….....……..……...…91
Table IV.2. Inter-planar distances (dhkl) of Cobalt Oxide.....……..…92
Table IV. 3.Cobalt Oxide crystallite's sizes (D_{hkl})..……..……92
Table IV. 4.The *dislocation density (δ_{hkl})* of Cobalt *Oxide*. …….....……93
Table IV. *5. Micro-stress values (εhkl) of Cobalt Oxide*…….…….……93
Table IV. *6. Texture coefficient (TChkl) of* Co_3O_4*layers fabricated at various concentration*……...……....94
Table IV. 7. The mean values versus of D, ε and δ of fabricated samples with various concentration……..*95*
Table IV. *8. Elementary analysis of Co_3O_4layers*……..……...…….*99*
Table IV. 9. Resistivity and Conductivity of Co_3O_4layers for different concentration……..……..105

GENERAL INTRODUCTION

General introduction

Transparent and conductive oxides (TCOs) are exceptional materials in many fields. Their dual property of electrical conductivity and transparency in the visible spectrum makes them ideal candidates for photovoltaic and optoelectronic applications [1]. Among TCOs, cobalt oxide is considered the most promising semiconductor material for technological applications such as energy storage due to its high absorbance in the UV-VIS range [2].

In recent years, the Co_3O_4 thin film has gained considerable importance for various applications, including photo-thermal conversion, pigments for paints used in aeronautics and space, thermolysis, NTC-type thermal resistances, high-charge capabilities, catalysis, and gas sensors. Cobalt oxide (Co_3O_4), which is stable at room temperature, crystallizes in the cubic spinel structure [3]. It is a p-type semiconductor with two direct bands at room temperature [4, 5].

Co_3O_4 thin films are currently made using several thin film deposition methods, including reactive evaporation (RE), electrochemical deposition (ECD), chemical vapor deposition (CVD), sol-gel process (SGP), 400 °C molecular beam epitaxy (MBE), magnetron sputtering (MST), pulsed laser deposition (PLD), and the pyrolysis spray method. Among these methods, a homemade pyrolysis spray method is used to deposit Co_3O_4 thin films. This method can create uniform thin films with remarkably consistent crystallite sizes[6, 7]. PSM offers several advantages, including solution concentration control, temperature stabilization, glass substrate control, spraying time control, large-area spraying, and composition control for film morphology (film density or thickness). Therefore, PSM is one of the most important methods for the preparation of functional Co_3O_4thin films.

This study aims to investigate how solution concentration and temperature influence the properties of cobalt oxide (Co_3O_4) deposited on glass substrates through pyrolysis spray. Additionally, it seeks to examine how these properties vary under different conditions. A cobalt chloride solution ($CoCl_2 \cdot 6H_2O$) was used as the source of cobalt. This research was conducted at the LEVRES laboratory at the University of El Oued.

This thesis is divided into four chapters:

- Chapter one provides a comprehensive bibliography and a general analysis of transparent conductive oxides (TCOs), along with a special study of cobalt oxide thin films and their applications.
- The second document details the pyrolysis spray method used to prepare cobalt oxide (Co_3O_4) thin films, explaining the deposition process mechanism and the characterization techniques employed to analyze the prepared films.
- The focus of the third chapter is on how substrate temperature affects the structural, morphological, optical, and electrical characteristics of cobalt oxide (Co_3O_4).
- The fourth chapter examines the influence of molarity on the structural, morphological, optical, and electrical properties of cobalt oxide (Co_3O_4).

In conclusion, this publication provides a comprehensive summary of all the important findings we have covered so far.

References

[1] T.J. Coutts, D.L. Young, X. Li, Characterization of transparent conducting oxides, Mrs Bulletin 25 (2000) 58-65.

[2] A. Abed, R. Abed, Characterization effect of copper oxide and cobalt oxide nanocomposite on poly (vinyl chloride) doping process for solar energy applications, Progress in Color, Colorants and Coatings 15 (2022) 235-241.

[3] J. Chen, X. Wu, A. Selloni, Electronic structure and bonding properties of cobalt oxide in the spinel structure, Physical Review B-Condensed Matter and Materials Physics, 83 (2011), 245204.

[4] S. Vladimirova, V. Krivetskiy, M. Rumyantseva, A. Gaskov, N. Mordvinova, O. Lebedev, M. Martyshov, P. Forsh, Co_3O_4 as p-type material for CO sensing in humid air, Sensors, 17 (2017), 2216.

[5] A. Miquelot, M. Despotopoulou, C. Vahlas, C. Villeneuve, N. Dragoe, N. Prud'Homme, O. Debieu, Morphological, structural, optical, and electrical study of nanostructured thin films: Charge transport mechanism of p-type Co_3O_4, Materials Chemistry and Physics, 240 (2020), 122059.

[6] W. Daranfed, N. Guermat, K. Mirouh, Experimental study of precursor concentration the Co_3O_4 thin films used as solar absorbers, Annales de Chimie-Science des Matériaux, 2020, pp. 121-126.

[7] S.S. Chiad, H.A. Noor, O.M. Abdulmunem, N.F. Habubi, Optical and structural properties of Ni-doped Co_3O_4Nanostructure thin films via CSPM, Journal of Physics: Conference Series, IOP Publishing, 2019, pp. 012115.

Chapter I

Bibliographic Study of Cobalt Oxide Thin Films

I.1. Introduction

In this chapter, we present a bibliographic study of transparent conducting oxides (TCOs), focusing specifically on cobalt oxide (Co_3O_4). We discuss its main properties and applications.

I.2.Transparent Conductive Oxides (TCOs)

Because of their excellent electrical characteristics and high optical transmittance in the visible wavelength, transparent conductive oxides (TCOs) are becoming more and more popular in a variety of optoelectronic applications. However, the use of some TCOs is limited due to their high cost, high sheet resistance, and limited transmittance in infrared wavelengths. TCO films have remarkable optical transmittance (>80%) in the visible wavelength range (380–700 nm) and advantageous electrical characteristics (resistivity of $<10^{-4}$ Ω.cm), which has led to their use in various optoelectronic applications. Examples of these uses include thin-film transistors, solar cells, organic light-emitting diodes (OLEDs), flat-panel displays, liquid crystal displays, and plasma display panels [1, 2].

TCO films can be deposited using various methods, such as sol-gel deposition, ion beam-assisted deposition, thermal evaporation, chemical vapor deposition, electron-beam evaporation, pulsed laser deposition, and magnetron sputtering [3-6]. The most widely used of these processes is magnetron sputtering. This is due to its high accumulation rates and moderate substrate temperatures. It is also suitable for industrial applications and can guarantee the film's superior optoelectronic performance[4, 7] .

I.1.1.1.What are TCO materials?

Highly conductive metals are opaque to visible light because of plasmonic reflection and a high density of free carriers. In contrast, most wide band-gap materials, which are transparent to visible light, are electrically insulating. Transparent conductive oxides (TCOs) are a unique class of metal oxides that exist in the form of thin films, typically a few hundred nanometers thick. These materials demonstrate both high transparency to visible light and high electrical conductivity. They are used as transparent electrodes in flat panel displays, solar cells, and electroluminescent devices.

TCOs exhibit strong electrical conductivity in the range of 1–10^4 S/cm and high optical transmission in the visible region. However, transparency and electrical conductivity are incompatible. Achieving these seemingly contradictory properties requires careful engineering of the material's composition and structure. To obtain transparent conducting oxides (TCOs), transparent insulators must be converted into highly conducting semiconductors[8, 9].

I.3.Properties of transparent conducting oxides (TCOs)

I.3.1.Electrical properties of TCOs

Although stoichiometric oxide materials are known for their high optical transparency, they generally do not exhibit high electrical conductivity. According to the Drude theory, which describes charge transport in metals through a free-electron gas, this behavior is not expected in stoichiometric oxides, which typically lack free carriers. The electrical conductivity in this case is:

$$\sigma = n_e e \mu_e = \frac{n_e e^2 \tau}{m_e} \qquad (I.1)$$

In this case, **σ** stands for electrical conductivity, $\mathbf{n_e}$ for the number of charge carriers, $\mathbf{m_e}$ for their effective mass, $\boldsymbol{\mu_e}$ for their mobility, **e** for the electronic charge, and **τ** for relaxation time.

Due to their broad optical band, stoichiometric TCO materials are insulating. Shallow donor and acceptor levels are produced close to the conduction and valence bands by intrinsic defects such as cation interstitials or anion vacancies.The electrical characteristics of the material can be improved by thermally ionizing these extra charge carriers.

TCO materials generate high concentrations of mobile free charge carriers in wide-bandgap semiconductors and insulators using appropriate dopants. Indium-tin oxide (ITO), for instance, can be effectively used by substituting Sn^{4+} cations for In^{3+} cations, which results in donor defects below the conduction band minimum and high electrical conductivity of 10^4 S/cm at room temperature [10]. Highly effective TCO materials, such as ITO, ZnO, SnO_2, and CdO, have similar structural, chemical, and electronic properties. Post-transition metal oxides have dense structures with strong interactions between metal ns and oxygen 2p orbitals, which leads to a forbidden gap between the valence and conduction bands. A large dispersion of conduction bands is

observed, especially in rocksaltCdO, due to octahedral coordination with oxygen anions [11].

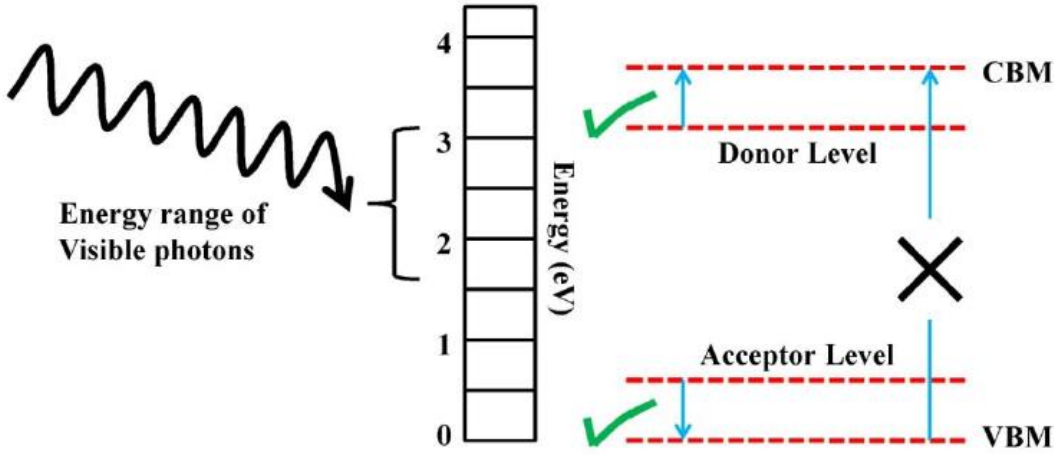

Figure I. 1. Band gap engineering of TCO material.

Due to their low energy, electrons cannot be excited directly from the valence band to the conduction band by visible photons. However, they have enough energy to excite holes from the acceptor level to the valence band in p-type TCO or electrons from the donor level to the conduction band in n-type TCO. Permitted and prohibited transitions are denoted by the symbols (✓) and (×), respectively.

Highly effective transparent conducting oxides (TCOs) exhibit excellent electrical conductivity at room temperature due to the low mass of charge carriers. They can be modified by introducing counter cations or anions, which results in remarkable optoelectronic properties in a single material [12].

Removing or replacing oxygen anions in n-type transparent conducting oxide (TCO) materials increases the supply of electrons, whereas p-type TCOs generate excess charge carriers around vacant sites due to their higher formation energies. Conventional TCOs have low formation energy and a higher charge carrier density, which leads to deep acceptor levels [13].

I.3.2.Optical propertiesof TCOs

Maxwell's electromagnetic wave equation determines the refractive index of uncharged semiconducting materials by exposing conflicting electrical and optical characteristics[14, 15]:

$$n^2 = \frac{\varepsilon}{2}\left[\left\{1 + \left(\frac{2\sigma}{\nu}\right)^2\right\}^{1/2} + 1\right] \text{(I. 2)}$$

$$k^2 = \frac{\varepsilon}{2}\left[\left\{1 + \left(\frac{2\sigma}{\nu}\right)^2\right\}^{1/2} - 1\right] \text{(I. 3)}$$

Drude's model gives an equation for a free electron gas's dielectric constant and explains how TCO material is absorbed in the infrared spectrum[16][17].

$$\varepsilon(\omega) = \frac{1 - \frac{4\pi n e^2}{m}}{\omega^2 + i\frac{\omega}{\tau}} \text{(I. 4)}$$

where **n** represents the material's refractive index, **ε** the dielectric constant, **σ** the electrical conductivity, **k** the extinction coefficient,**τ** is relaxation time,**ν** the electromagnetic wave frequency,and **ω** is frequency of EM waves.

FromDrude's theory, it is revealed that EM waves cannot travel through a material with a negativevalue of dielectric constant because its wave vector is imaginary and decays exponentially. The EM waves incident on that material gets reflected. The plasma frequency or cut-off frequency can be determined by:

$$\omega_p = \left(\frac{ne^2}{m^*\varepsilon_0}\right)^{1/2} \text{(I. 5)}$$

where, **ωp** is a plasma or cut-off frequency, **ϵ_o** is permittivity of free space, **n** is the number density of charge carriers, and **m*** is its effective mass. The material is transparent to those EM radiations whose frequency is greater than plasma frequency. Hence, TCO materials are transparent in visible and near infra-red (NIR) regions and reflect IR radiation (below plasma frequency), as shown in figure I.2.

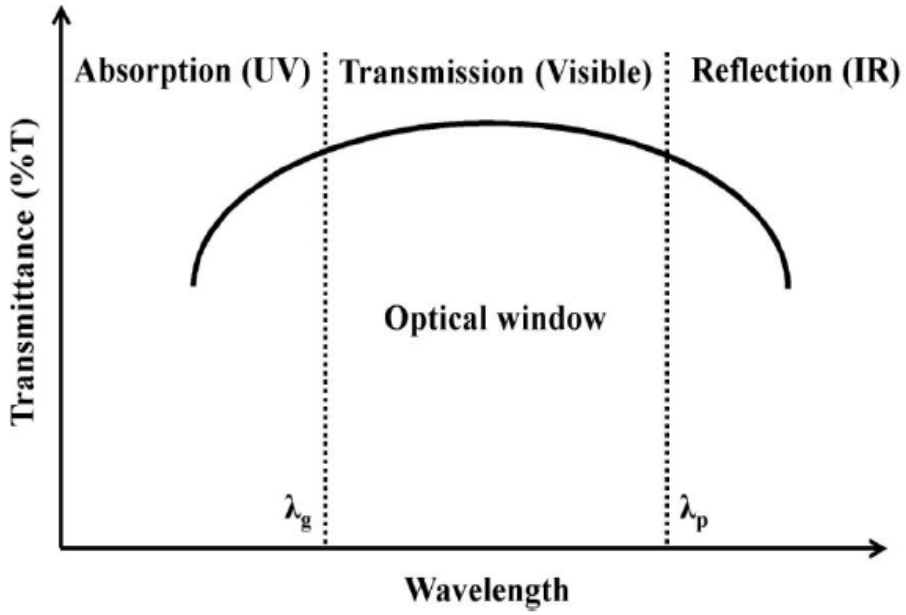

Figure I.2. Transmittance spectrum of TCO material.

TCO materials are transparent in the range of shorter wavelength band gaps to higher plasma wavelengths. This range is governed by plasmon frequency and mobility. They absorb incident photons with energies higher than the material's band gap, reflecting them at lower frequencies. Plasma frequencies in the near-infrared (NIR) region provide high optical transparency. By tailoring the plasmon frequency, infrared regions can be blocked or transmitted [18].

The Fermi level is pushed to a higher energy state when a material is degenerately doped with an appropriate counter cation, causing surplus produced charge carriers to occupy the lower energy level of the conduction band. In this instance of degenerate doping, an electron can only be stimulated to a higher energy level if it possesses enough energy to move into the vacant conduction band energy level and beyond the bottom filled energy levels of the occupied conduction band. It leads to the material's band gap expanding, which is good for its optical characteristics. This shift in optical band energy is known as Burstein-Moss shift or BM shift and can be determined by:

$$\Delta E_{BM} = \frac{\hbar^2}{2m^*}(3\pi^2 n)^{2/3} \quad (\text{I}.6)$$

where **m*** is the effective mass, **n** is the carrier concentration, and ΔE_{BM} is the BM-shift magnitude. The plasma edge will move toward the red portion of the visible

spectrum if the transparent material is extensively doped and the charge carrier concentration is high enough.

The secondary gapE_{sg}, in TCO materials is a difference in the two lowest conduction bands, where electrons at Fermi level can jump into the adjacent unoccupied energy band. A high E_{sg} value prevents intra-band transitions and shows high optical transparency, similar to p-type TCO materials.

The physical properties of TCO materials are interconnected, so a single material cannot meet all requirements. The most important property is the type of charge carrier, since basic functionalities can be determined from a single material, though most electronic devices require both types.

I.3.3.Optical and electrical performance

Improved Performance: TCOs are made up of important optical and electrical characteristics that are inversely correlated. In order to evaluate TCO material performance, researchers created a reliable metric known as the figure of merit (FOM). The following formula can be used to calculate the FOM value:

$$FOM = \frac{\sigma}{\alpha} = \frac{-1}{R_{sh} lnT} \text{(I. 7)}$$

Where **α** is the TCO material's absorption coefficient and **σ** is its electrical conductivity. **T** is the transmittance in the visible spectrum, and **Rs** is the sheet-resistance (thickness-independent parameter) of the thin-film of TCO material.

The FOM value is used to assess the performance of various TCO materials by producing a single number that integrates both qualities in a specific manner. This figure can also serve as a standard for measuring all TCO materials.

When using the Figure of Merit (FOM) as a performance parameter in solar cells and display applications, it is essential to consider several factors. These include maximum transmittance, peak values, and selecting low optical bandgap materials that exhibit high FOM values. Additionally, it's important to note that two materials can have the same FOM value while demonstrating different optoelectronic properties. Therefore, a thorough comparison of FOM values should be made for materials that possess significant optical transparency.

I.4.Types of TCOs

Transparent Conductive Oxides (TCOs) can be categorized into two types based on their conduction properties: n-type and p-type. Below is a detailed explanation of each type of TCO.

I.4.1.*n*-type TCOs

It is widely accepted that a single material cannot possess high electrical conductivity and good optical transparency in the visible spectrum at room temperature. Extrinsic doping is extremely challenging due to the material's broad optical bandgap, which is equal to or greater than 3.1 eV. However, TCOs can achieve high conductivity comparable to metal (10^4 S/cm) and outstanding transparency (80%) comparable to ceramics in the visible range by adding dopants and/or nonstoichiometry [19].

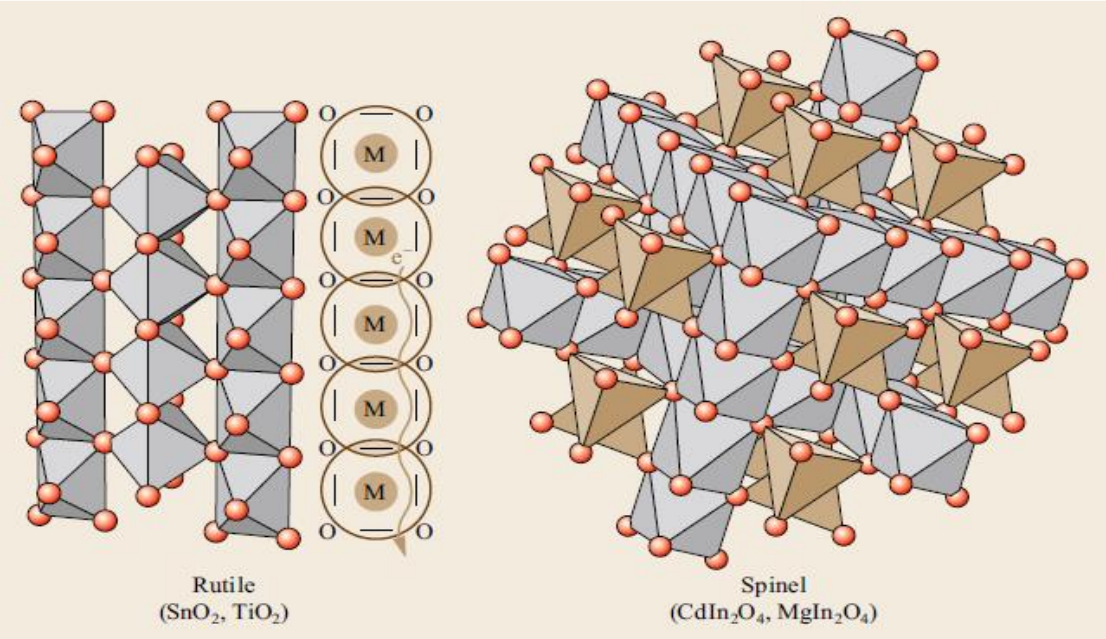

FigureI.3. Crystal structures of typical n-type TCOs.

The emphasis is on creating TCO materials that exhibit high optical transparency and substantial carrier mobility. The first n-type transparent conductor, CdO, was developed in 1907 by Babekar, however, it suffered from incomplete thermal oxidation during post-annealing heating[11].

Technical interest was aroused after the discovery of CdO as the first transparent conductor. Despite its poisonous nature, CdO is not widely used these days. However,

its high carrier mobility still attracts a lot of interest. Since then, significant effort has gone into creating higher-performance TCOs that can support a broad range of optoelectronic device applications. Examples of these TCOs include Sn/F/Sb/Mo-doped In_2O_3, In/Al/F/B/Ga-doped ZnO, Sb/F-doped SnO_2, $MgIn_2O_4$, Cd_2SnO_4, Y-doped $CdSb_2O_6$, Sn-doped $CdIn_2O_4$, Zn_2SnO_4, $Zn_2In_2O_5$, and $ZnSnO_3$. , $In_4Sn_3O_{12}$, Ge/Sn-doped $GaInO_3$, Sn-doped $AgInO_2$, $BaSnO_3$, and other highly effective, commercially used TCOs are available [18, 20].

The majority of n-type oxides acquire a valence band made up of O 2p orbitals and a conduction band made up of spatially dispersed metal ns orbitals. These bands have high n-type conductivity and a large optical band gap due to the ionic character of the host. The best-performing oxide is indium-tin oxide (ITO). According to a 1954 report, TCO has a conductivity of approximately 10^4 S/cm and a transparency of 80%[10].As a result, its special optoelectronic qualities increase its use as transparent electrodes in solar cells and flat panel displays[21].

I.4.2.p-Type TCOs

Unlike n-type TCOs, p-type TCOs use full valence bands rather than empty conduction bands to form conduction channels for positive holes. However, developing hole conduction paths is more difficult than developing electron conduction channels. For this reason, p-type TCOs are uncommon [22].

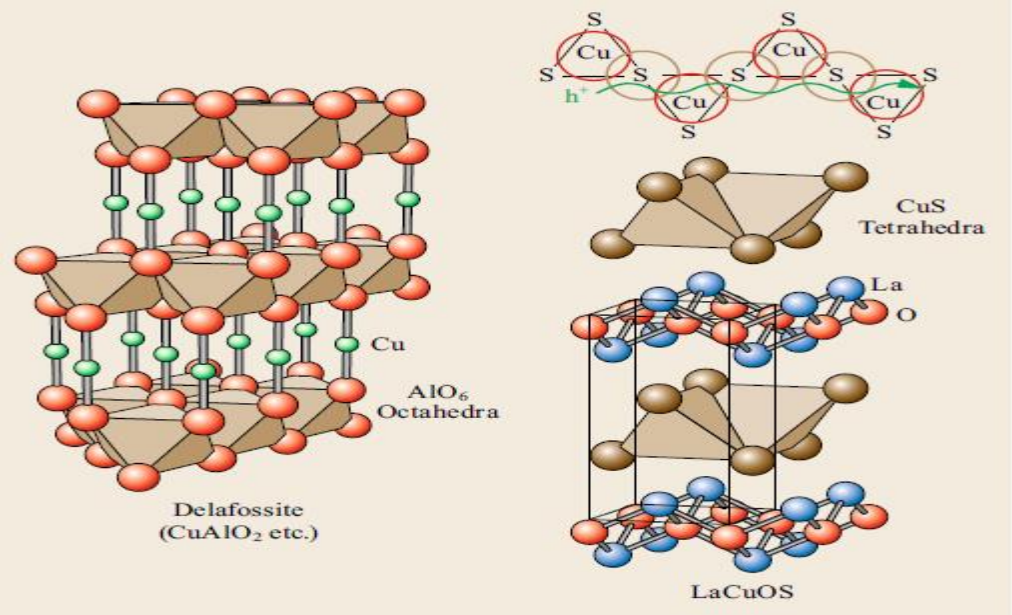

Figure I.4. Crystal structures of typical p-type TCOs.

I.5. Cobalt

I.5.1. It's discovery

In 1735, G. Brandt discovered cobalt in bismuth minerals. Later, in 1780, T. O. Bergman was able to isolate cobalt in its metallic form. Additionally, ancient Egyptians, Greeks, and Romans used cobalt compounds to create blue-colored glass. A necklace featuring blue glass beads, dating back to 2250 BC, was found in Persia.

I.4.2.Its name

The name "cobalt" is derived from the German term "Kobolden," which refers to the "spirits of the mountain." Ancient mountaineers and miners believed that these malevolent spirits were responsible for their inability to extract metal from cobalt ores, which closely resembled copper or silver ores, using the rudimentary methods available at the time. Eventually, the term was altered to "cobalt" and later Latinized to "cobaltum".

I.4.3.Structure of cobalt:

Cobalt can crystallize in a hexagonal close-packed structure or in a face-centered cubic structure. The two types α-Co (hexagonal close-packed cell) and β-Co (face-centered cubic cell) are shown in FigureI. 5[23].

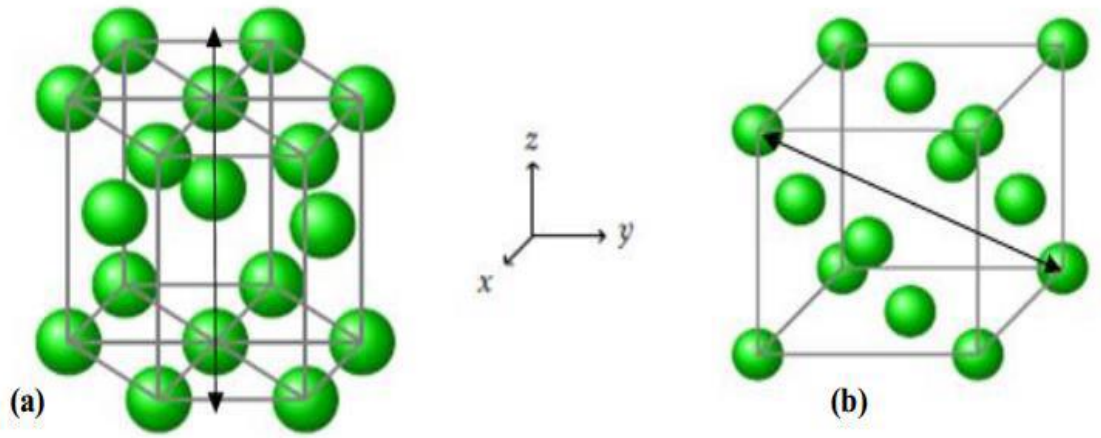

Figure I.5.Axis of easy magnetization: a) α-Co and b) β-Co.

The structural properties of these materials can be summarized in the table I. 1.

Table I. 1.Crystal structure and lattice parameters of Co[23].

Element	structure	a(°A)	c(°A)	c/a
Cobalt	Cfc Hcp	3.55 2.51	~ 4.07	~ 1.62

I.5.5.Properties of Cobalt

I.5.5.1. Physicochemical properties

Cobalt is a hard, ductile, gleaming, blue-gray metal. Its surface reacts with diluted acids, but not with oxygen. It is in group B7 of the ninth column of the periodic table of elements and comes before iridium and rhodium[24].

I.4.5.2. Thermal and thermodynamic properties

The thermal and thermodynamic properties of cobalt are shown inTable I.2.

Table I.2. The different thermal and thermodynamic parameters[25, 26].

Melting point	1768 K (1495°C)
Boiling point (under 1.013 Pa)	2648 K(2375°C) à 3823 K (3550 °C)
Critical temperature	5400 K(5127°C)
Enthalpy of fusion	15.2 KJ/mole
Enthalpy of evaporation	382.4KJ/mole
Enthalpy of atomization	423.082KJ/mole
coefficient of linear expansion at room temperature	$12.5*10^{-6}$/°C
coefficient of linear expansion at transformation temperature	$14.2*10^{-6}$/°C

I.5.5.3. Reduction potentials

Table I. 3: The different potentials of the half-reactions of Cobalt reductions[26].

Demis's reactions	E°(V)
$Co^{+3} + e \rightarrow Co^{+2}$	+1.808
$Co^{+2} + 2e \rightarrow Co_{(s)}$	-0.277
$Co_3O_{4(s)} + 8H^+ + 2e \rightarrow 3Co^{+2} + 4H_2O$	+2.110
$Co_2O_{3(s)} + 6H^+ + 2e \rightarrow 2Co^{+2} + 3H_20$	+1.750
$Co(OH)_{2(s)} + 2e \rightarrow Co_{(s)} + 2OH^-$	-0.730
$Co(NH_3)_6^{+3} + e \rightarrow Co(NH_3)_6^{+2}$	-0.100
$CoO(OH)_{(s)} + H_2O + e \rightarrow CO(OH)_{2(s)} + OH^-$	-0.170

I.6. cobalt oxides

Among transition metal oxides, cobalt oxide is one of the most versatile materials. It exists in three distinct p-type crystalline forms: cobalt monoxide (CoO), cobaltic oxide (Co_2O_3), and cobaltite (Co_3O_4). Due to its chemical stability, Co_3O_4 is the most commonly used form in research projects. Cobalt Oxide, also known as: CoO (II), Co_2O_3 (II), and Co_3O_4 (II, III)[27]**.**

I.6.1.Cobalt Oxide "CoO type"

Cobalt Oxide, also known asCobalt monoxide or "CoO type," has a Néel temperature (TN) of 290K and behaves in an antiferromagnetic manner. However, the TN value in thin film structures is slightly affected by the thickness of the CoO oxide.Its crystalline structure is of the fcc type (Nacl-type structure) due to the interpenetration of Co^{2+} and O^{2-} lattices (Figure 6). The lattice parameter of theCoO structure is 4.260 Å, and each Co^{2+} ion is surrounded by six O^{2-} ions in an octahedral pattern, and vice.Despite the large hopping integrals between the Co 3d and O 2p orbitals, there is little hybridization between the Co and O orbitals because the oxygen orbitals require less energy.

The electronic configuration of CoO is $Co\ 3d^7 O\ 2p^6$.

In the ground state, the O 2p band is fully occupied whereas the Co 3d band is only partially occupied. According to band theory, CoO will still exhibit metallic properties even if the valence band is only half occupied.

Experiments have shown that cobalt oxide (CoO) is an insulator with a band gap of 2.5 eV. The strong electron-electron interaction in the 3d band significantly impacts the electronic structure of CoOand is responsible for this disparity. Consequently, a d-d character is necessary for the valence-to-conduction band transitions. However, Shen et al.'s research has revealed that these transitions are p-d in nature. Therefore, the O2p band appears to be significant and must be considered when examining the valence band structure [28] .

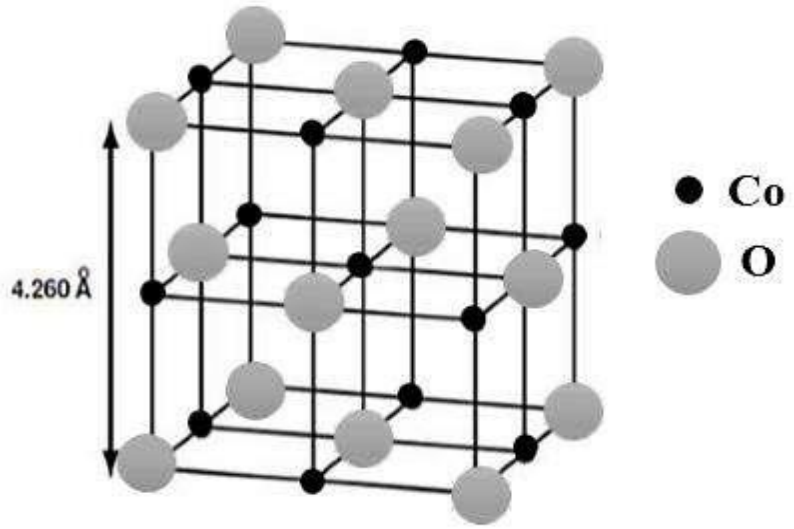

Figure I.6.CoO cell, where O and Co atoms are face-centered cubic (fcc)[29] .

I.6.2.CobaltOxide"Co_2O_3type"

This type of oxide is highly metastable, although its existence in the solid state has not yet been confirmed. According to the literature, cobalt(II) oxide (Co_2O_3) has a hexagonal close-packed (hcp) structure with lattice values of a = 4.640 Å and c = 5.750 Å. Brundle et al. examined the interaction of oxygen and air with clean cobalt surfaces using X-ray photoelectron spectroscopy (XPS), but they were unable to demonstrate the existence of such an alloy [28].

I.6.3.Cobalt Oxide "Co_3O_4 type"

Cobalt oxide is a p-type semiconductor material. It has three distinct stoichiometric phases as we have seen: cobaltous oxide (CoO), which has a cubic structure; cobaltic oxide (Co_2O_3), also with a cubic structure; and cobalt oxide (Co_3O_4), which features a cubic spinel structure of the type AB_2O_4. In this structure, Co^{+3}ions occupy the octahedral sites, while Co^{+2}ions occupy the tetrahedral sites[30]. Among these phases, Co_3O_4 is the most stable[31], and our focus will be on Co_3O_4 thin films.It can be used for a variety of purposes, including as catalyst for gas sensors [32] and catalysts[33, 34], supercapacitors[35], a solar selective absorber due to its the p-type semiconductingproperties[36], energy storage[37],and photocatalysis [38]due to its high absorption in the visible spectrum, strong electrical conductivity, and good crystallinity.

Table 1 summarizes the physical and chemical properties of Co_3O_4 thin films. The material was found to have a low band gap energy (Eg) and a refractive index of 2.4. Research on Co_3O_4 thin films has been conducted using chemical and physical methods on various substrates to improve their structural, optical, and electrical properties. These thin films can be prepared using various techniques, such as magnetron sputtering (MST), pulsed laser deposition (PLD), chemical vapor deposition (CVD), the sol-gel process (SGP), reactive evaporation (RE), electrochemical deposition (ECD), and spray pyrolysis (SPT).

The spray techniques are preferred over other methods because they allow for temperature stabilization control for glass substrates, concentration control of the solution, large-area spraying, time control for spraying, composition control, and large-area spraying.

Table I.4.An overview of the fundamental chemical and physical characteristics of Co_3O_4 thin films.

Property	value
Appearance	Fine dark gray to balck
Molecular mass	74.9326g/mol
Stable phase Energy at 298.15 K	9.23 eV
Conductivity (σ)	10^{-4}- 10^{-2}
Melting Point	895°C
Refractive index	2.4
Density (Volumic mass)	6.11g/mol
Direct band gap energy (E_g)	2.0-2.7eV
Crystal structure	Cubic spinel
Lattice parametre	8.080°A
Space group	Fd-3m
Electrical properties at room temperature	P-type

Studying the physical and chemical characteristics of Co_3O_4 thin films is the primary goal of this work. In this study, we have suggested a review of previous studies on spray-prepared nanostructured Co_3O_4.

I.6.3.1.Structural and microstructural properties Co_3O_4 thin films

Several growth techniques, including magnetron sputtering (MST), spray pyrolysis technique (SPT), chemical vapor deposition (CVD), sol-gel process (SGP), reactive evaporation (RE), electrochemical deposition (ECD), and pneumatic spray method (PSM), have been employed to elaborate Co_3O_4 thin films.Due to recent

developments, the production of more crystalline Co_3O_4 thin films has become feasible under improved growth conditions. Chemical vapor deposition (CVD) has been employed to create cobalt oxide thin films on glass at various temperatures [39]. The cobalt oxide films are polycrystalline and have a cubic spinel structure (As shown in Figure 7). C. Ravi Dhas et al. [41] examined how the molarity of the precursor affected the structural property. The films exhibited a preferential orientation along the (311) plane due to variations in deposition molar concentrations, which influenced their structural properties.

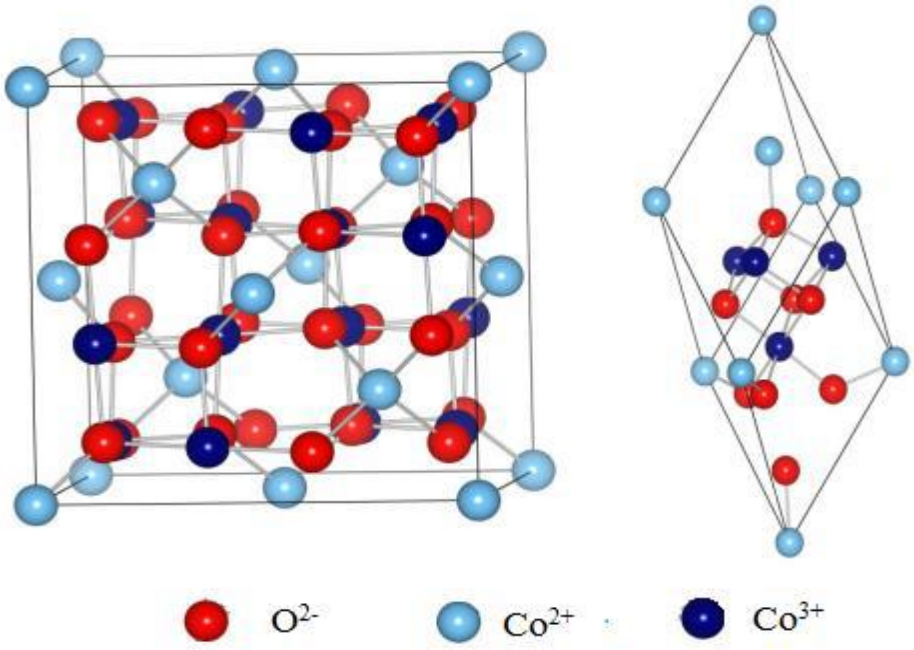

Figure I.7.Unit cell (on the left) and primitive cell (on the right) of Co_3O_4[40].

I.6.3.2.Optoelectronic PropertiesCo3O4 thin films

- **Transmittance**

The optical properties of Co_3O_4 thin films produced by chemical vapor deposition (CVD) were examined to understand the impact of substrate temperatures [39].

Figure 8 shows the optical transmittance spectra of Co_3O_4 thin films formed at different substrate temperatures. The spectra are plotted as a function of wavelength in the visible and near-infrared regions. As the substrate temperature increases, the transmittance values also rise. This phenomenon can be attributed to the increased convective flow of hot air, which results in less mass being transferred to the heated substrate.

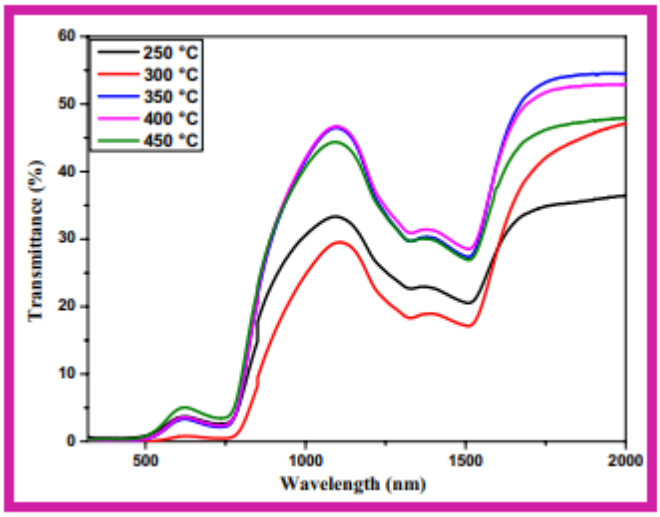

Figure I.8. Optical transmittance of Co_3O_4 thin films as a function of substrate temperatures [39].

❖ Optical Band Gap

Table I. 5. optical parameter values of the thin layers of Co_3O_4 that were deposited[29].

Concentration (mol/l)	E_{g1}(eV)	E_{g2}(eV)
0.05	1.41	1.92
0.1	1.44	1.94
0.15	1.45	2.02
0.2	/	1.47

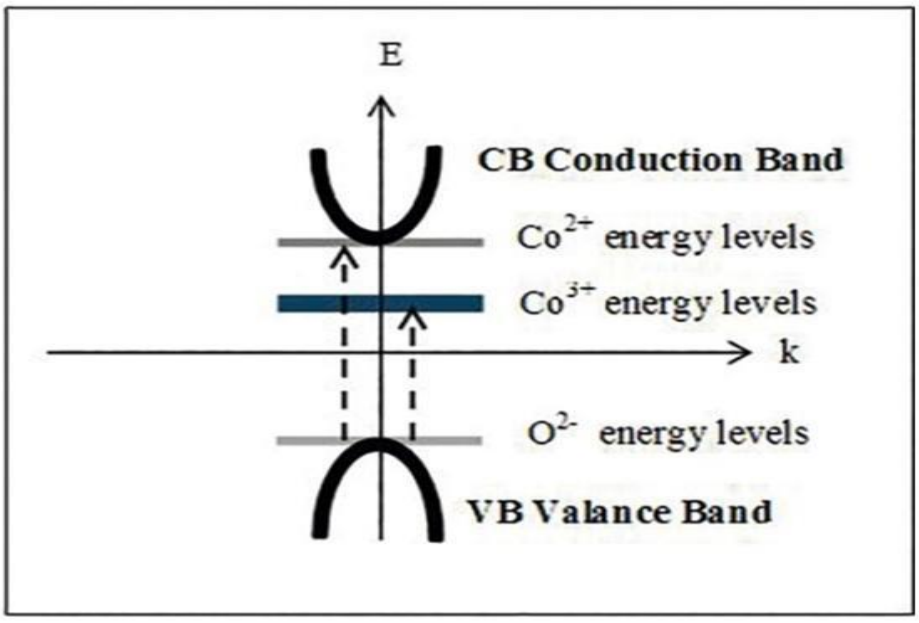

Fig I.9. Schematic representations of the band structure of Co_3O_4.

Figure I.9 and Table I.5 clearly show that the strong O 2p character of the valence band explains the presence of two band gaps. Meanwhile, the Co (II) 3d orbitals mainly contribute to the conduction band [42].

❖ **Electrical Properties**

Figure I.10 illustrates how electrical conductivity varies with substrate temperature. The conductivity, σ, increases with substrate temperature up to 400 °C but then decreases. The electrical properties of stoichiometric Co_3O_4 are affected by adsorbed oxygen.

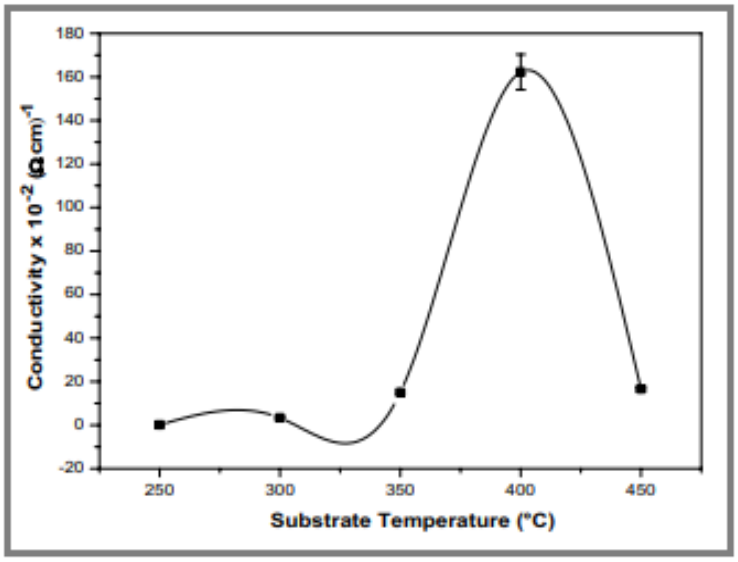

Figure I.10.Dependence of electrical conductivity in Co_3O_4 films on substrate temperature[39].

I.7.Applications of Cobalt Oxide Co_3O_4 thin film:

Due to their unique physical, chemical, and electrochemical properties, cobalt oxide (Co_3O_4) thin films are highly versatile and have a variety of applications in many industries. A few well-known uses are listed below:

I.7.1.Energy Storage Devices

- Batteries**:**Due to their high specific capacity and exceptional cycling stability, lithium-ion batteries (LIBs) and other rechargeable batteries use them as electrode materials [44, 45].
- **Supercapacitors:**Its superior redox characteristics make it an ideal active component for pseudo capacitors [46].

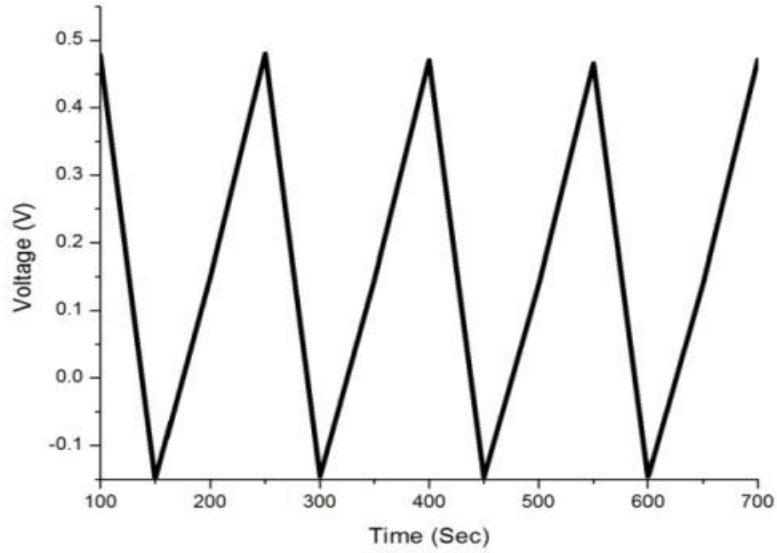

FigureI.11. Charge /discharge curves of Co_3O_4thin film[47].

I.7.2. Gas Sensors

• Cobalt oxide thin films are appropriate for industrial safety and environmental monitoring since they are sensitive to gases like CO, H_2S, and NOx[48].

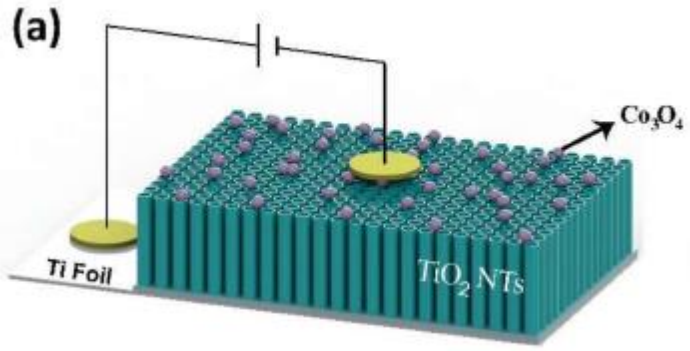

Figure I. 12. Measurement scheme of (a) Co_3O_4/TiO2 heterostructures[49].

I.7.3. Catalysis

• Water Splitting: In water electrolysis, it acts as an electrocatalyst for the oxygen evolution reaction (OER)[50, 51].

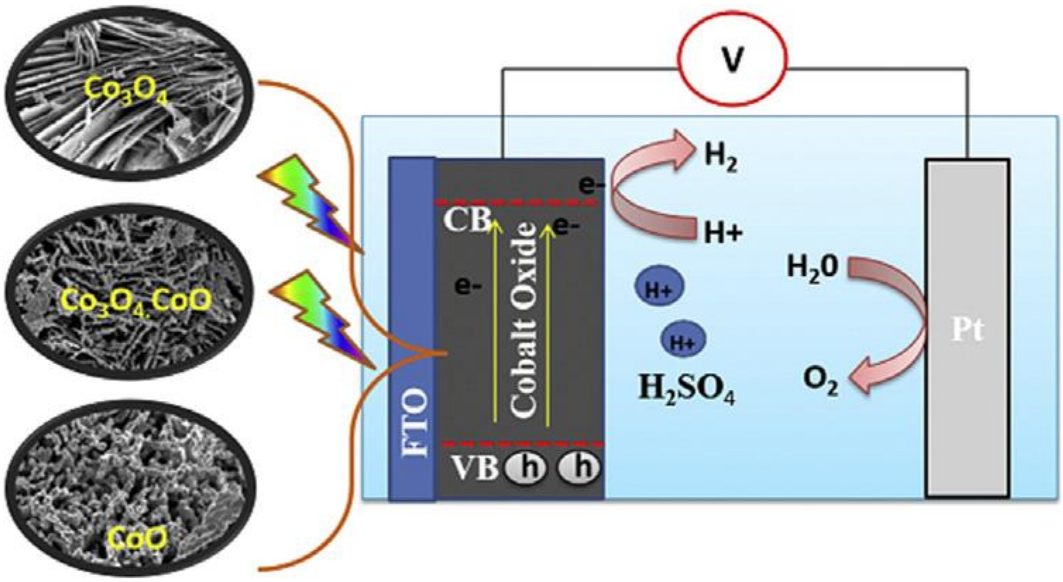

FigureI.13.Cobalt oxide as photocatalyst for water splitting[52].

- **Heterogeneous Catalysis** is utilized in processes such as the reduction of nitrogen oxides and the oxidation of hydrocarbons because of its high catalytic activity[32].

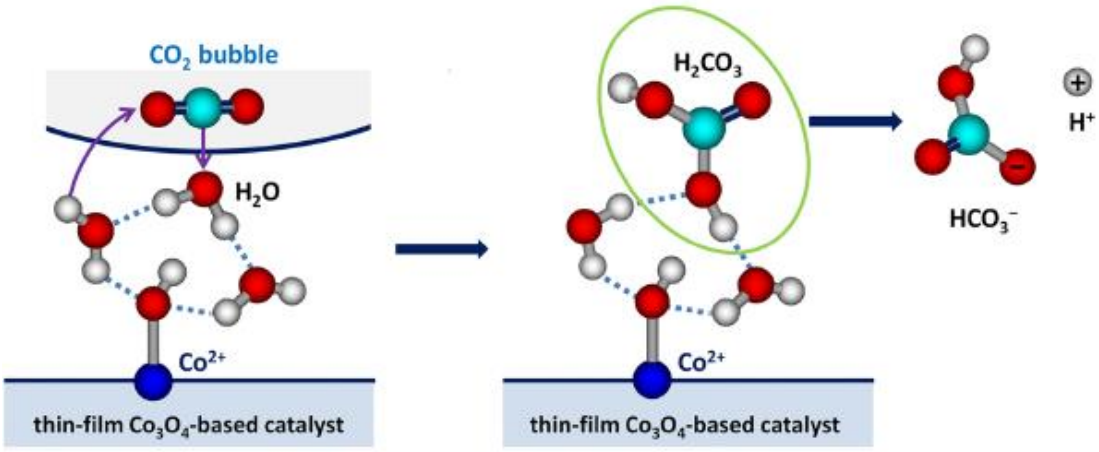

Figure I. 14. Diagram of the suggested CO_2 hydration process that is aided by the thin film of Co_3O_4 produced by plasma[53].

I.7.4. Electrochromic Devices

- Co_3O_4 thin films are used in smart windows and displays because of their capacity to alter optical characteristics in response to applied voltage[54].

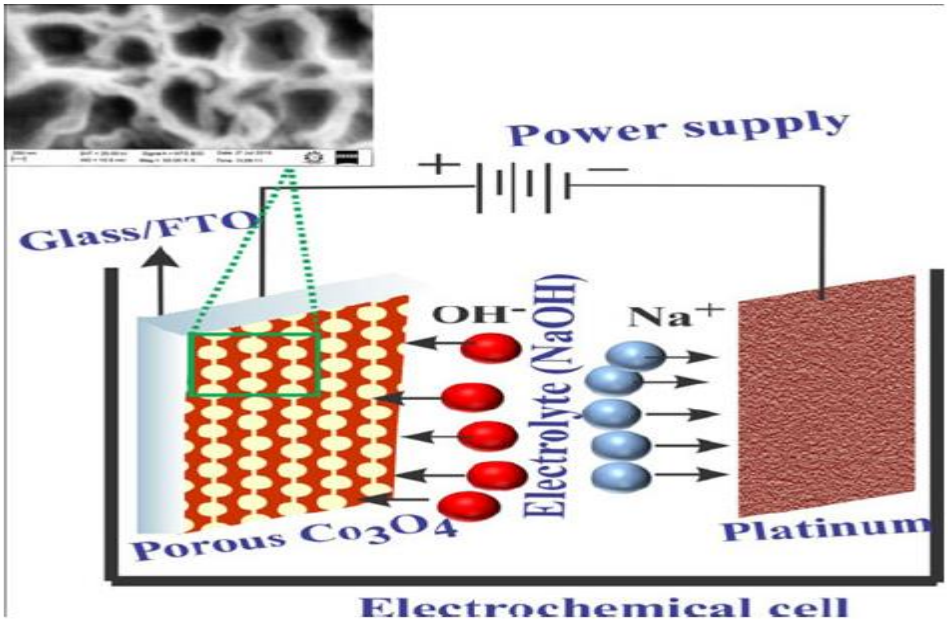

Figure I. 15.Electrochromic device cell (ECD) schematic illustration employingCo_3O_4 film[54].

I.7.5. Photovoltaics and Photodetectors

- Its advantageous optical bandgap makes it suitable for use as an absorber or buffer layer in solar cells [55, 56].
- Applied in photodetectors for applications that involve visible and ultraviolet light [57, 58].

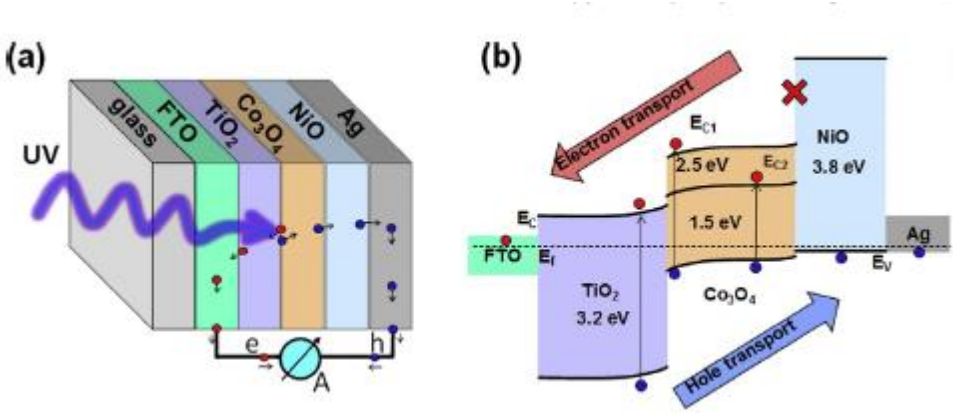

Fig I. 16. (a) Device schematic showing self-bias ultraviolet photodetection. (b) Energy band diagram of the TiO_2/Co_3O_4 UV photodetector (red and blue circles represent the photogenerated electrons and holes, respectively, and the cross symbol represents the electron blocking function)[59].

I.7.6. Magnetic Applications

• Cobalt oxide can be used in magnetic sensors and spintronic devices because of its low-temperature antiferromagnetic characteristic[60].

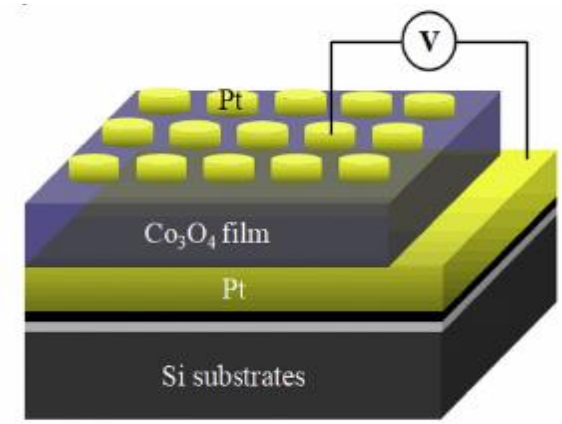

Fig I.17. The schematic diagram of a sandwiched Pt/Co_3O_4/Pt structure[61].

I.7.7. Antimicrobial Coatings

• Because of their antibacterial qualities, Co_3O_4thinfilms are appropriate for sanitary surfaces and medical equipment[62, 63].

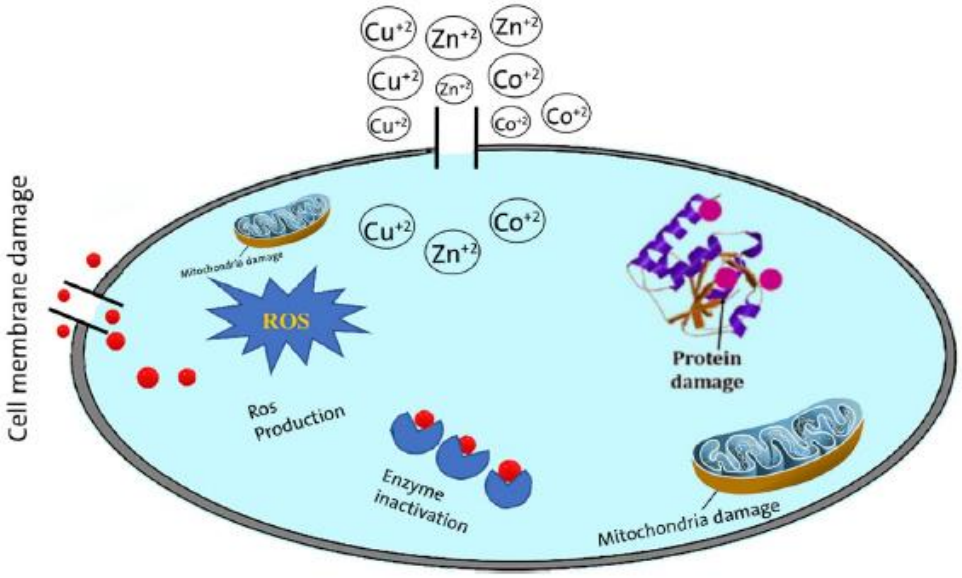

Figure I.18. Mechanism of antibacterial and antifungal activity of CuO,ZnO, Co_3O_4 nanoparticals and CuO- ZnO- Co_3O_4 nanocomposite.

I.7.8. Thermoelectric Devices

• Co_3O_4 thin films are being investigated for energy harvesting applications in waste heat recovery due to their strong thermoelectric qualities[64].

I.7.9. Protective and Decorative Coatings

• The hardness, chemical stability, and visual appeal of cobalt oxide thin films make them useful as protective and decorative coatings [65, 66].

I.7.10. Chemical and Biological Sensors

• Cobalt oxide's electrochemical activity makes it perfect for sensors that identify chemical species like hydrogen peroxide and glucose or biomolecules[67].

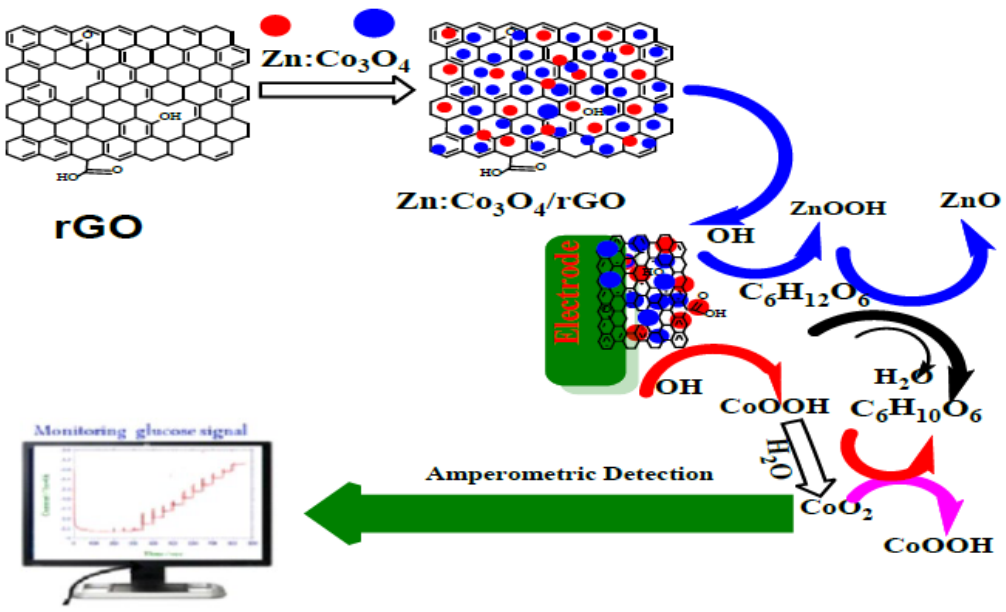

Figure I.19. Schematic illustration for the fabrication of $ZnCo_3O_4$/rGO/CPE modified electrode and its mechanism for amepriometric detection of glucose[68].

I.8.Conclusion

In this chapter, we introduced transparent conducting oxides (TCOs) and the spinel structure. We discussed the different forms, or phases, of cobalt oxides and reviewed the general properties and applications of cobalt oxide (Co_3O_4).

References

[1]H. Xu, L. Lan, M. Xu, M. Li, D. Luo, P. Xiao, J. Peng, Low-Roughness and Easily-Etched Transparent Conducting Oxides with a Stack Structure of ITO and IZO, ECS Journal of Solid State Science and Technology 2 (2013) R245.

[2]S. Trukhanov, Peculiarities of the magnetic state in the system La0. 70Sr0. 30MnO3− γ (0≤ γ≤ 0.25), Journal of Experimental and Theoretical Physics 100 (2005) 95-105.

[3]G. Gonçalves, E. Elangovan, P. Barquinha, L. Pereira, R. Martins, E. Fortunato, Influence of post-annealing temperature on the properties exhibited by ITO, IZO and GZO thin films, Thin solid films 515 (2007) 8562-8566.

[4]L. Raniero, I. Ferreira, A. Pimentel, A. Goncalves, P. Canhola, E. Fortunato, R. Martins, Role of hydrogen plasma on electrical and optical properties of ZGO, ITO and IZO transparent and conductive coatings, Thin Solid Films 511 (2006) 295-298.

[5]M.I. Panasyuk, T.I. Zubar, T.I. Usovich, D.I. Tishkevich, O.D. Kanafyev, V.A. Fedkin, A.N. Kotelnikova, S.V. Trukhanov, D. Michels, D. Lyakhov, Mechanism of bubbles formation and anomalous phase separation in the CoNiP system, Scientific Reports 13 (2023) 5829.

[6]A. Ferreira, F. Silva, A. Pinto, V. Sousa, Characterization of Thin Chromium Coatings Produced by PVD Sputtering for Optical Applications .Coatings 2021, 11, 215, s Note: MDPI stays neutral with regard to jurisdictional claims in published …, 2021.

[7]A. Seyhan, E. Kartal, Optical, Electrical and Structural Properties of ITO/IZO and IZO/ITO Multilayer Transparent Conductive Oxide Films Deposited via Radiofrequency Magnetron Sputtering, Coatings 13 (2023) 1719.

[8]D.S. Ginley, J.D. Perkins, Transparent conductors, Handbook of transparent conductors, Springer, (2010), pp. 1-25.

[9]C. Kittel, Int. to Solid State Physics, 8th edn., Maruzen, John Wiley & Sons, Inc., New York, 2005.

[10]G. Rupprecht, Untersuchungen der elektrischen und lichtelektrischen Leitfähigkeit dünner Indiumoxydschichten, Zeitschrift für Physik, 139, (1954), 504-517.

[11]K. Badekar, Electrical conductivity and thermoelectricpower of some heavy metal compounds, Annalen der Physik (Leipzig), 22, (1907), 749.

[12]C.G. Van de Walle, Hydrogen as a cause of doping in zinc oxide, Physical review letters, 85, (2000), 1012.

[13]G. Brunin, F. Ricci, V.-A. Ha, G.-M. Rignanese, G. Hautier ,Transparent conducting materials discovery using high-throughput computing, npj Computational Materials, 5, (2019), 63.

[14]R. GOVIND, UNIVERSITY RAMGARH, JHARKHAND.

[15]E.C. Jordan, C. Andrews, Electromagnetic waves and radiating systems, American Journal of Physics, 19, (1951), 477-478.

[16]C. Kittel, Introduction to solid state physics.(7thedn), john willey and sons inc, New York, (1996), 308.

[17]H. Hartnagel, Semiconducting Transparent Thin Films, Institute of Physics Publishing, (1995).

[18]T.J. Coutts,D.L. Young, X. Li, Characterization of transparent conducting oxides, Mrs Bulletin, 25, (2000), 58-65.

[19]K. Chopra, S. Major, D. Pandya, Transparent conductors—a status review, Thin solid films 102 (1983) 1-46.

[20]H. Kawazoe, M. Yasukawa, H. Hyodo, M .Kurita, H. Yanagi, H. Hosono, P-type electrical conduction in transparent thin films of CuAlO2, Nature 389 (1997) 939-942.

[21]H. Hosono, Recent progress in transparent oxide semiconductors: Materials and device application, Thin solid films 515 (2007) 6.6014-000

[22]H. Kawazoe, H. Yanagi, K. Ueda, H. Hosono, Transparent p-type conducting oxides: design and fabrication of pn heterojunctions, Mrs Bulletin 25 (2000) 28-36.

[23]M. Tinouche, Élaboration et caractérisations de couches minces à base de cobalt, 2018.

[24]W. Betteridge, Cobalt and its Alloys, (No Title) (1982.(

[25]L. Harbraken, Techniques de l'ingénieur, Propriétés de Cobalt et de ses alliages, M.

[26]E. Generalic, Copyright© 1998-2003 Cobalt, Tableau périodique des élements. htm (2018.(

[27]M.B. Sabah Haffas, Caractérisation des couches minces Co3O4: Cu élaborée par la technique spray pneumatique.

[28]H.M. Garad, L'anisotropie magnétique perpendiculaire induite par oxydation et recuit thermique: De la structure au magnétisme, Universitéde Grenoble, 2012.

[29]N. Kouidri, Contribution à l'étude de couches minces d'oxydes transparents conducteurs à base de zinc et cobalt par spray pneumatique, University of Mohamed Khider, BISKRA, 2019.

[30]R.M. Obodo, U. Chime, A.C. Nkele, A.C. Nwanya ,A. Bashir, I. Madiba, M. Asjad, I. Ahmad, T. Zhao, N. Thovhogi, Effect of annealing on hydrothermally deposited Co3O4-ZnO thin films for supercapacitor applications, Materials Today: Proceedings 36 (2021) 374-378.

[31]A.C. Nwanya, D. Obi, R.U. Osuji, R .Bucher, M. Maaza, F.I. Ezema, Simple chemical route for nanorod-like cobalt oxide films for electrochemical energy storage applications, Journal of Solid State Electrochemistry 21 (2017) 2567-2576.

[32]R. Perekrestov, A. Spesyvyi, J. Maixner, K. Mašek ,O. Leiko, I. Khalakhan, J. Maňák, P. Kšírová, Z. Hubička, M. Čada, The comparative study of electrical, optical and catalytic properties of Co3O4 thin nanocrystalline films prepared by reactive high-power impulse and radio frequency magnetron sputtering ,Thin Solid Films 686 (2019) 137427.

[33]O. Kilo, J. Jabbour, R. Habchi, N. Abboud, M. Brouche, A. Khoury, D. Zaouk, Electrospray deposition and characterization of cobalt oxide thin films, Materials science in semiconductor processing 24 (2014) 57-61.

[34]P. Shi, R. Su, S. Zhu, M. Zhu, D. Li, S. Xu, Supported cobalt oxide on graphene oxide: Highly efficient catalysts for the removal of Orange II from water, Journal of hazardous materials 229 (2012) 331-339.

[35]S.G. Kandalkar, J. Gunjakar, C. Lokhande ,Preparation of cobalt oxide thin films and its use in supercapacitor application, Applied Surface Science 254 (2008) 5540-5544.

[36]A. Lakehal, B. Benrabah, A. Bouaza, C. Dalache, B. Hadj, Tuning of the physical properties by various transition metal doping in Co3O4: TM (TM= Ni, Mn, Cu) thin films: A comparative study, Chinese journal of physics 56 (2018) 1845-1852.

[37]L. Yao, H. Yao, G. Xi, Y. Feng, Recycling and synthesis of LiNi 1/3 Co 1/3 Mn 1/3 O 2 from waste lithium ion batteries using d, l-malic acid, Rsc Advances 6 (2016) 17947-17954.

[38]A. Vennela, D. Mangalaraj, N. Muthukumarasamy, S. Agilan, K. Hemalatha, Structural and optical properties of Co3O4 nanoparticles prepared by sol-gel technique for photocatalytic application, International Journal of Electrochemical Science 14 (2019) 3535-3552.

[39]N. Kouidri, S. Rahmane, A. Allag, Substrate temperature-dependent properties of sprayed cobalt oxide thin films, Journal of Materials Science: Materials in Electronics 30 (2019) 1153-1160.

[40]J .Chen, X. Wu, A. Selloni, Electronic structure and bonding properties of cobalt oxide in the spinel structure, Physical Review B—Condensed Matter and Materials Physics 83 (2011) 245204.

[41]C.R. Dhas, R. Venkatesh, R. Sivakumar, A.M.E. Raj, C. Sanjeeviraja, Effect of solution molarity on optical dispersion energy parameters and electrochromic performance of Co3O4 films, Optical Materials 72 (2017) 717-729.

[42]A. Lakehal, B. Bedhiaf, A. Bouaza, B. Hadj, A. Ammari, C. Dalache, Structural, optical and electrical properties of Ni-doped Co 3 O 4 prepared via Sol-Gel technique, Materials Research 21 (2018) e20170545.

[43]D. Barreca, C. Massignan, S. Daolio, M. Fabrizio, C. Piccirillo, L. Armelao, E. Tondello, Composition and microstructure of cobalt oxide thin films obtained from a novel cobalt (II) precursor by chemical vapor deposition, Chemistry of Materials 13 (2001) 588-593.

[44]R.M. Obodo, I.C. Nwodo, P.C. Ani, E. Omugbe, C. Mbamara, U.C. Elejere, C.U. Eze, I. Ahmad, M. Maaza, J.N. Aniezi, Review onperformance optimization of Lithium Sulphur Batteries (LiSBs) using carbon based electrodes, Recent Advances in Natural Sciences (2024) 64-64.

[45]Y. Zhang, Y. Zhang, Y. Feng, Y. Wang, L. Zhang, Fabrication of Zn-doped Co3O4 as cathode material for aqueous rechargeable Zn-ion batteries, International Journal of Electrochemical Science 18 (2023) 100268.

[46]A. Jagadale, V. Kumbhar, C. Lokhande, Supercapacitive activities of potentiodynamically deposited nanoflakes of cobalt oxide (Co3O4) thin film electrode, Journal of colloid and interface science 406 (2013) 225-230.

[47]S. Jogade, D. Sutrave, S. Gothe, Electrochemical analysis of cobalt oxide thin film for supercapacitor, Int. J. Adv. Res. Phys. Sci 2 (2015) 36-41.

[48]G. Eranna, B. Joshi, D. Runthala, R. Gupta, Oxide materials for development of integrated gas sensors—a comprehensive review, Critical Reviews in Solid State and Materials Sciences 29 (2004) 111-188.

[49]O. Alev, A. Kılıç, Ç. Çakırlar, S. Büyükköse, Z.Z. Öztürk, Gas sensing propertiesof p-Co3O4/n-TiO2 nanotube heterostructures, Sensors 18 (2018) 956.

[50]J. Li, J. Li, J. Ren, H. Hong, D. Liu, L. Liu, D. Wang, Electric-field-treated Ni/Co3O4 film as high-performance bifunctional electrocatalysts for efficient overall water splitting ,Nano-Micro Letters 14 (2022) 148.

[51]H.S. Jeon, M.S. Jee, H. Kim, S.J. Ahn, Y.J. Hwang, B.K. Min, Simple chemical solution deposition of Co_3O_4 thin film electrocatalyst for oxygen evolution reaction, ACS Applied Materials & Interfaces, 7 (2015), 24550-24.555

[52]S.N.F. Moridon, M.I. Salehmin, M.A. Mohamed, K. Arifin, L.J. Minggu, M.B. Kassim, Cobalt oxide as photocatalyst for water splitting: Temperature-dependent phase structures, International journal of hydrogen energy, 44 (2019), 25495-25504.

[53]H .Kierzkowska-Pawlak, E. Kruszczak, J. Tyczkowski, Catalytic activity of plasma-deposited Co_3O_4-based thin films for CO_2 hydration–A new approach to carbon capture applications, Applied Catalysis B: Environmental, 304 (2022), 120961.

[54]C.R. Dhas, R. Venkatesh, R. Sivakumar, A.M.E. Raj, C. Sanjeeviraja, Fast electrochromic response of porous-structured cobalt oxide (Co_3O_4) thin films by novel nebulizer spray pyrolysis technique, Ionics 22 (2016), 1911-1926.

[55]A. Faccin, Advanced AFM techniques to characterize all-oxide solar cells at the nanoscale.

[56]A.Q. Mugheri, A.A. Otho, G.M. Kaleri, S. Ghanghro, A. Kandhro, H. Fouad, M.S. Akhtar, ZnO and ZnO/Co_3O_4 nanorods for enhanced photovoltaic and

photosensors applications, Journal of Nanoelectronics and Optoelectronics, 16 (2021), 2003-2010.

[57]A.K. Rana, M. Patel, T.T. Nguyen, J-H. Yun, J. Kim, Transparent Co_3O_4/ZnO photovoltaic broadband photodetector, Materials Science in Semiconductor Processing, 117 (2020), 105192.

[58]M. Patel, M. Kumar, H.-S. Kim ,W.-H. Park, E.H. Choi, J. Kim, Reactive sputtering growth of Co3O4 thin films for all metal oxide device: a semitransparent and self-powered ultraviolet photodetector, Materials Science in Semiconductor Processing 74 (2018) 74-79.

[59]P. Mahala, M. Patel ,D.-K. Ban, T.T. Nguyen, J. Yi, J. Kim, High-performing self-driven ultraviolet photodetector by TiO2/Co3O4 photovoltaics, Journal of Alloys and Compounds 827 (2020) 154376.

[60]Z.N. Kayani, S. Arshad, S. Riaz, S. Naseem, Investigation of structural, optical and magnetic characteristics of Co3O4 thin films, Applied Physics A 125 (2019) 196.

[61]C. Yao, W. Hu, M. Ismail, S.K. Thatikonda, A. Hao, S. He, N. Qin, W. Huang, D. Bao, Coexistence of resistive switching and magnetism modulation in sol-gel derived nanocrystalline spinel Co3O4 thin films, Current Applied Physics 19 (2019) 1286-1295.

[62]N.E. Volofu, Synthesis, characterisation and assessment of antimicrobial activity of doped zinc oxide nanoparticles against selected waterborne pathogens, Vaal University of Technology (South Africa), 2019.

[63]R. Garg, S. Gonuguntla, S. Sk, M.S. Iqbal, A.O. Dada, U. Pal, M. Ahmadipour, Sputtering thin films: Materials, applications, challenges and future directions, Advances in Colloid and Interface Science (20.103203 (24

[64]A. Soffientini, Synthesis and characterization of nanostructured oxides for thermoelectric applications, (2018.(

[65]S. Nanthini, P. Veluswamy, H. Shankar, Protective Coatings for High Temperature Thermoelectric Materials, Coatings for High-Temperature Environments: Anti-Corrosion and Anti-Wear Applications, Springer2023, pp. 311-349.

[66]I. Barauskienė, Synthesis, structure and electrochemical properties of cobalt oxide films, Kauno technologijos universitetas, 2019.

[67]A.M. Ndala, Amperometric detection of nitrite using Co3O4 thin film, Cape Peninsula University of Technology, 2021.

[68]A. Yayesew, Synthesis and Characterization of Nanocomposite of Zn Doped Co3o4 and Reduced Graphene Oxide for Electrochemical Non-Enzymatic GlucoseSensor, 2022.

Chapter II

Elaboration and Characterizations Techniques

II. 1. Introduction

The thin-film technique is an impressive art form and a cutting-edge scientific method. The use of thin films dates back to the early metal era. One notable example is gold beating; an ancient art practiced for at least 4,000 years. Gold's exceptional malleability allows it to be hammered into extremely thin sheets. Its aesthetic appeal and resistance to chemical deterioration make gold ideal for providing durable protection and decoration. Thanks to advancements in thin-film materials, professional electronics performance has increased dramatically over the last 20 years, and the cost of mass-produced components has decreased. Since the invention of the transistor in 1947, hundreds of components (such as semiconductor components) have been integrated. Therefore, gadgets that offer significantly more computational power and memory than original computers have become trivialized, such as calculators and personal computers[1].

This chapter provides thin layers and explores their applications. It discusses physical and chemical deposition methods, focusing particularly on the spray pyrolysis process, the mechanisms involved in thin layer formation, and their advantages.A brief description of the various characterization techniques employed is provided, including energy dispersive spectroscopy (EDS), UV-Vis spectroscopy, X-ray diffraction, and four-point probe measurements.

II. 2. Thin films

A "thin film" is a layer of material that extends infinitely in two dimensions while being restricted in the third dimension, known as thickness. The thickness of a thin film can range from a few nanometers to several micrometers [2]. Thin films are formed through the random nucleation and growth of individual atoms, ions, or molecules that condense or react on a solid surface, which is referred to as a substrate.

First, the absorptive species are not in thermodynamic equilibrium with the substrate, so they move across its surface until they reach the same temperature as the substrate. During this movement, when they arrive at favorable sites (such as crystalline defects or impurities), they create seeds that grow to form the film.

II. 2.2.Application of Thin Films

Due to their unique electrical, optical, mechanical, magnetic, and chemical properties, thin films have a broad range of applications across multiple fields. Typically ranging from a few nanometers to several micrometers in thickness, these films are used to improve the functionality, performance, or durability of devices and surfaces. Table II.1 categorizes these fundamental properties and provides examples of common applications for each category.

Table II. 1. Thin Film Applications.

Thin-film Property category	**Typical applications**
Optical	Reflective/antireflective coatings, interference filters, decoration (color, luster), memory discs (CDs), waveguides and static-free coatings.
Electrical	Insulation, conduction, semiconductor devices, piezoelectric drivers, transparent electrodes in flat panel displays, electrochromic devices and transparent semiconducting device and photovoltaic cells etc.
Magnetic	Memory discs
Chemical	Barriers to diffusion or alloying, protection against oxidation or corrosion, gas/liquid sensors etc.
Mechanical	Tribological (wear-resistant) coatings, hardness, adhesion, micromechanics
Thermal	Barrier layers, Heat sink

II. 3. Classification of Deposition Technologies

There are dozens of deposition technologies for material creation [3, 4]. Classifying these technologies is easier when the number of technologies studied is restricted. Here, the focus is on thin-film deposition techniques for creating layers ranging in thickness from a few nanometers to around 10 micrometers. Essentially, there are two types of thin-film deposition technologies: purely physical ones, such as evaporative techniques, and purely chemical ones. Many glow discharge and reactive sputtering-based procedures incorporate both chemical and

physical reactions. These overlapping processes are known as physical-chemical methods.A classification scheme is presented in Table II.2, where there is a group of thin-film deposition technologies according to evaporative glow discharge, gas-phase chemical, and liquid-phase chemical processes.

Table II. 2. classification of thin-film deposition techniques.

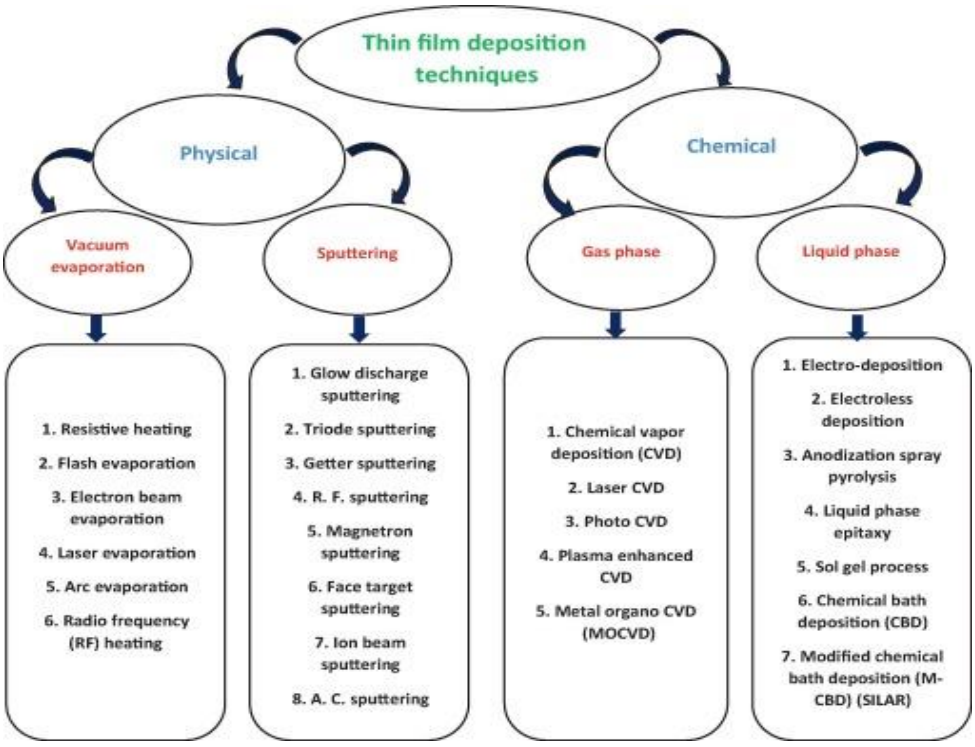

II. 3. 1.Physical Vapor Deposition (PVD)

This process uses a variety of techniques, including molecular beam epitaxy, evaporation, sputtering, and pulsed laser deposition.

II. 3. 1.1.Thermal evaporation by resistive heating

Thermal evaporation by resistive heating is a popular method for preparing thin films of metals, alloys, and compounds. It requires a vacuum environment with sufficient heat to achieve the required vapor pressure. The evaporated material condenses on a substrate, reducing oxide formation and impurity incorporation. Evaporation typically occurs at (10-5)

Torr pressure, with film characteristics and quality influenced by substrate temperature, deposition rate, and ambient pressure[2].

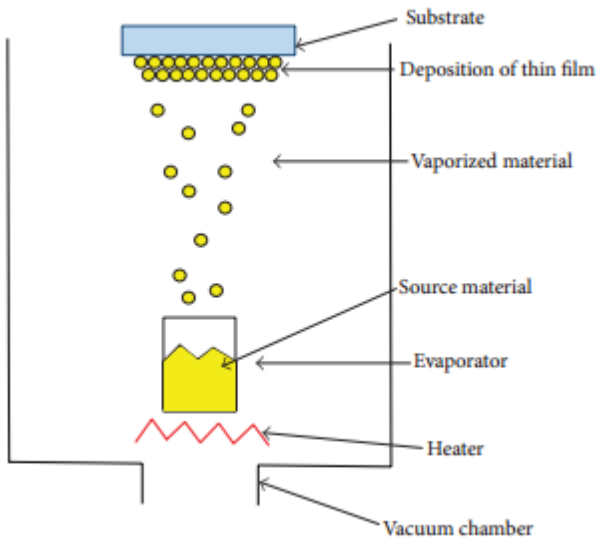

Figure II. 1.Diagram of resistive heating for thermal evaporation[5].

II. 3. 1.2.Electron beam evaporation

Electron beam evaporation (EBE) involves accelerating electrons through (5-10)kV fields onto a material's surface, causing it to melt and evaporate. This direct heating method is essential for evaporating materials from water-cooled crucibles, avoiding reactions with crucible walls. EBE can be classified into thermionic and plasma electron categories, with thermionic electrons generated from heated metal filaments or plasma extracted from confined spaces[2].

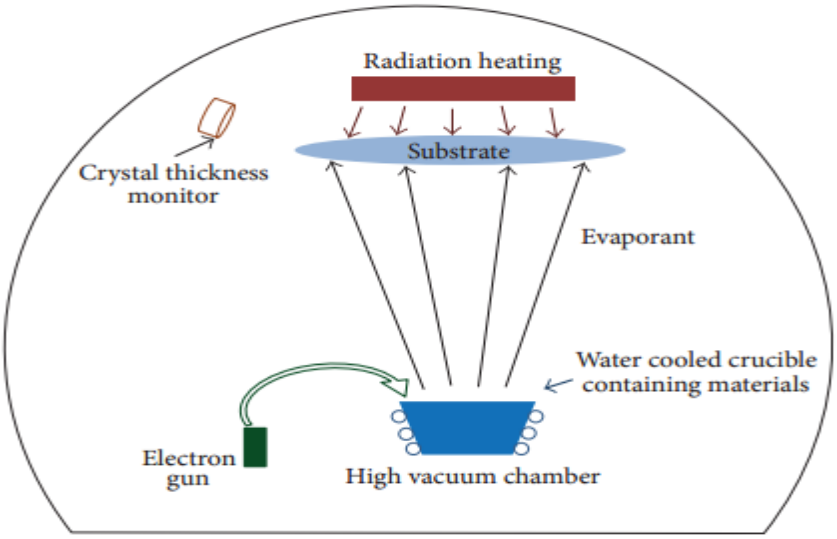

Figure II.2. General diagram of Electron Beam Evaporator[6].

II. 3. 1.3.Sputtering

Sputtering is a versatile technique used for producing high-quality transparent conductor films. It creates a gas plasma by applying voltage between a cathode and anode, causing intense bombardment by ions. The particles are ejected from the cathode and diffuse away, depositing a thin film onto a substrate. Sputtering can be powered by DC or RF biasing, with DC sputtering restricted to conducting materials. Magnetron sputtering uses a magnetic field at the target surface for high deposition rates and low substrate temperatures[2].

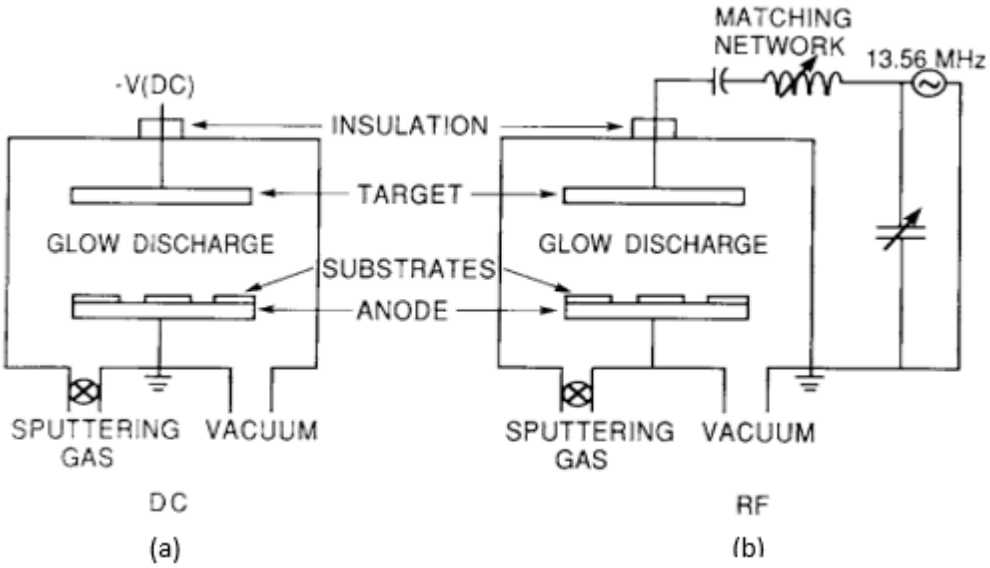

Figure II. 3. Schematics of simplified sputtering systems: (a) DC, (b) RF[1].

II. 3. 1.4.Pulsed laser deposition (PLD)

In pulsed laser deposition, an impulse laser beam is focused on a sizable target inside a vacuum-enveloped enclosure; the substrate temperature, gas pressure, and laser energy all affect the quality of the deposit:

- ✓ Stoichiometric transfer of target matter facilitates multi-element material deposit, with target purity influencing deposits.
- ✓ The choice of material is vast, limited by absorption to laser wavelength, and the purity of targets is critical.

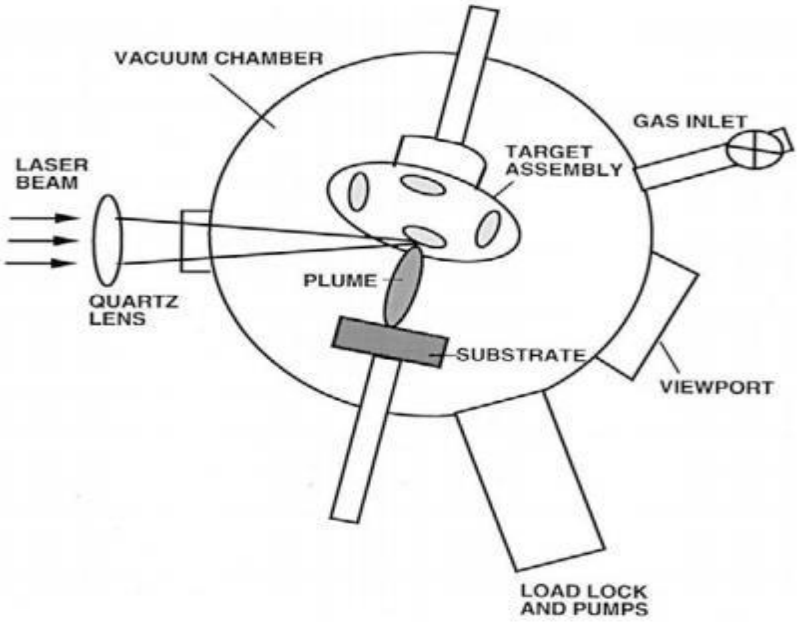

Figure II. 4. General diagram of PLD[1].

II. 3. 1.5.Molecular Beam Epitaxy (MBE)

Effluent cells heat selected elements in vacuum furnaces, forming lattices on monocrystalline wafers. Growth in ultra-high vacuum chamber with (10-11) mbar pressure and cryopannels is cooled by liquid nitrogen.

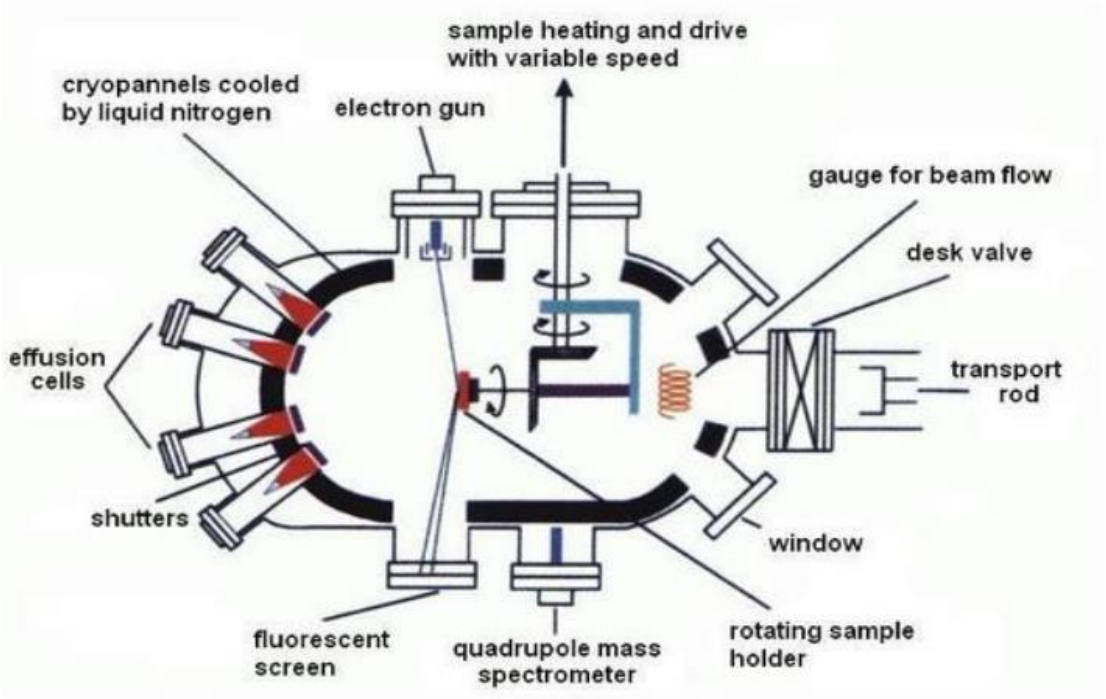

Figure II. 5. The MBE growth chamber design, the sample is fixed in the chamber center on a rotating holder[7].

II. 3. 2.Chemical Vapor Deposition

Chemical vapor deposition (CVD) and thermal oxidation are crucial methods for film formation in solid-state electronics, enabling easy synthesis of simple and complex compounds at low temperatures, with deposition variables determining deposit film properties [8]. Macroscopically following three fundamental steps play critical role in the growth of a film:

• Transfer of the precursor to the gas phase.

• Transport of the gas phase to the substrate.

• Deposition onto substrate and film growth.

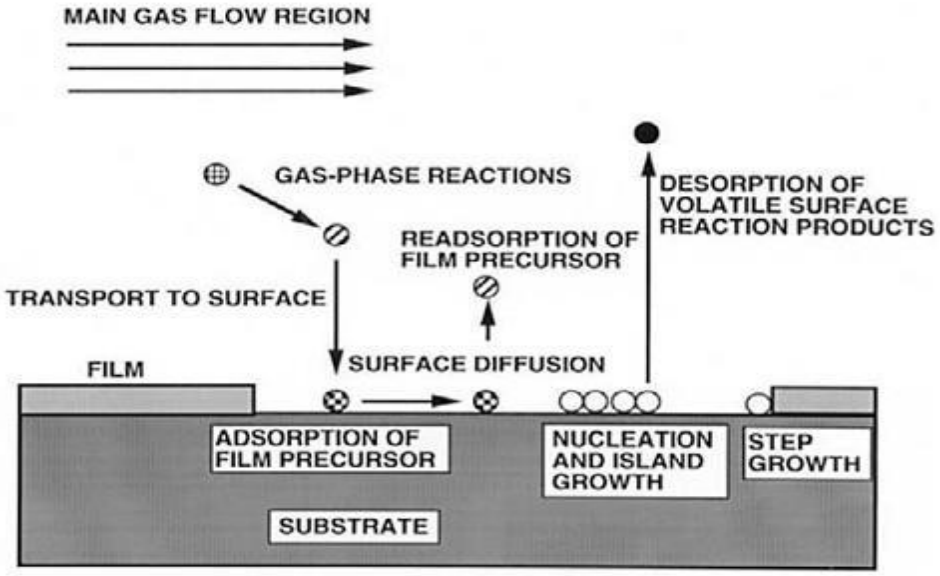

Figure II.6.Sequence of gas transport and reaction processes contributing to CVD film growth[1].

II. 3. 3.Spray Pyrolysis

The spray pyrolysis technique is a method that has been widely used for more than two decades, due to its simple, inexpensive technique and possibility to produce large area films[9, 10]. Because the film formation is carried out in air by a simple apparatus in SPD, the technique is one of the most attractive film preparation methods. This technique dissolves elements of the compound material in solution and solution fed into the spray nozzle at a predetermined pressure and flow rates. A heater power source with a feedback circuit regulates the substrate temperature. An aerosol or ultrasonic spray generator creates tiny droplets of the solution, which are then sprayed onto a heated substrate. Gas pressure or gravity can be used to force the spray nozzle. In order to prevent chemical interactions between the compound components, gas pressure can be controlled by flow and utilized as part of the compounds, such as oxygen or dry air, to deposit oxides and nitrogen or inert gas. The evaporation of the reactant or solvent and the droplet landing process are what cause the film to form.

When the solvent is totally eliminated when the droplet gets close to the substrate where the chemical reaction takes place, it is the optimal deposition setting [11]. While volatile byproducts evaporate and diffuse away from the surface, the reactant molecules go through processes of absorption, surface diffusion, and chemical reaction that result in nucleation and

layer development[12]. However, heating the substrate sufficiently to ensure that the compound solvents are totally evaporated is also crucial. The solution concentration and deposition duration determine the film's thickness.

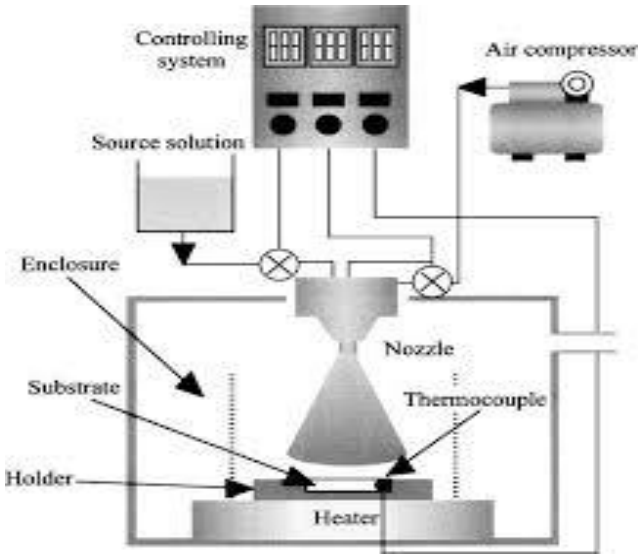

Figure II.7.Schematic representation of a spray pyrolysis deposition (SPD).

II. 3.4.Advantages of Spray Pyrolysis Deposition:

1. Inexpensive technique.

2. Possibility to produce large area film.

3. ability to form crystalline or amorphous deposition.

4. ability to control deposition parameters such as deposition temperature, deposition rate, thickness etc.

5. Particles are more uniform in size.

6. Simple & continuous operation.

7. Easy fabrication.

8. Easy to control.

9. Vacuum less.

II.3.5.Specific Aspects of Chemically Sprayed Thin Films to Consider:

When the falling drops hit the hot substrate, a chemical reaction occurs; as a result, the necessary material will go through the steps listed above to form a thin film. Numerous drops will crystallize independently as they reach the heated substrate[13], forming a patchy film as seen in figures II.8.

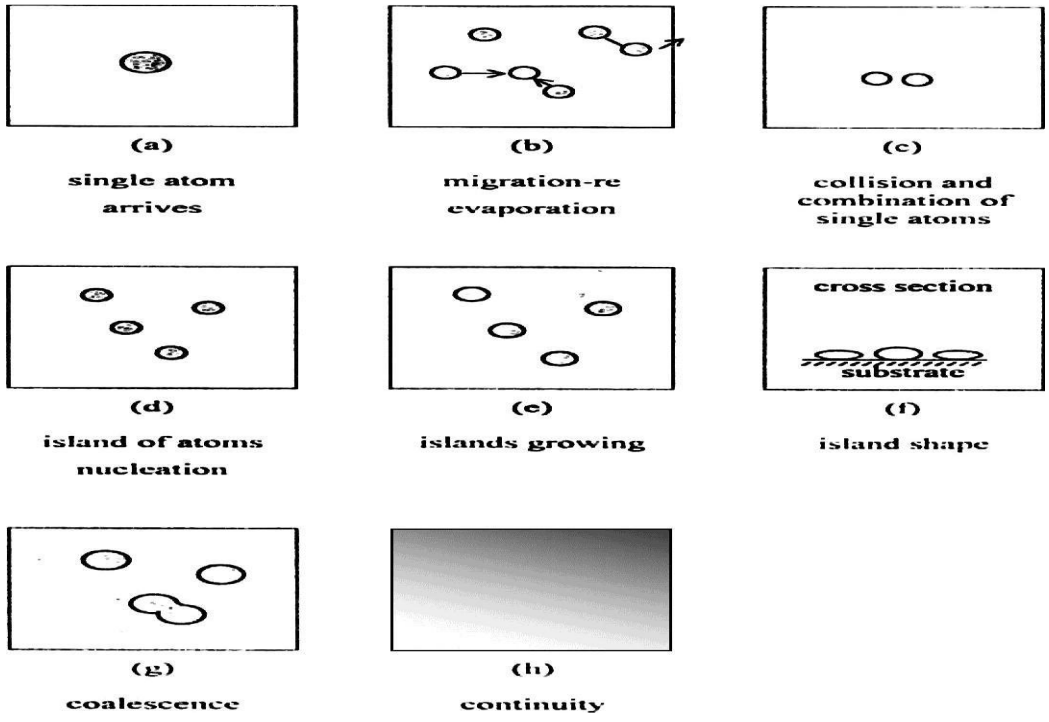

Figure II.8: Formation Stages of Thin Film[14].

- ✓ **Growth kinetics during for deposition:**

Thermal evaporation, chemical breakdown, and/or the evaporation of source materials by the irradiation of energetic species or photons are the methods used to deposit thin films on a substrate. There are three primary processes in any thin-film deposition process:

1.Creation of the suitable ionic, molecular, or atomic species.

2.These organisms are transported to the substrate.

3.Formation of a solid deposit by condensation on the substrate, either directly or by a chemical and/or electrochemical reaction.

Unit species are adsorbed on substrate surfaces, forming larger clusters that are unstable and desorb based on deposition parameters. Clusters can grow if collided with other species. After reaching a critical size, nuclei form stable, chemisorbed nuclei. Critical nuclei grow until a saturation density is reached, influenced by factors like energy, rate of impingement, activation energies, and substrate temperature.The next stage is the coalescence stage.

Larger islands form porous networks, revealing channels and holes in the substrate, transforming the film's structure from discontinuous to continuous[15].

- ✓ **Growth modes**

Research on thin films focuses on understanding growth mechanisms for better control, with nanoparticles self-assembling to form two-dimensional or three-dimensional crystals [16].

Atomic thin film growth involves three basic modes: Frank van der Merwe, Stranski-Krastanov, and Volmer-Weber growth, resulting from competing energy terms during film deposition, and processes like adsorption, desorption, and diffusion[17-19].

As in the case of atoms, the interplay of various free energy terms determines the way on how the nanoparticles (NPs)films will grow. These are in detail[20]:

The text outlines the interaction energy between NPs, the entropic contribution E_{TS}, inter-particle energy E_p[21] , and NP-to-substrate interaction energy E_s, and the diffusion energy barrier E_d.

After attaching to the substrate, the NPs will either remain stationary in one spot or freely wander in search of energetically more suitable places, depending on the relative magnitudes of Ed and k_BT_s.

From a comparison of these free energy terms one finds [19, 20]that three different growth modes follow: Frank-van-der-Merwe growth mode (FvdM) occurs when NP-to-substrate energy dominates, with stable clusters of NPs attaching at the periphery of the nucleus in contact with the substrate.

Planar film growth is accelerated by the ratio of E_d and k_BT_s, resulting in polycrystalline or single-crystalline superlattices. Immobility nucleates multiple crystallites, while large mobility promotes single-crystal growth[16].

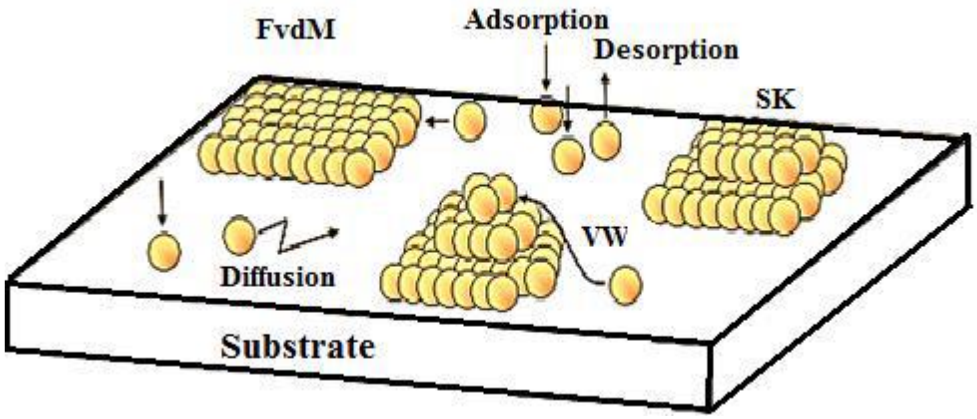

Figure II. 9.Schematic representation of the three known film growth modes[19].

II.4. Characterization methods

For the study of thin-film materials and technologies, a measurement of thin-film properties is essential. When assessing thin films, one must take into account their crystalline structure, chemical makeup, and optical, electrical, and morphological characteristics.

II.4. 1.X rays diffraction (XRD)

The crystalline quality of the Co_3O_4 thin films is investigated using X-ray diffraction (figure II.9). This straightforward, non-destructive analysis method allows for the identification of several phases and their distribution inside the sample, as well as the evaluation of internal stress, average grain size, texture, and other factors.

X-rays are electromagnetic waves with wavelength (0.5-50Å)comparable to atomic separation distances. When propagating through a crystal, the X-rays interact with the lattice and are diffracted according to the Bragg's law [16]:

$$2dd_{hkl}\sin\theta = n\lambda \quad (II.1)$$

d_{hkl} :The interplanar spacing.

n:The integer.

θ:The scattering angle.

λ :The wavelength.

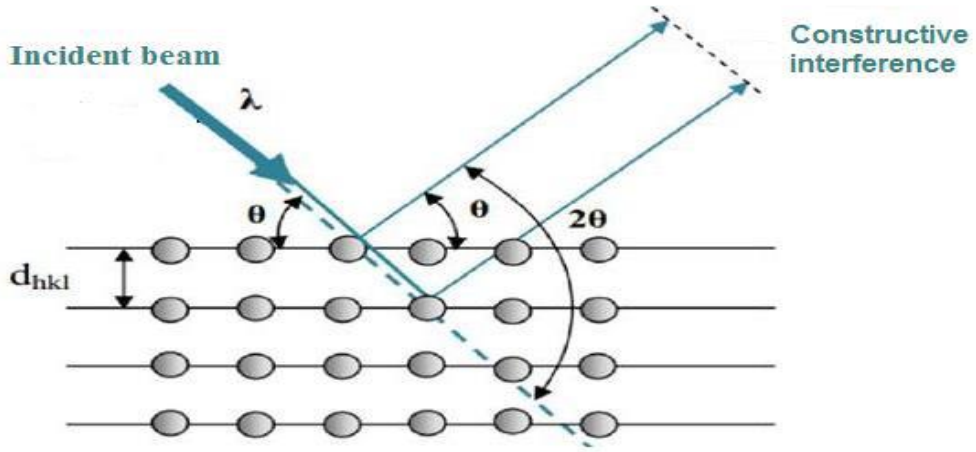

Figure II.10.Schematic diagram of Bragg diffraction[22].

The technique detects diffracted radiation using a counter tube, recording intensities on a computer system. The X-ray diffraction data is compared with JCPDS data to identify unknown materials, with crystallite size estimated using Scherrer's formula[16]:

$$D = \frac{0.9\lambda}{\beta cos\,\theta} \qquad \text{(II. 2)}$$

D:The crystallite size(nm).

λ: The wavelength of X-ray(nm).

β:The full width at half maxima of the peak (FWHM)in radians.

θ:The Bragg's angle(rd).

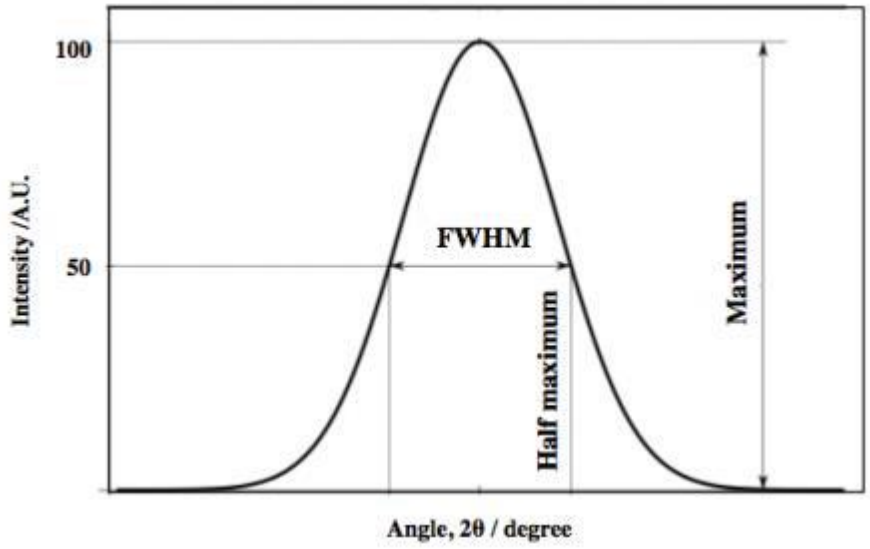

Figure II.11.Illustrate the peak widths FWHM ($\Delta\theta$=β)[23].

It can be calculating the dislocations density using the grains size values according to the following relationship[16]:

$$\delta = \frac{1}{D^2} \qquad \text{(II. 3)}$$

The micro-strain is calculated using, a Williamson-Hall plot method[24]*:*

$$\beta * cos\,\theta = \frac{0.9 * \lambda}{\mathrm{D}} + 4\varepsilon * sin\theta \qquad \text{(II. 4)}$$

The lattice parameter values for Cubic system can be calculated from the following equations using the (hkl) parameters and the interplanar spacing d[25]:

$$\frac{1}{\mathrm{d}_{\mathrm{hkl}}^2} = \left(\frac{\mathrm{h}^2 + \mathrm{k}^2 + \mathrm{l}^2}{\mathrm{a}^2}\right) \qquad \text{(II. 5)}$$

II.4. 2.FT-IR spectroscopy:

To identify the composite material in the samples, organic and inorganic chemists employed Fourier Transform Infra-Red spectroscopy (FTIR) (figure II.12).

An IR beam hits a sample, transmitting and absorbing radiation, resulting in different peaks representing the sample compounds measured at different frequencies.

Figure II.12.Fourier Transform Infra-Red spectroscopy.

The FTIR spectroscopy can be used to analyze solid, liquid and gas samples [26],it is utilized for identifying unknown materials, determining the quality or consistency of a sample, and determining the amount of components in a mixture[26].

II.4. 3.Scanning Electron Microscopy (SEM):

SEM is a type of microscope that produces high-resolution pictures of surface topography. Its acceleration voltage parameter is between 0.5 and 30.0 kV, and its magnification range is between 5 and 300,000 times[27].This microscope provides surface properties (chemical composition, electrical conductivity) (Paul et al., 2012)[28].

Figure II.13 displays the JEOL JSM-6060LV Low Vacuum Scanning Electron Microscope that was utilized to image the materials.

Figure II.13.Scanning Electron Microscopy (SEM).

II.4.4.Energy dispersive X-ray spectroscopy (EDS)

The analytical method known as energy dispersive X-ray spectroscopy (EDS) is employed to analyze the elements of nanoparticles and nanomaterials. It is an essential component of both transmission electron microscopy (TEM) and scanning electron microscopy (SEM)[29].EDS characterizes the elemental composition of a component by using Xray emissions[30]. A schematic of an EDS system is offered in figure (II.14).

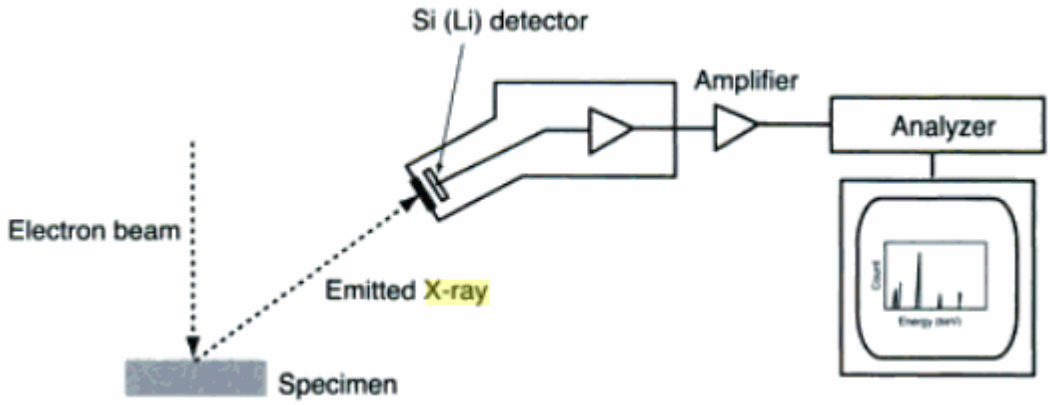

Figure II.14.Schematic diagram of an energy dispersive X-ray spectroscopy system.

II.4. 5.Optical spectrophotometry (Ultraviolet-visible Spectroscopy)

Optical spectrophotometry is a non-destructive technique used to determine material optical properties. It uses transmittance measurements with wavelengths between 300 nm and 2000 nm. Ultraviolet-visible spectroscopy focuses on photon spectroscopy in the ultraviolet and visible regions, using the Beer-Lambert law for quantitative concentration determination.

In UV-VIS-NIR Spectroscopy, the following principle is involved: When a monochromatic light beam passes through a homogeneous medium of an absorbing substance, the rate at which the intensity of the radiation decreases with respect to the thickness of the absorbing medium is directly proportional to the intensity of incident radiation and the medium's concentration (figure II.15):

$$I = I_0 e^{-\alpha d} \qquad \text{(II. 6)}$$

Where d is the film thickness, α is the absorption coefficient, and I_0 and I are the incident and transmitted beam intensities, respectively.

The absorption coefficient (α) can be calculated using the following expression:

$$\alpha = \frac{1}{d} ln \frac{100}{T(\%)} \qquad \text{(II. 7)}$$

Where $T(\%)$ is the transmittance (quantity of the transmitted light), and can be directly measured by[31]:

$$T(\%) = \frac{I}{I_0} \times 100 \qquad \text{(II. 8)}$$

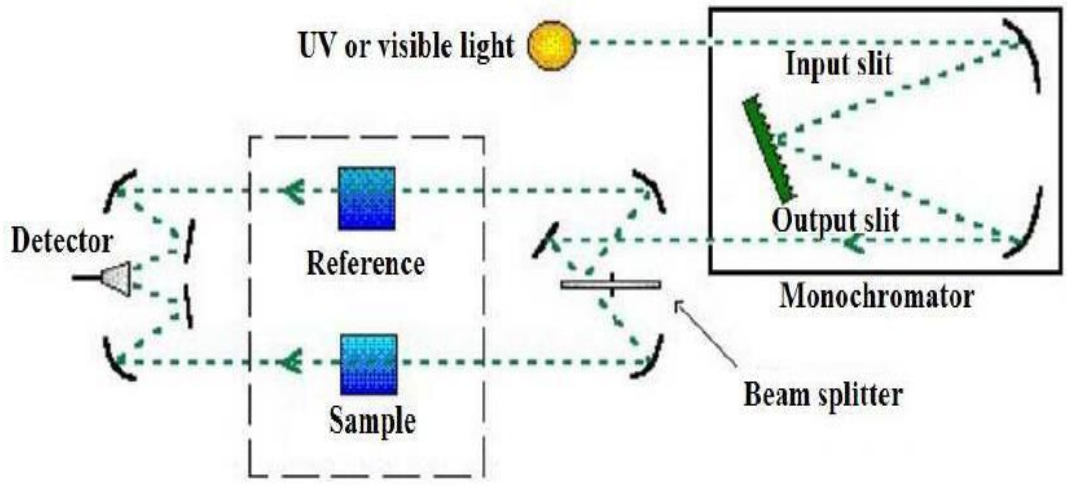

Figure II.15.Schematic representation of constituent elements of a Spectrophotometer UV-VIS-NIR[22, 32].

- **Optical bad gap Eg :**

Electronic transitions between wide states of band-to-band cause absorption at high energies. Tauc law is typically used to describe it[33]:

$$(\alpha h\nu)^n = \mathrm{A}\left(\mathrm{h}\nu - \mathrm{E_g}\right) \qquad \text{(II. 9)}$$

Where E_g is the optical gap and $h\nu$ is the photon energy. The integers n and A define the optical type of transition, where n can be either 2 or 1/2, where 2 or 1/2 denotes permitted direct transitions or authorized indirect transitions, respectively. The curves $(\alpha h\nu)^2 = f\ (h\nu)$ will be plotted in order to ascertain the type of transition from the films produced in this investigation[34]. We can obtain Egvalue as it showing in figure II.16.

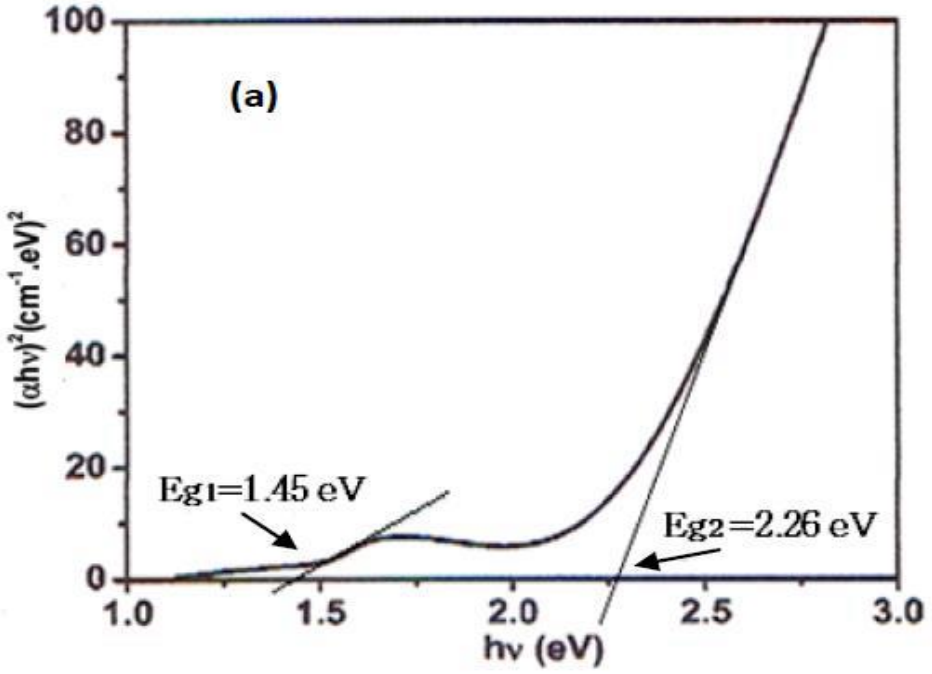

Figure. II.16. Curve represent the function $(\alpha h\upsilon)2=f(h\upsilon)$[16].

II.4. 6.Four-point probe resistivity measurements

Four-point probe measurements involve four probes spaced along the sample's surface, measuring voltage across the inner probes. High-impedance voltmeters minimize contact resistance by forcing current through the outer probes.

$$V_2 = \frac{\rho I}{2\pi}.\left(\frac{1}{S_1} - \frac{1}{S_2 + S_3}\right) \qquad (\text{II. } 10)$$

$$V_3 = \frac{\rho I}{2\pi}.\left(\frac{1}{S_1 + S_2} - \frac{1}{S_3}\right) \qquad (\text{II. } 11)$$

Then, by measuring $V=V_2-V_3$, the voltage drops between probes 2and 3, and the current I through probes1 and 4, the resistivity can be determined using for equations(10) and (11) as:

$$\rho = \frac{2\pi V/I}{\left(\frac{1}{S_1} + \frac{1}{S_2} - \frac{1}{S_2+S_3} - \frac{1}{S_1+S_2}\right)} \qquad (\text{II. } 12)$$

Thus, a direct measurement of the resistivity can be made using a high-impedance voltmeter and a current source. When the probe spacing are equal ($S1=S2=S3=S$),which is the most practical case, then equation(17) becomes:

$$\rho = 2\pi S.\frac{V}{I} \text{(II. 13)}$$

Equations(12) and (13) are only valid for semi-infinite samples with large thickness and surface, and probe locations far from boundaries. Correction factor f is often needed to account for finite thickness and surface. Further, for epitaxial layers, f must also consider the nature of the substrate-whether it is a conductor or an insulator. Thus, equation (II. 14) becomes:

$$\rho = 2\pi S.\frac{V}{I}.f \text{(II. 14)}$$

For a thin semiconductor wafer or thin semiconducting layer deposited on an insulating substrate, and for the condition $t<S2/$, which represents most practical cases because the probe spacing S is usually on the order of a millimeter, then the correction factor due to the thickness is:

$$f = \frac{t/S}{2ln2} \text{(II. 15)}$$

So that:

$$\rho = 4.532.t.\frac{V}{I} \text{(II. 16)}$$

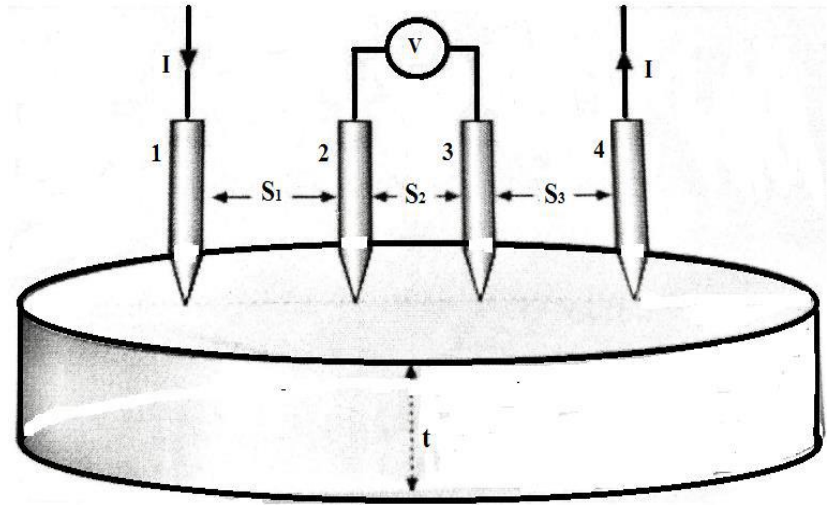

Figure II.17.Linear four-point probe configuration[35].

II.5.Conclusion

Techniques for thin film preparation are the focus of this chapter. Therefore, we made an effort to provide a thorough explanation of the spray pyrolysis method. Because of its ease of usage, spray pyrolysis technology is also the most used technique for depositing metals, alloys, and many chemicals. It works well and is reasonably priced. The various characterisation methods used to examine and measure the various optical, structural, morphological, and electrical characteristics of the resulting films were covered in the second section of this chapter.

References

[1] M. Ohring, Materials science of thin films: depositon and structure, 2nd Edition, October 15, (2001), Academic press.

[2] U. Rau, M. Scmidt, Thin Solid Films, 387, (2001), 141

[3] L.I. Maissel, M.H. Francombe, An introduction to thin films, CRC Press1973.

[4] S.K. Ghandhi, VLSI fabrication principles: silicon and gallium arsenide, John Wiley & Sons1994.

[5] M.C. Sharma, B. Tripathi, S. Kumar, S. Srivastava, Y. Vijay, Low cost CuInSe2 thin films production by stacked elemental layers process for large area fabrication of solar cell application, Materials Chemistry and Physics 131 (2012) 600-604.

[6] N. Xu, S.E. Huq, Novel cold cathode materials and applications, Materials Science and Engineering: R: Reports 48 (2005) 47-189.

[7] J. Singh, Physics of Semiconductors and their Heterostructures, (No Title) (1993).

[8] R.K. Bhakta, Rational development of precursors for MOCVD of TiO2: precursor chemistry, thin film deposition, mechanistic studies, Bochum, Univ., Diss., 2005.

[9] L. Isac, A. Duta, A. Kriza, S. Manolache, M. Nanu, Copper sulfides obtained by spray pyrolysis—possible absorbers in solid-state solar cells, Thin Solid Films 515 (2007) 5755-5758.

[10] M. Krunks, O. Bijakina, V. Mikli, H. Rebane, T. Varema, M. Altosaar, E. Mellikov, Sprayed CuInS2 thin films for solar cells: The effect of solution composition and post-deposition treatments, Solar energy materials and solar cells 69 (2001) 93-98.

[11] P.S. Patil, Versatility of chemical spray pyrolysis technique, Materials Chemistry and physics 59 (1999) 185-198.

[12] S. Oktik, G. Russell, A. Brinkman, Properties of ZnO layers deposited by “photo-assisted” spray pyrolysis, Journal of crystal growth 159 (1996) 195-199.

[13] G. Slewah, Study of Electrical and Optical Properties of Thin Film of CdS and CdS: In Prepared by Spray Pyrolysis Technology, M. Sc. Thesis, College of Sciences, University of Basrah, 1990.

[14] I.R. Agool, H.M. Mohammed, S.M. Abd Al Hussan, Synthesis, Characterization and Optoelectronic Properties of Solar Cells Device for Vacuum Thermally Evaporated Pure and Gallium Doped CdSe Thin Films, IOP Conference Series: Earth and Environmental Science, IOP Publishing, 2021, pp. 012086.

[15] R. MESSEMCHE, Elaboration and characterization of undoped and doped titanium dioxide thin layers by sol gel (spin coating) for photocatalytic applications, 2021.

[16] Y. Benkheta, Elaboration and characterization of thin layers of zinc oxide (ZnO) deposited by ultrasonic spray for photovoltaic and optoelectronic applications, University Mohamed Khider of Biskra, 2019.

[17] J. Venables, Introduction to surface and thin film processes, Cambridge university press2000.

[18] A. Pimpinelli, J. Villain, Physics of crystal growth, 1999.

[19] L.B. Freund, S. Suresh, Thin film materials: stress, defect formation and surface evolution, Cambridge university press2004.

[20] K.J. Bishop, C.E. Wilmer, S. Soh, B.A. Grzybowski, Nanoscale forces and their uses in self-assembly, small 5 (2009) 1600-1630.

[21] I.-C. Robin, Solid State Material Systems for Light Emission and Light Detection, Université Joseph-Fourier-Grenoble I, 2011.

[22] N. Kouidri, Contribution à l'étude de couches minces d'oxydes transparents conducteurs à base de zinc et cobalt par spray pneumatique, University of Mohamed Khider, BISKRA, 2019.

[23] H. Yilmazer, M. Niinomi, T. Akahori, M. Nakai, Y. Todaka, Effect of high–pressure torsion processing on microstructure and mechanical properties of a novel biomedical β–type Ti–29Nb–13Ta–4.6 Zr after cold rolling, International Journal of Microstructure and Materials Properties 7 (2012) 168-186.

[24] A.K. Zak, W.A. Majid, M.E. Abrishami, R. Yousefi, X-ray analysis of ZnO nanoparticles by Williamson–Hall and size–strain plot methods, Solid State Sciences 13 (2011) 251-256.

[25] M. Dahnoun, Preparation and characterizationof Titanium dioxide and Zinc oxide thin films via Sol-Gel (spin coating) technique for optoelectronicapplications, University Mohamed Khider Biskra, 2020.

[26] C.E. Smith, S. Frank, Handbook of instrumental techniques for analytical chemistry, Frank, S., ed, 1997.

[27] V.O.R. Baerga, Laser shockwave sintering of micro and nanoscale powders of yttria-stabilized zirconia, Iowa State University2010.

[28] A.R. Barron, Physical methods in chemistry and nano science, (2015).

[29] M. He, T.-M. Lu, Metal-dielectric interfaces in gigascale electronics: thermal and electrical stability, Springer Science & Business Media2012.

[30] A. Naranjo, Plastics testing and characterization: Industrial applications, Hanser Verlag2008.

[31] A. Yahia, Optimization of indium oxide thin films properties prepared by sol gel spin coating process for optoelectronic applications, University Mohamed Khider of Biskra, 2020.

[32] A. Jrad, Elaboration, Characterization and Design of ZnS Thin Films for Optoelectronic Applications, 2017.

[33] J. Tauc, R. Grigorovici, A. Vancu, Optical properties and electronic structure of amorphous germanium, physica status solidi (b) 15 (1966) 627-637.

[34] Z. Bencharef, A. Chala, R. Messemeche, Y. Benkhetta, The physical properties of spinel cubic Co 3O 4 thin films prepared by a PSM, Main Group Chemistry 21 (2022) 329-340.

[35] A. Bouhdjer, Study of Thin Layers of Indium Oxide (In2O3) Elaborated by Chemical Means, Université Mohamed Khider-Biskra, 2016.

Chapter III

The Effect of substrate temperature on the properties of CO_3O_4 thin films

III.1. Introduction

This study aims to create cobalt oxide layers using the spray pyrolysis approach. During this process, a cobalt chloride ($COCl_2.6H_2O$) aqueous solution is sprayed onto preheated glass substrate at temperatures in the range of 250°C to 400°C. To evaluate and characterize the structural, optical, morphological, and electrical characteristics of the obtained samples, several techniques were employed, including X-ray diffraction (XRD), scanning electron microscopy, optical absorption measurements, and the four-point probe process. Structural analysis of the X-ray diffraction displayed that Co_3O_4 developed in a controlled manner, forming a cubic structure. The films were found to grow preferentially along the (111) or (331) directions depending on the temperature of the substrate. Furthermore, XRD analysis clearly indicated that the average Co_3O_4 grain size increased with higher substrate temperatures. Observations of the surface morphology indicated some overgrowth of cobalt oxide clusters alongside the presence of nanocrystalline grains, and small spherical particles are well distributed at both substrate temperatures of 250°C and 400°C.Optical measurements revealed a direct bandgap values ranging from 1.46 to 2.05 eV.

The highest conductivity measured was 1.29 S/cm at a substrate temperature of 400°C.It's observed that as the substrate temperature rises, the electric conductivity of the prepared samples also increases.

III.2. Experimental details

III.2.1. Films Preparation

An aqueous sol of 0.05 M was produced by dissolving cobalt chloride hexahydrate in demineralized water, followed by stirring by a magnetic stirrer for 20 min to attain a clear and uniform solution. The obtained layers were found to be deep gray with a uniform crystalline structure. The current density values of the resulting layers were found to be equivalent to those of Co_3O_4 layers using the thermal breakdown process[1].As a result, a homogeneous and highly adhering cobalt oxide layer formed. The following is the potential chemical reaction that occurs:

$$3COCl_2 + 2H_2O + O_2 \xrightarrow{\Delta} CO_3O_4 \downarrow + 3Cl_2 \uparrow + 2H_2 \uparrow \quad \text{(III. 1)}$$

Thin, adhering coatings of cobalt oxide formed on the glass substrate. These films were darkly tinted when deposited. These thin cobalt oxide films were then used for further characterization. For the estimation of the film thickness, the weight approach (microbalance) was used, which calculates the film thickness using the following formula[2].

$$e = \frac{m}{\rho * S} \quad \text{(III. 2)}$$

Wherein e is the thickness of the film, m the mass, S the surface, and ρ the density (ρ=6.10 g/cm3)[3].

III.2.2. Characterization Techniques

For the evaluation and characterization of Co_3O_4 thin films that were prepared at 250°C, 300°C, 350°C and 400°C, the following characterizations were used:X-ray diffraction analysis (a Philips PW-3710 diffractometer)was used in the 2θ range from 10° to 80° using a Cu-Kα target with a wavelength of λ=0.15418 nm at room temperatureto derive the phase compositions of the films. The surface morphology was evaluatedfor basic evaluation utilizing a scanning electron microscope system. The SEM was instrumentedwith an energy dispersionspectrometer.Using an infrared transmission spectrometer, the types of chemical bonding identified in the materials were between 400 and 4000 cm^{-1}. For the wavelength range of 300 to 900 nm, the transmittance was measured with a two-beam UV-vis spectrophotometer (UV-3101; Shimadzu), while the electrical conductivity and specific resistance of the Co_3O_4 films were determined using the four-electrode technique.

III.3. Results and Discussion

III.3.1. X-Ray Diffraction

Fig III. 1 displays the XRD pattern of the deposited Co_3O_4layersat a variety of substrate temperatures. The films crystallography is good, exhibiting five main peaks with 2θ values of about 19, 31, 37, 44, and 60◦, which can perfectly match the (1 1 1), (22 0), (3 3 1),

(4 0 0), and (5 1 1) planes of the Co_3O_4cubic structure, respectively. They are verified by comparing the 2θ peak positions of the XRD patterns of the layers with the reference X-ray diffraction data file (JCDPS card #01-074-2120). The films were found to grow preferentially along the (111) or (331) directions depending on the temperature of the substrate.

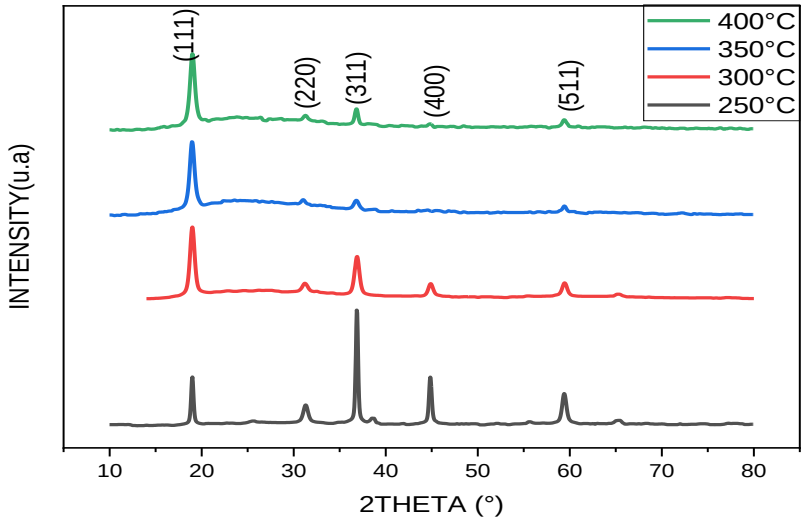

Figure III.1. XRD spectra of Cobalt Oxide at various temperatures.

Table III.1 presents a summary of the interplanar distances derived from the XRD profiles. The observed variations in these interplanar distances denote the forming of a strained lattice, accompanied by the development of micro-stress as the films crystallize[4]. The interplanar spacing ($\mathbf{d_{hkl}}$) was estimated utilizing the Bragg equation[5, 6]:

$$2d_{hkl}\sin\theta = n\lambda \qquad \text{(III. 3)}$$

Whereas, $\boldsymbol{n}$ is the order of diffraction, (**hkl**) miller indices, $\boldsymbol{\lambda}$is the X-ray wavelength,$\boldsymbol{d_{hkl}}$the inter-planar spacing, and the Bragg angel isθ.

Table III.1. Inter-planar distances (d_{hkl}) of Co_3O_4samples for various temperatures.

Substrate temperature	(a): 250°C	(b): 300°C	(c): 350°C	(d): 400°C
d_{111}(Å)	4.6723	4.6725	4.6783	4.6691
d_{220}(Å)	2.8573	2.8652	2.8815	2.8581
d_{311}(Å)	2.4381	2.4369	2.4414	2.4407
d_{400}(Å)	2.0211	2.0192	2.03221	2.0232
d_{511}(Å)	1.5556	1.5545	1.5548	1.5558

It is well known that for the cubic structures (a=b=c) can be calculated using the following relation[7]:

$$\frac{1}{d_{hkl}^2} = \left(\frac{h^2 + k^2 + l^2}{a^2}\right) \text{(III. 4)}$$

Whereas: (**h k l**) are the Miller plane indices and **a** is lattice constant.

The volume of unit cell **V** was estimated as follow:

$$V = a^3 \text{(III. 5)}$$

Table III.2. The parameters (a, b and c) and volume of the unit cell Vvalues comparing to the data listed onJCPDS card #**2120-074-01**.

Substrate temperature	Latice parameters			Unit cell volume (10*6 pm*3)			Δa(Å)	ΔV(10*6 pm*3))
	Our data		JCPDS card	Our data		JCPDS card		
	a=b =c(Å)		a=b =c(Å)	$V = a^3$		$V = a^3$		
(a): 250°C	8.0856		8.0840	528.621		528.30	0.0016	0.3214
(b): 300°C	8.0867		8.0840	528.846		528.30	0.0028	0.5457
(c): 350°C	8.1117		8.0840	533.774		528.30	0.0277	5.4737
(d): 400°C	8.0885		8.0840	529.194		528.30	0.0046	0.8944

Table III.2indicates that our estimated values closely match the data listed on JCPDS card #01-074-2120.The XRD data were used to make an estimate of the lattice expansion of the nanocrystals. The lattice parameter has been calculated to be 8.084Å. A slight lattice contraction was observed in the Co_3O_4, which may be due to the lattice strain caused by the high surface-to-volume fraction. It is suggested that the size reduction contributes to this lattice contraction[4].

Moreover, the unit cell volume increases with the rise in the annealing temperature, owing to an improved crystal growth in the films.

The crystallite size $\boldsymbol{D_{hkl}}$, the dislocation density **δ** and the stresses **ε** in Co_3O_4 films have been determined from X-ray diffraction spectra. Firstly, The crystallite sizes ($\boldsymbol{D_{hkl}}$) were calculated using Scherer formula[8, 9]:

$$D_{hkl} = \frac{k\lambda}{\beta_{1/2}\cos\theta} \text{ (III. 6)}$$

Where: (**k** = 0.90), **β1/2** the FWHM of the diffraction peak, **θ** the Bragg angle and **λ**= 1.5406 Å is the X-ray radiation wavelength.

Table III.*3.The crystallites size (*$\boldsymbol{D_{hkl}}$*) of* Co_3O_4 thin films at a variety of temperatures.

Substrate temperature	(a): 250°C	(b): 300°C	(c): 350°C	(d):400°C
D_{111}(nm)	13.6424	13.6424	13.6419	13.6421
D_{220}(nm)	13.9731	13.9701	16.7567	13.9728
D_{311}(nm)	14.1822	14.1829	14.1801	21.2708
D_{400}(nm)	14.5543	14.5566	21.8113	21.8276
D_{511}(nm)	18.5853	15.4914	23.2355	23.2309

Second, the length of dislocation lines per unit volume is the dislocation density ($\boldsymbol{\delta_{hkl}}$), which is a measure of the amount of defects in a crystal.We have used the following expression in order to calculate this value[6, 10]:

$$\delta_{hkl} = \frac{1}{D_{hkl}^2} \text{(III. 7)}$$

Table III.4.The *dislocation density* $\boldsymbol{\delta_{hkl}}$*of* Co_3O_4 *thin films at a variety of substrate temperature*.

Substrate temperature	(a): 250°C	(b): 300°C	(c): 350°C	(d):400°C
δ_{111}(10^{15} lines/ m^2)	5.3729	5.3734	5.3729	5.3728
δ_{220} (10^{15} lines/ m^2)	5.1217	3.5614	5.1239	5.1219
δ_{311} (10^{15} lines/ m^2)	4.9718	4.9733	4.9713	2.2102
δ_{400} (10^{15} lines/ m^2)	4.7208	2.1020	4.7193	2.0989
δ_{511} (10^{15} lines/ m^2)	2.8951	1.8522	4.1669	1.8529

Finally, the microstrain ($\boldsymbol{\varepsilon_{hkl}}$), was evaluatedby the use of the following expression[5]:

$$\varepsilon_{hkl} = \frac{\beta_{1/2}\ \cos\theta}{4} \text{(III. 8)}$$

Table III. 5. Microstress values (ε_{hkl}) of Co_3O_4 films at various substrate temperature.

Substrate temperature	(a): 250°C	(b): 300°C	(c): 350°C	(d):400°C
ε_{111} ($line^{-2}$ .m^{-4})	0.0025	0.0025	0.0025	0.0025
ε_{022} ($line^{-2}$ .m^{-4})	0.0025	0.0025	0.0020	0.0024
ε_{113} ($line^{-2}$ .m^{-4})	0.0024	0.0024	0.0024	0.0016
ε_{004} ($line^{-2}$ .m^{-4})	0.0023	0.0023	0.0015	0.0015
ε_{115}($line^{-2}$ .m^{-4})	0.0018	0.0022	0.0014	0.0014

Otherwise, the texture coefficient ($\mathbf{TC_{hkl}}$), is provided as the ratio of the intensity of each orientation ($\mathbf{I_{hkl}}$) to the corresponding JCPDS card intensity ($\mathbf{I_{0_{hkl}}}$), The coefficient($\mathbf{TC_{hkl}}$) also provides information about the probability of growth according to an orientation (hkl). The coefficient ($\mathbf{TC_{hkl}}$) is given through the following equation[11]:

$$\boldsymbol{TC_{hkl} = \frac{I_{hkl}/I_{0_{hkl}}}{N^{-1}(\sum_{i=1}^{n} \frac{I_{hkl}}{I_{0_{hkl}}})}} \qquad \textbf{(III. 9)}$$

where **N** is the quantity of peaks in diffraction.

Table III.6. Texture coefficient (TC_{hkl}) of Co_3O_4 thin films at a variety of substrate temperature.

Substrate temperature	(a): 250°C	(b): 300°C	(c):350°C	(d):400°C
TC_{111}	0.9149	2.3821	3.3959	3.0285
TC_{220}	0.3307	0.1274	0.2356	0.3000
TC_{311}	1.9251	1.3972	0.6481	1.1350
TC_{400}	1.0942	0.5398	0.1046	0.0493
TC_{511}	0.7352	0.5534	0.6157	0.4871

Table. III.6 compiles the $\mathbf{TC_{hkl}}$values that were obtained.As we can see, peak (111) corresponds to the greatest value of the texture coefficient, suggesting that orientation is preferred. Hence, in comparison to the other peaks, peak (111) has the maximum intensity. Most of the crystallites are aligned parallel to the substrate's plane.

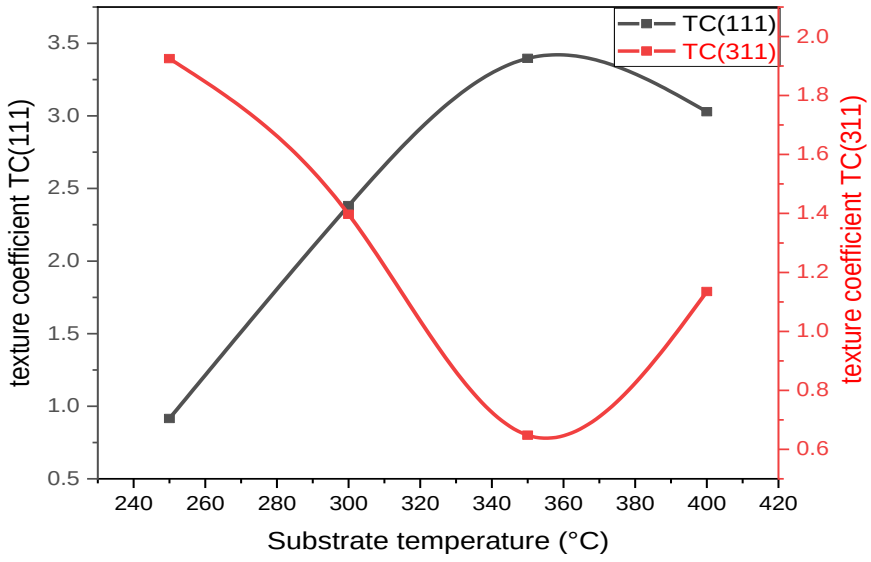

Figure III.2.TC values of Co_3O_4layers vs substrate temperatures.

Figure III.2 shows that as the substrate temperature is raised, the TC values at the (311) peak continuously decrease, while those at the (111) peak increase, the same phenomenon was reported[12], which is attributed to the increasing oxygen density

and decreasing cobalt density in the thin layer. The following formulas[13, 14]can be used to determine the medium value of crystallite size $\prec D \succ$, medium value of microstress $\prec \varepsilon \succ$, and medium value of dislocation density $\prec \delta \succ$ of the layers:

$$\begin{cases} \langle \boldsymbol{D} \rangle = \dfrac{\sum \boldsymbol{TC_{hkl} * D_{hkl}}}{\boldsymbol{n}} (\textbf{III. 10}) \\ \langle \boldsymbol{\varepsilon} \rangle = \dfrac{\sum \boldsymbol{TC_{hkl} * \varepsilon_{hkl}}}{\boldsymbol{n}} (\textbf{III. 11}) \\ \langle \boldsymbol{\delta} \rangle = \dfrac{\sum \boldsymbol{TC_{hkl} * \delta_{hkl}}}{\sum \boldsymbol{TC_{hkl}}} (\textbf{III. 12}) \end{cases}$$

Table III.7. The average values of D, ε and δ of Co_3O_4 thin films at various substrate temperature.

Substrate temperature	$\prec D \succ$ (nm)	$\langle \boldsymbol{\varepsilon} \rangle$(lines^{-2} m^{-4})	$\prec \delta \succ$ (10^{15} lines/m^2)
(a): 250°C	14.7985	0.002365	4.6948
(b): 300°C	14.1052	0.002461	5.0503
(c):350°C	15.2108	0.002357	4.7341
(d): 400°C	16.4089	0.002219	4.2646

The dislocation density and microstrain of the Co_3O_4 films are summarized in Table III.7 and are found to be decreased with the rise of substrate temperature.

III.3.2.SEM & EDS Analysis

Morphological characterization focuses on the surface features and microstructure of thin films, including their roughness, grain size, porosity, and overall texture. Scanning electron microscopy (SEM) is used to observe the surface morphology of spray-depositedCo_3O_4thin layers.

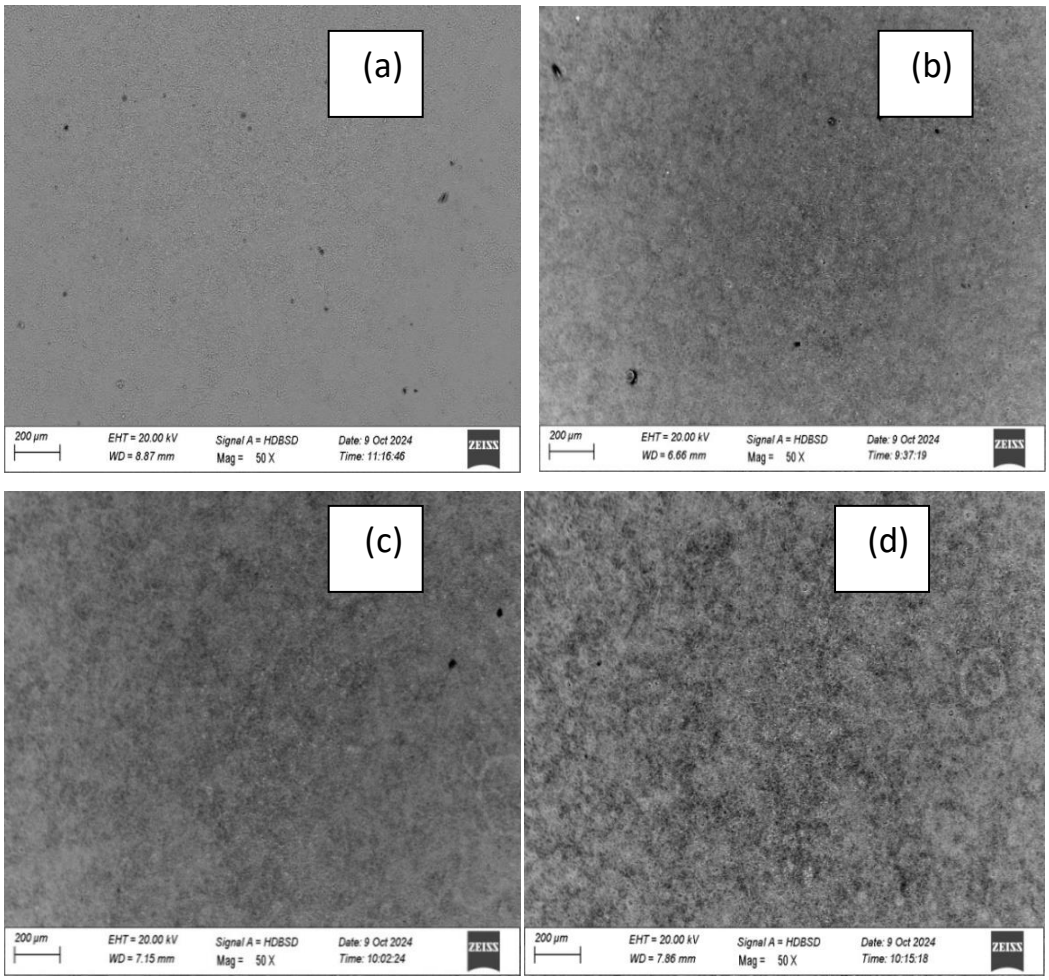

Figure III.3. SEM of Co_3O_4 thin layers fabricated at: (a): 250°C, (b): 300°C, (c): 350°C, and (d): 400°C.

The SEM images of thin layers of cobalt oxide, prepared at various substrate temperatures (250°C - 400°C) are displayed in Figure III.3. The images indicate that small spherical particles are well distributed at both substrate temperatures of 250°C and 400°C. Additionally, Figure III.3 illustrates the spherical structure of the fabricated layers. Furthermore, XRD analysis clearly indicated that the average Co_3O_4 grain size increased with higher substrate temperatures, as shown in Table III.7.

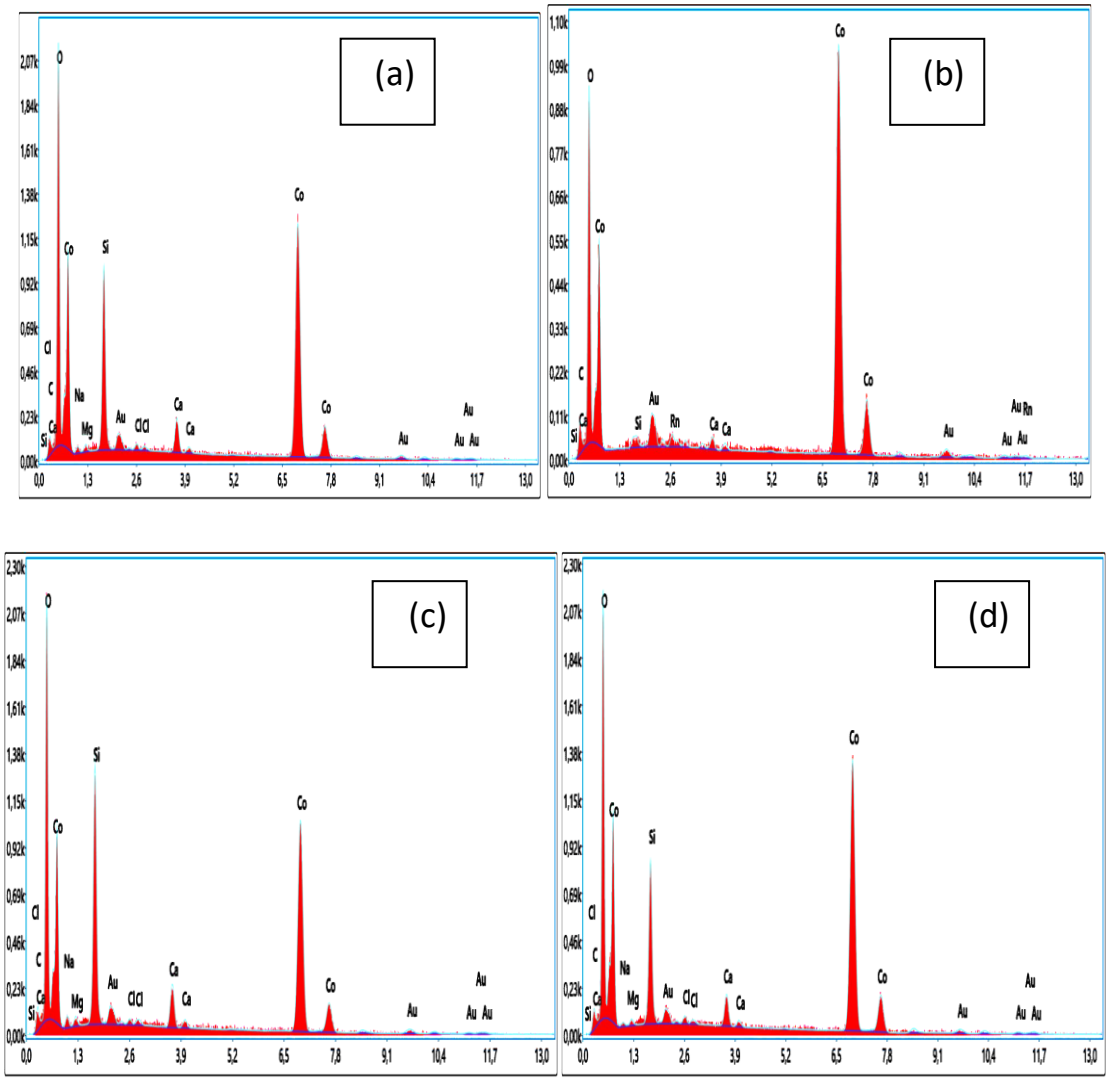

Figure III.4. EDS micrographs of Co_3O_4 thin films prepared with various substrate temperature (a):250°C, (b): 300°C, (c):350 °C and (d): 400°C.

The EDS compositional analysis of Co_3O_4 films is shown in figure III.4. These images prove the existence of Co and O elements in the Co_3O_4 layers at a variety of substrate temperatures. The appearance of silicon and carbon peaks may be due to contamination of the glass substrate. The increase in oxygen content as the substrate temperature increases could be due to the chemisorption of oxygen from the atmospheric air[15].

III.3.3. FTIRAnalysis

The functional group characteristics and purity of the synthesized metal oxide nanoparticles were determined by FTIR spectroscopy.

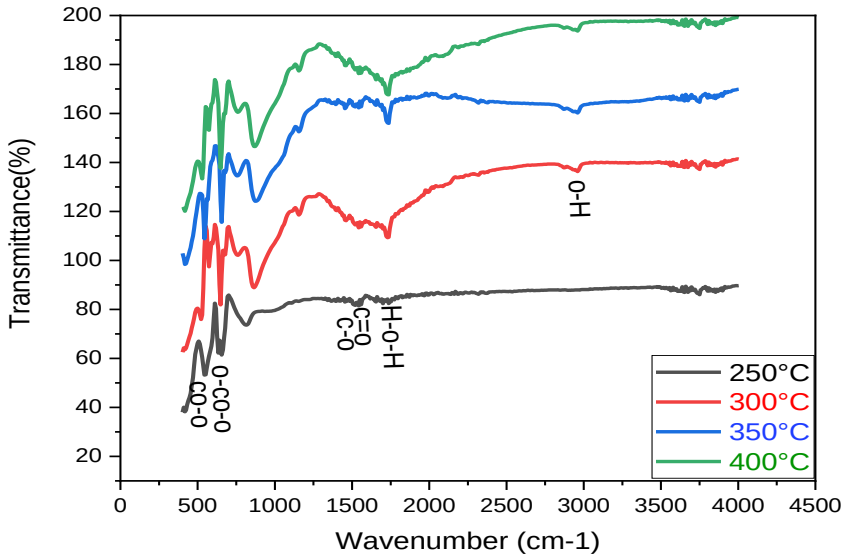

Figure III.5. Transmittance spectra of Cobalt Oxide at various substrate temperature.

From Figure III.5, a large sharp band was observed at 550.95cm^{-1} which ascribes the symmetric stretching to Co-O[16, 17]and at 650.47 cm^{-1} to O-Co-O[18]. These two dips 550.95 cm^{-1} and 650.47 cm^{-1} closely resemble the optical vibrating modes of Co_3O_4[19, 20].Therefore, the existence of some impurities of CoO in the Co_3O_4 thin films may not be neglected. The dip at 1524.62 cm^{-1} was the symmetric stretching because of the existence of C-O and 1575.5 cm^{-1} corresponds to C=O[21]. Whilst bridging vibrations of the O–Co–O and Co–O–Co functionalities are responsible for the peaks at 864.9 and 765.37 cm^{-1}, respectively[22]. The broadband at2959.90 cm^{-1}is assigned to the O-H stretching. The weak IR bands at 1681.6 and1714.3cm^{-1}represent symmetrical and asymmetrical stretching of H-O-H due to moisture adsorption. These OH and H-O-H humidity bands can be viewed because

the sample pellets are exposed to air. This is due to the stretching and vibration of the water molecules[23, 24].

III.3.4. Optical Properties

The optical transmittance for the wavelength range 350-900 nm is used to estimate the optical characteristics such as transmittance and bandgap of Co_3O_4 thin layers.Fig III. 6 illustrates the optical transmission spectrum of the prepared Co_3O_4 layers at temperatures of 250 - 400 °C of the substrate.

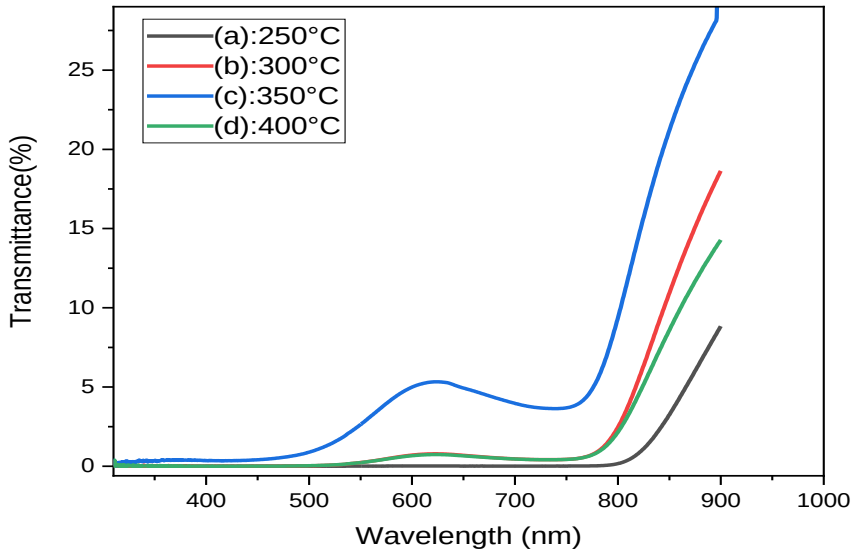

Figure III.6. Transmittance spectra of Cobalt Oxide at various temperatures: (a): 250°C, (b):300°C, (c):350°Cand (d): 400°C.

The maximum transmittance of Co_3O_4 films is in the infrared range (up to 900 nm) with a variation from 8.93% to 28.69% and the visible range exhibits low transmittance. The transmittance spectrum obtained for Co_3O_4 at a variety of temperatures are presented in Figure III.6.We find that transmittance increases with increasing wavelength and also increases with increasing temperature, whereas the film thickness reduces. It is clearly visible due to its deep black hue. This picture also shows that the viewable region has two basic

absorption edges. The average optical transmission of the fabricated layers was determined to be 8.93;18.63;28.69 and 14.28% for the films prepared at the following temperature respectively: 250°C, 300°C, 350°C and 400°C.The absorption coefficient (α) can be obtained from the transmittance and reflectance spectra using the relation[25]:

$$\alpha=1/e \ \ln((1-R)^2/T) \quad (III.13)$$

Whereas: e the layer thickness, T the transmittance, R reflectance.

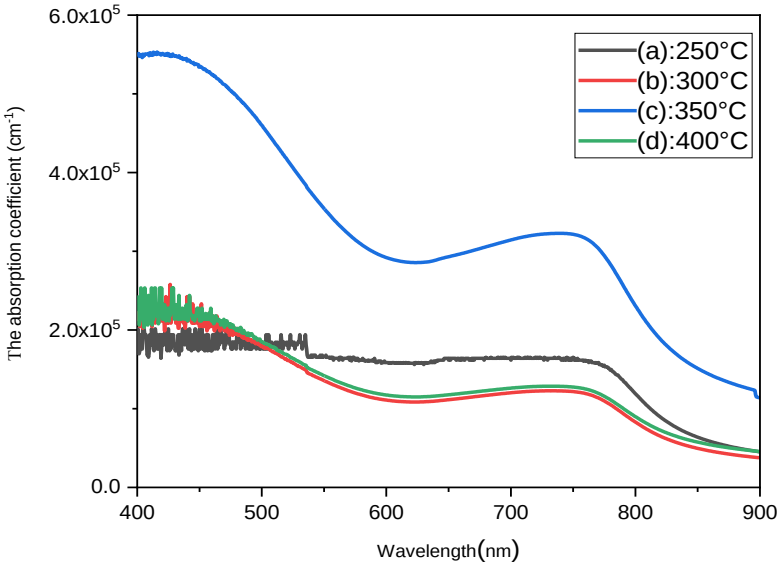

Figure III.7. Development of the absorption coefficient (α) of the Cobalt Oxideat a various temperatures : (a): 250°C, (b):300°C, (c):350°C and (d): 400°C.

The mean value of the absorption coefficient ($\langle\alpha\rangle > 10^5 cm^{-1}$) for the samples also confirms the direct bandgap nature of the samples[26]. The investigated films have an absorption coefficient (α) obeying the following relationship[27]for high photon energies (hν).

$$\alpha h\nu=B(h\nu-Eg)^p \quad (III.14)$$

Whereas: B is a constant; p an integer equal of 1/2 or 2 for direct or indirect transitions, respectively.

In FigIII.7. The variation of the absorption coefficient (α) as a function of wavelength (λ) of preparedCo_3O_4layers is presented. For the different temperatures 250°C, 300°C, 350°C, and 400°C the average absorption coefficient is 16×10^4, 20×10^4, 51×10^4, and $24\times10^4 cm^{-1}$, respectively. The intensity of the strong visible emission rises as the temperature of the substrate increases up to 350 °C and then it is reduced due to the reduced number of oxygen vacancies.

The improved crystal growth of Co_3O_4 films is attributed to higher temperatures, the removal of defects, and a reduction in the number of grain boundaries. In addition, the values of the absorption coefficient are very close to the values found in the literature.

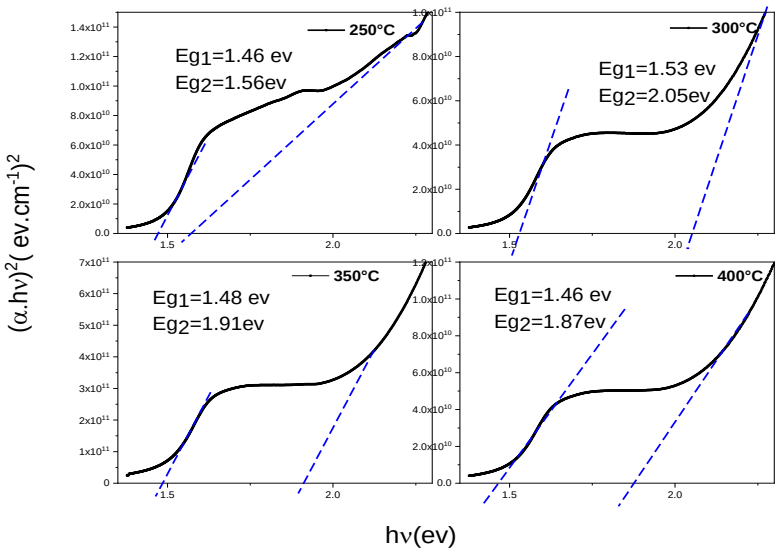

Figure III. 8. Plots of $(ah\nu)^2$against hν of $Co_3O_4$for temperatures :(a): 250°C, (b):300°C, (c):350°C and(d): 400°C.

FigureIII.8 illustrates the graphs of $(\alpha h\nu)^2$against the energy (hν) for Co_3O_4layer fabricated at different temperatures: 250°C, 300°C, 350°C and 400°C.Two straight lines were observed. This indicates the existence of two direct band gap values of cobalt oxide, which is consistent with the literature.The bandgaps (Eg) of the deposited layers ranged from1.46 to

1.53 eV for the lower energies and 1.56 to 2.05 eV for the higher energies, which are in accordance with the reported band structures of Co_3O_4[28, 29],recommended that the $O^{-II} \rightarrow CO^{III}$charge transfer mechanism (basic optical band gap energy or valence to conduction band excitation) be linked to the larger bandgap (2.05 eV). Co(III) centers in Co_3O_4 result in the formation of a sub-band inside the energy gap. Therefore, the $O^{-II} \rightarrow CO^{III}$charge transfer (with CO located beneath the conduction band) can be linked to the 1.47 eV bandgap[30, 31].

The values of Eg_1 and Eg_2 vary from 1.46 to 1.53 eV and 1.56 to 2.05 eV respectively. These values are in agreement with the literature[32].

III.3.5. Electrical Properties

The electrical conductivity and resistivity of Co_3O_4 films are measured using the four-probe electrical method. The resistivity of Co_3O_4layers is estimated using the following expression:

$$\rho = \frac{R.A}{l} \qquad (III.15)$$

In this context, **ρ** represents resistivity, **R** stands for resistance, A is the cross-sectional area, and **l** denotes the distance between the probes. Conductivity is calculated using the formula σ = 1/ρ, where **σ** stands for conductivity. Values for resistivity and conductivity are determined at various working temperatures and are presented in Table III.8.

Table III.8. Resistivity and conductivity of Co_3O_4layers at various substrate temperature.

T(°c)	R_{SHEET}(ohm)	l(nm)	ρ(ohm.cm)	$\sigma(ohm.cm)^{-1}$
250	1.38E+05	4.27E-07	5.89E+00	0.17
300	5.04E+07	5.37E-05	3.05E+03	3.28E-04
350	9.49E+04	1.03E-07	9.74E-01	1.03E+00
400	1.73E+04	4.46E-05	7.35E-01	1.29

.

The data presented in Table III. 8 indicate that conductivity rises with higher substrate temperatures (250°C, 300°C, 350°C, and 400°C). This rise in conductivity can be attributed to the growing size of the crystallites. As the crystallite size increases, the gaps between them decrease, leading to improved conductivity.At this level, complete bonds exist between the atoms, resulting in a decrease in the number of defects that trap free charge. These findings align with the researchers' conclusions[28, 29]. The results presented in Figure III.8 are corroborated by the findings from the DRX and EDS analyses. As the substrate temperature rises, the conductivity of the prepared samples also increases. This trend indicates a developing semi-conducting nature in the material[33]. By developing more grains and achieving good crystallinity in the film prepared at 400°C, the maximum room temperature conductivity (1.29 S/cm) is observed.

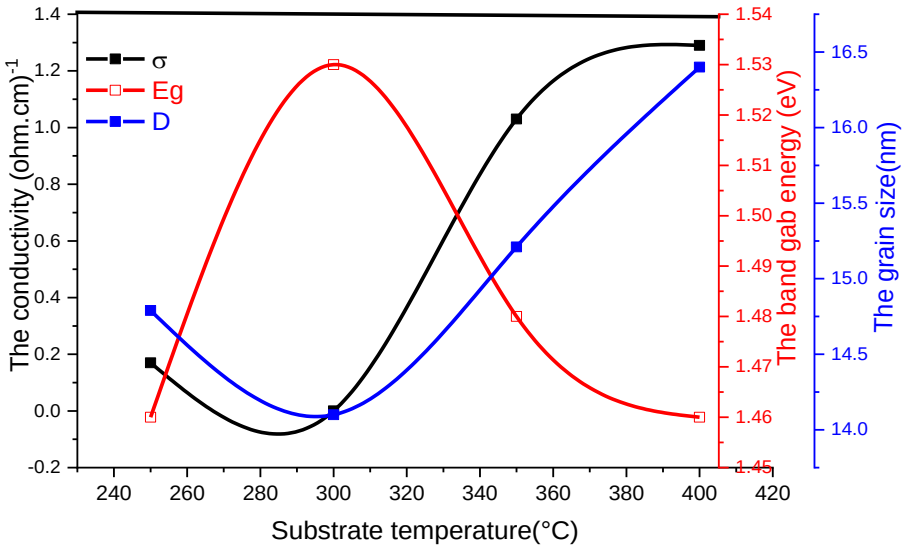

Figure III. 9. Variation of the opticalgap (E_g), grain size (D) and conductivity as a function of the various temperature of the Cobalt Oxide films.

III.4.Conclusion

The morphological, optical, and structural characteristics of Cobalt Oxide (Co_3O_4) layers made by spray pyrolysis process and placed on substrates of glass were the main focus of this study. The Co_3O_4 layers formed are monophase and polycrystalline, with a cubic structure and intense peak at the (111) plane, according to the diffraction of X-ray data except for T=250°C.It was found that the crystallite sizes were enlarged from 14.1052 to 16.4089 nm as the substrate temperature rose, and the transmittance of the produced layers was also improved. The bandgap widths vary slightly with the substrate temperature and are in the interval of 1.46-1.53 eV for the low-energy domain and 1.56-2.05 eV for the high-energy domain. The optical absorption coefficient is in the order of $10^5 cm^{-1}$. Electrical conductivity rises from 3.28× 10−4 to 1.29 (Ω cm) $^{-1}$ for Co_3O_4layers.The successful fabrication of a high-quality cobalt oxide layer on glass substrates using a manual spray pyrolysis process at temperatures in the range of 250 - 400 °C has beenaccomplished.

Ultimately, the current study made it abundantly evident that the substrate temperature is a crucial factor that has a big impact on the physical characteristics of Co_3O_4 films. According to these characteristics, Co_3O_4 films which are produced particularly at temperatures between 350°C and 400°C can be employed for electrochemical applications, as an absorber layer for gas sensing and solar applications.

Future research could focus on optimizing the deposition process and adjusting the parameters by doping the films with various chemical elements to produce high-quality, miniaturized films that can be integrated into device architectures.

References

[1] E. Laouini, M. Hamdani, M. Pereira, J. Douch, M. Mendonça, Y. Berghoute, R. Singh, Preparation and electrochemical characterization of spinel type Fe–Co_3O_4 thin film electrodes in alkaline medium, international journal of hydrogen energy 33 (2008) 4936-4944.
[2] L. Kathwate, G. Umadevi, P. Kulal, P. Nagaraju, D. Dubal, A. Nanjundan, V. Mote, Ammonia gas sensing properties of Al doped ZnO thin films, Sensors and Actuators A: Physical 313 (2020) 112193.
[3] M. Ahmed, A. Tawfik, M. El-Nimr, A. El-Hasab, Physical and electrical properties of Ni-Al ferrites, Journal of materials science letters 10 (1991) 549-551.
[4] Q. Jiang, L. Liang, D. Zhao, Lattice contraction and surface stress of fcc nanocrystals, The Journal of Physical Chemistry B 105 (2001) 6275-6277.
[5] A. Beggas, B. Benhaoua, A. Attaf, M. Aida, Growth study of CdS thin films deposited by chemical bath, Optik 127 (2016) 8423-8430.
[6] A. Gahtar, A. Benali, S. Benramache, C. Zaouche, Effect of annealing time on the structural, morphological, optical and electrical properties of NiS thin films, Chalcogenide Letters 19 (2022).
[7] J. Pal, P. Chauhan, Study of physical properties of cobalt oxide (Co_3O_4) nanocrystals, Materials characterization 61 (2010) 575-579.
[8] M. Pan, F. Lu, Y. Zhu, G. Huang, J. Yin, F. Huang, G. Chen, Z. Chen, Thermodynamic, exergoeconomic and multi-objective optimization analysis of new ORC and heat pump system for waste heat recovery in waste-to-energy combined heat and power plant, Energy Conversion and Management 222 (2020) 113200.
[9] M. Salavati-Niasari, A. Khansari, F. Davar, Synthesis and characterization of cobalt oxide nanoparticles by thermal treatment process, Inorganica Chimica Acta 362 (2009) 4937-4942.
[10] S. Marouf, A. Beniaiche, H. Guessas, A. Azizi, Morphological, structural and optical properties of ZnO thin films deposited by dip coating method, Materials Research 20 (2016) 88-95.
[11] V. Kumar, H. Sharma, S.K. Singh, S. Kumar, A. Vij, Enhanced near-band edge emission in pulsed laser deposited ZnO/c-sapphire nanocrystalline thin films, Applied Physics A 125 (2019) 1-7.
[12] M. Manickam, V. Ponnuswamy, C. Sankar, R. Mariappan, R. Suresh, Influence of substrate temperature on the properties of cobalt oxide thin films prepared by nebulizer spray pyrolysis (NSP) technique, Silicon 8 (2016) 351-360.

[13] F. Khan, W. Khan, S.-D. Kim, High-performance ultraviolet light detection using nano-scale-fin isolation AlGaN/GaN heterostructures with ZnO nanorods, Nanomaterials 9 (2019) 440.
[14] D. Souad, S. Benramache, A. Ammari, A. Gahtar, Effect of substrate temperature on the structural, optical, electrical, and morphological properties of zinc oxide thin films, Iranian Journal of Physics Research 22 (2022) 185-191.
[15] C.R. Dhas, R. Venkatesh, R. Sivakumar, A.M.E. Raj, C. Sanjeeviraja, Effect of solution molarity on optical dispersion energy parameters and electrochromic performance of Co3O4 films, Optical Materials 72 (2017) 717-729.
[16] J. Feng, H.C. Zeng, Size-controlled growth of Co3O4 nanocubes, Chemistry of materials 15 (2003) 2829-2835.
[17] G. Rathika, V. Suba, D.S. Lakshmi, R. Rani, Exploring the Biosynthesized Metal Nanoparticles for their Catalytic Degradation of Toxic Water Wastes and Antimicrobial Potential, Journal of Inorganic and Organometallic Polymers and Materials 32 (2022) 3153-3169.
[18] S.-H. Wu, D.-H. Chen, Synthesis and characterization of nickel nanoparticles by hydrazine reduction in ethylene glycol, Journal of Colloid and Interface Science 259 (2003) 282-286.
[19] P. Nkeng, J.-F. Koenig, J. Gautier, P. Chartier, G. Poillerat, Enhancement of surface areas of Co3O4 and NiCo2O4 electrocatalysts prepared by spray pyrolysis, Journal of Electroanalytical Chemistry 402 (1996) 81-89.
[20] M. Pudukudy, Z. Yaakob, Sol-gel synthesis, characterisation, and photocatalytic activity of porous spinel Co 3 O 4 nanosheets, Chemical Papers 68 (2014) 1087-1096.
[21] S. Alias, A. Ismail, A. Mohamad, Effect of pH on ZnO nanoparticle properties synthesized by sol–gel centrifugation, Journal of Alloys and Compounds 499 (2010) 231-237.
[22] A.M. Amanulla, S.J. Shahina, R. Sundaram, C.M. Magdalane, K. Kaviyarasu, D. Letsholathebe, S. Mohamed, J. Kennedy, M. Maaza, Antibacterial, magnetic, optical and humidity sensor studies of β-CoMoO4-Co3O4 nanocomposites and its synthesis and characterization, Journal of Photochemistry and Photobiology B: Biology 183 (2018) 233-241.
[23] S. Haq, F. Abbasi, M.B. Ali, A. Hedfi, A. Mezni, W. Rehman, M. Waseem, A.R. Khan, H. Shaheen, Green synthesis of cobalt oxide nanoparticles and the effect of annealing temperature on their physiochemical and biological properties, Materials Research Express 8 (2021) 075009.
[24] R.M. Obodo, S.M. Mbam, D.C. Iwueke, M. Ramzan, R. Ijeh, I. Ahmad, M. Maaza, F.I. Ezema, Annealing optimization of graphitized Co3O4@ CuO@ NiO composite electrodes for supercapacitor applications, Energy Storage 4 (2022) e347.
[25] R. Boughalmi, A. Boukhachem, M. Kahlaoui, H. Maghraoui, M. Amlouk, Physical investigations on Sb2S3 sprayed thin film for optoelectronic applications, Materials science in semiconductor processing 26 (2014) 593-602.
[26] A. Hammad, Z. Elmandouh, H. Elmeleegi, Structure and some physical properties of chemically deposited nickel sulfide thin films, Acta Physica Polonica A 127 (2015) 901-903.

[27] A. Gahtar, S. Benramache, B. Benhaoua, F. Chabane, Preparation of transparent conducting ZnO: Al films on glass substrates by ultrasonic spray technique, Journal of Semiconductors 34 (2013) 073002.
[28] R.V. Kumar, Y. Diamant, A. Gedanken, Sonochemical synthesis and characterization of nanometer-size transition metal oxides from metal acetates, Chemistry of Materials 12 (2000) 2301-2305.
[29] G. Wang, X. Shen, J. Horvat, B. Wang, H. Liu, D. Wexler, J. Yao, Hydrothermal synthesis and optical, magnetic, and supercapacitance properties of nanoporous cobalt oxide nanorods, The Journal of Physical Chemistry C 113 (2009) 4357-4361.
[30] D. Barreca, C. Massignan, S. Daolio, M. Fabrizio, C. Piccirillo, L. Armelao, E. Tondello, Composition and microstructure of cobalt oxide thin films obtained from a novel cobalt (II) precursor by chemical vapor deposition, Chemistry of Materials 13 (2001) 588-593.
[31] A. Gulino, P. Dapporto, P. Rossi, I. Fragalà, A novel self-generating liquid MOCVD precursor for Co3O4 thin films, Chemistry of materials 15 (2003) 3748-3752.
[32] A. Agbogu, A. Ekwealor, F. Ezema, INFLUENCE OF PRECURSOR CONCENTRATION ON STRUCTURAL AND OPTICAL PROPERTIES OF CoxOy THIN FILMS, Digest Journal of Nanomaterials and Biostructures 9 (2014) 1289-1296.
[33] L. Kadam, P. Patil, Thickness-dependent properties of sprayed cobalt oxide thin films, Materials chemistry and physics 68 (2001) 225-232.

Chapter IV

Effect of the concentration on the properties of Co_3O_4 thin films

IV.1.Introduction

It is widely recognized that the properties of materials are affected by both the deposition process and the preparation parameters used. Among these parameters, concentration is particularly important in determining the characteristics of the material. By controlling the concentration, one can achieve the desired properties suitable for specific applications. In this study, thin layers of cobalt oxide with varying concentrations have been fabricated, and the effects of solution concentration on the optical, electrical, and structural properties have been investigated.

IV.2.Results and Discussion

IV.2.1.Film Thickness

The gravimetric approach involves using a high-precision electronic balance to measure the change in substrate weight resulting from film deposition. This method can be employed to quantify the thickness of the fabricated layers. If the surface area of the layer and the density of Co_3O_4 (ρ = 6.054 g/cm³) are known, the film thickness(d) can be calculated as follows[1]:

$$d = \frac{m}{(A \times \rho)} \qquad \text{(IV. 1)}$$

In this context, A, m, and ρ represent the area, mass, and density of Co_3O_4, respectively. Based on the calculated results of the prepared films thickness using Equation (1), we observe that the thickness

increases with higher concentrations of the prepared solution. Specifically, the film thickness (d) varied from 1.03E-05 cm to 5.37E-05 cm as the molar concentration of the cobalt precursor was increased.

IV.2.2.X-Ray Diffraction

The objective of this study was to elucidate the structural characteristics of the deposited thin films at varying solution molarities (0.025, 0.05, 0.075, and 0.1 mol/L). XRD patterns of deposited cobalt sulfide

films were recorded between 10 and 80°2θ using Cu-Ka radiation with a wavelength of 1.5406 Å. The voltage source was set at 40 kV, and the current was set at 40 mA, as illustrated in Figure IV.1.

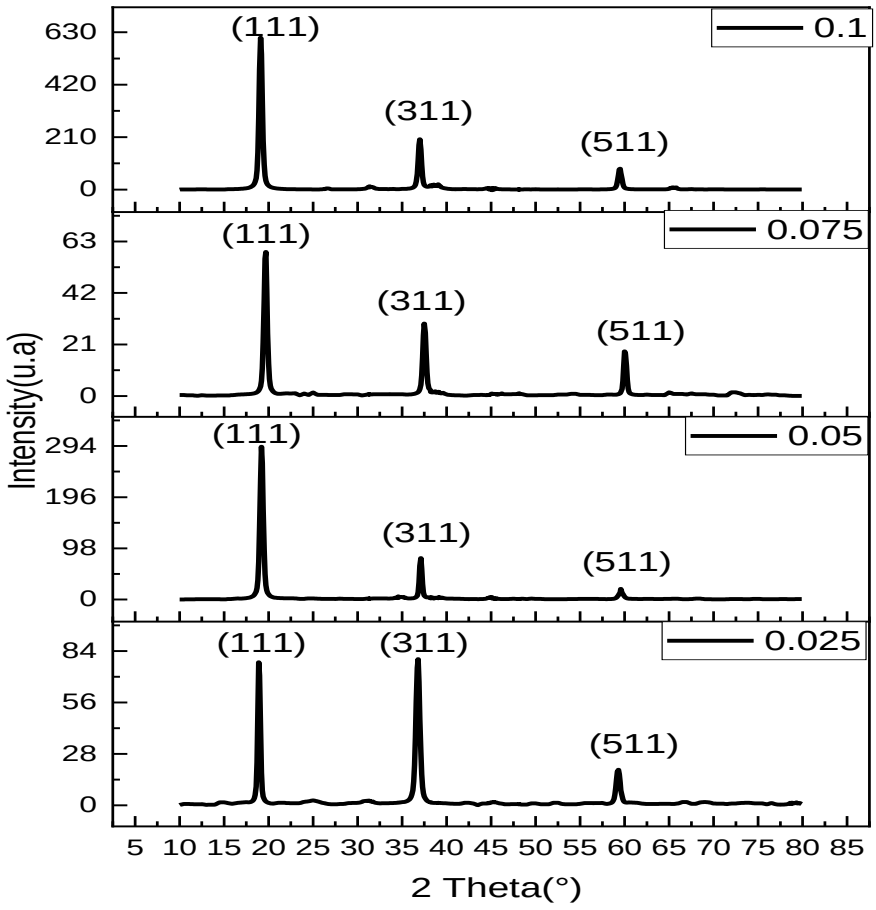

FigureIV.*1.DRX spectra of Cobalt Oxide: (a):C=0.025, (b):C=0.075, (c): C=0.05 and (d): C=0.1mol/l.*

As demonstrated in Figure IV.1, the X-ray spectra of the cobalt oxide layers produced by spray pyrolysis are presented. A thorough examination of the layers reveals the presence of multiple diffraction peaks at 2θ = 19.045°, 36.93°, and 59.5°, corresponding to the (1 1 1), (3 1 1), and (5 1 1) diffraction planes, respectively. This observation is indicative of the polycrystalline nature of these layers. The interplanar distance values corresponding to the (1 1 1), (3 1 1), and (5 1 1) planes were compared to the standard values for Co_3O_4, as documented in the JCPDS Data Card #01-074-1657. This comparison between the calculated dhkl values and the reference values confirms that the fabricated layers crystallize in a spinel-type cubic structure of Co_3O_4, specifically in the Fd3m space group, with a preferred orientation along the (111) plane. Previous studies by Hamdani et al. [2] and Avila et al.[3] have demonstrated that the (111) plane is the favored orientation for Co_3O_4 films produced through the spray pyrolysis process. Additionally, no peaks corresponding to other cobalt oxides, such as CoO or other forms of Co_2O_3, were observed. This indicates that Co_3O_4 exhibits greater stability compared to other cobalt oxides, a finding that aligns with results obtained

by other researchers[4-6] for Co_3O_4 films prepared using the spray pyrolytic process. The unit cell lattice parameter, denoted as 'a,' is determined from the peak positions using the cubic system formula:

$$\frac{1}{d_{hkl}^2} = \left(\frac{h^2 + k^2 + l^2}{a^2}\right) \text{(IV. 2)}$$

The value was estimated to be a = 8.0659 Å for a concentration c = 0.025 mol/l, which is close to the value given in JCPDS card #01-074-1657 (a = 8.0650).

Table IV.1. Lattice parameters (a, b, c, and d) and unit cell volume V compared to (JCPDS card #01-074-1657) values.

Concentration	**Latice parameters**		**Unit cell volume (10^3 pm^3)**		**Δa(Å)**	**ΔV (10^6 pm^3)**
	Our data	**JCPDS card**	**Our data**	**JCPDS card**		
	a=b =c(Å)	**a=b =c(Å)**	$V = a^3$	$V = a^3$		
(a): C=0.025	8.0659	8.0650	524.772	524.58	0.0009	0.192
(c): C=0.05	8.1146	8.0650	534.339	524.58	0.049	9.759
(d): C=0.075	7.9328	8.0650	499.361	524.58	0.1322	25.2
(b): C=0.1	8.0514	8.0650	521.953	524.58	0.01	2.627

As illustrated in Table 1, a comparative analysis of the structural parameter values obtained is presented, alongside their correlation with the relevant JCPDS card (card No. 01-074-1657). It is noteworthy that these values exhibit a high degree of similarity. The unit cell lattice parameter, denoted by ‘a’, is determined from the sites of the peaks according to the cubic system formula:

Table IV.2. Inter-planar distances (dhkl) of Cobalt Oxide.

Concentration	**(a): C=0.025M**	**(b): C=0.05M**	**(c): C=0.075M**	**(d): C=0.1M**
d_{111}**(Å)**	4.6459	4.6912	4.5191	4.6459
d_{311}**(Å)**	2.4325	2.4459	2.3998	2.4325
d_{511}**(Å)**	1.556	1.5601	1.5419	1.555

Table IV.2 recapitulates the interplanar spacings estimated through the XRD analysis. The observed mismatch in the interplanar spacings denotes the formation of a strained lattice, which is accompanied by the presence of microstresses as the films undergo the crystallization process.

The Bragg formula was utilized to estimate the interplanar distance (d_{hkl})[5, 7]:

$$2d_{hkl}\sin\theta = n\lambda \quad (IV.3)$$

Crystallite size D, dislocation density δ, and stresses ε in Co_3O_4layers have been estimated by the use of X-ray diffraction data.

First, the Scherer formula employed to determine the crystallite size (D_{hkl}) for all diffraction peaks [8, 9]:

$$D_{hkl} = \frac{k\lambda}{\beta_{1/2}\cos\theta} \quad (IV.4)$$

In this context, k is the Sherrer constant, typically 0.90, β1/2 refers to the (FWHM) of the diffraction peak, θ represents the Bragg angle, and λ = 1.5406 Å, the wavelength of the x-ray employed.

Table IV. 3.Cobalt Oxide crystallite's sizes (D_{hkl})

Concentration	**(a): C=0.025**	**(b): C=0.05**	**(c): C=0.075**	**(d): C=0.1**
$\mathbf{D_{111}}$**(Å)**	20.4674	27.2825	20.4839	20.4674
$\boldsymbol{D_{311}}$**(Å)**	21.2807	17.0142	21.3134	21.2807
$\boldsymbol{D_{511}}$**(Å)**	23.2382	18.5732	31.0743	23.2382

Second, the dislocation lines length per unit volume is defined as the dislocation density (δ_{hkl}), which measures the crystal's defects. The following formula was employed for its determination[10, 11]:

$$\delta_{hkl} = \frac{1}{D_{hkl}^2} \text{(IV. 5)}$$

Table IV. 4.The *dislocation density (δ_{hkl})*of Cobalt *Oxide*.

Concentration	**(a): C=0.025**	**(b): C=0.05**	**(c): C=0.075**	**(d):C=0.1**
$\boldsymbol{\delta_{111}}$**($10^{15}$lines/ m^2)**	2.3872	1.3435	2.3833	2.3871
$\boldsymbol{\delta_{311}}$**($10^{15}$lines/ m^2)**	2.2082	3.4545	2.2014	2.2081
$\boldsymbol{\delta_{511}}$**($10^{15}$lines/ m^2)**	1.8519	2.8988	1.0356	1.8518

And finally, the following formula was used to calculate the microstrain (ε_{hkl}) [12]:

$$\varepsilon_{hkl} = \frac{\beta_{1/2}}{4\,tan\,\theta} \text{(IV. 6)}$$

Table IV. *5. Micro-stress values (ε_{hkl}) of Cobalt Oxide .*

Concentration	**(a):C=0.025**	**(b): C=0.05**	**(c): C=0.075**	**(d): C=0.1**
$\boldsymbol{\varepsilon_{111}(10^{-3})}$	10.2061	7.7313	9.9195	10.2060
$\boldsymbol{\varepsilon_{311}(10^{-3})}$	5.13960	6.4639	5.0625	5.1396
$\boldsymbol{\varepsilon_{511}(10^{-3})}$	3.0099	3.7767	2.2311	3.0099

The texture coefficient (TC_{hkl}), estimated from X-ray data by employing a standard equation (7), evaluates the preferred orientation of Co_3O_4 layers[13]:

$$TC_{hkl} = \frac{I_{hkl}/I_{0_{hkl}}}{N^{-1}\left(\sum_{i=1}^{n} \frac{I_{hkl}}{I_{0_{hkl}}}\right)} \qquad \text{(IV. 7)}$$

In this context, (TC_{hkl}) represents the texture coefficient for the (hkl) plane, while (I_{hkl}) refers to the measured or normalized intensity. The value ($I_{0_{hkl}}$) corresponds to the standard intensity from the JCPDS database, and N denotes the number of reflections. The preferred orientation of a layer is associated with the (hkl) plane that exhibits the highest value of (TC_{hkl}).

Table IV. *6. Texture coefficient (TChkl) of* Co_3O_4*layers fabricated at various concentration.*

Concentration	**(a): C=0.025M**	**(b): C=0.05M**	**(c):C=0.075M**	**(d):C=0.1M**
$\boldsymbol{TC_{111}}$	2.2056	1.1106	1.9831	2.1953
$\boldsymbol{TC_{311}}$	0.4042	1.0158	0.5560	0.3952
$\boldsymbol{TC_{511}}$	0.3903	0.3878	0.4609	0.3713

The mean crystallite size$\langle D\rangle$, mean micro-stress $\langle\varepsilon\rangle$ and mean dislocation density $\langle\delta\rangle$of the layers, can be estimated by the use of the formulas below:

$$\begin{cases} \langle D \rangle = \dfrac{\sum TC_{hkl} * D_{hkl}}{n} \text{ (IV. 8)} \\ \langle \varepsilon \rangle = \dfrac{\sum TC_{hkl} * \varepsilon_{hkl}}{n} \text{ (IV. 9)} \\ \langle \delta \rangle = \dfrac{\sum TC_{hkl} * \delta_{hkl}}{\sum TC_{hkl}} \text{ (IV. 10)} \end{cases}$$

Table IV. 7. The mean values of D, ε and δ of fabricated samples with various concentration.

Concentration	$\langle D \rangle (nm)$	$\langle \varepsilon \rangle$**($10^{-3}$ lines^{-2} m^{-4})**	$\prec \delta \succ$ **(10^{15} lines/m^2)**
(a): C=0.025	20.9375	5.1524	2.2934
(b): C=0.05	21.0171	6.5858	2.6011
(c):C=0.075	22.2646	4.7029	2.1426
(d): C=0.1	20.9403	5.1524	2.2934

The variations of the crystallite size (D), the dislocation density (δ) and strain (ε) with respect to the solution concentration are illustrated in Fig.IV.2.

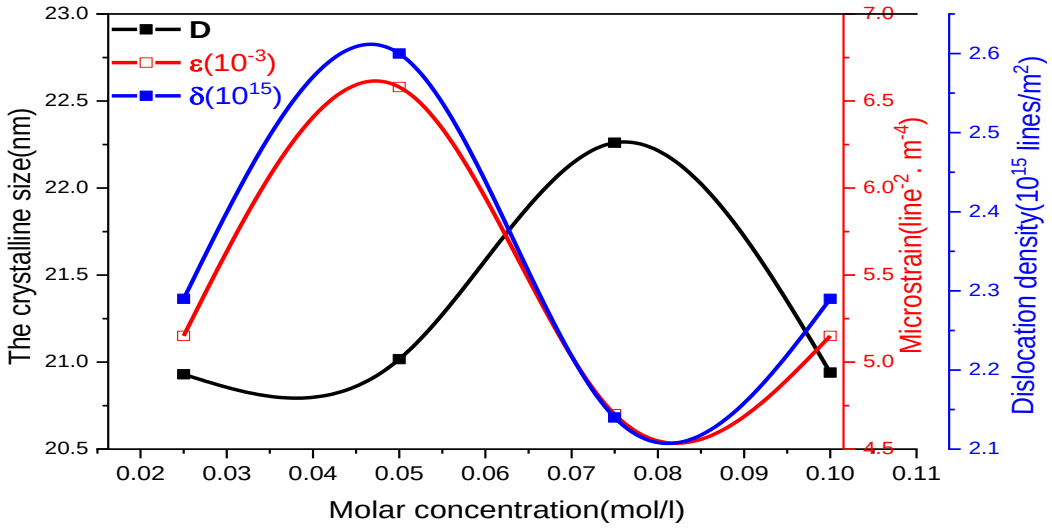

FigIV.2.Crystalline size, Microstrain, and dislocation density ofCo_3O_4layersversus the molar concentration.

It is evident from figure IV.3that the crystallite size grows as the molar concentration rises.

This phenomenon could be interpreted as follows: on the one hand, more cobalt ions reach the substrate where cobalt atoms condense more quickly, and faster crystallite nucleation leads to the creation of larger grains.

In addition, strain and dislocation density decrease as molar concentration rises and inversely with crystallite size. Because there are fewer barriers and the lattice can relax more readily, larger crystallites typically show less strain. The decrease of both and strain dislocation density shows that the lattice imperfections become less important along grain boundaries. The crystallites sizes, strain and dislocation density agree well with those of[14, 15].

IV.2.3.Morphological and Elemental Analysis

The morphology of the layers was analyzed using Scanning Electron Microscopy, which is the most commonly employed technique for examining microstructural and surface characteristics. Figure IV.4 (a-d) presents the SEM images of Co_3O_4 layers prepared at various concentrations.

The SEM images reveal that the layers exhibit a homogeneous morphology with very small grains, as well as a heterogeneous surface with a mesoporous structure. Notably, there are no visible cracks on the surface of the layers. The microporosity of Co_3O_4 is beneficial for applications in supercapacitors.

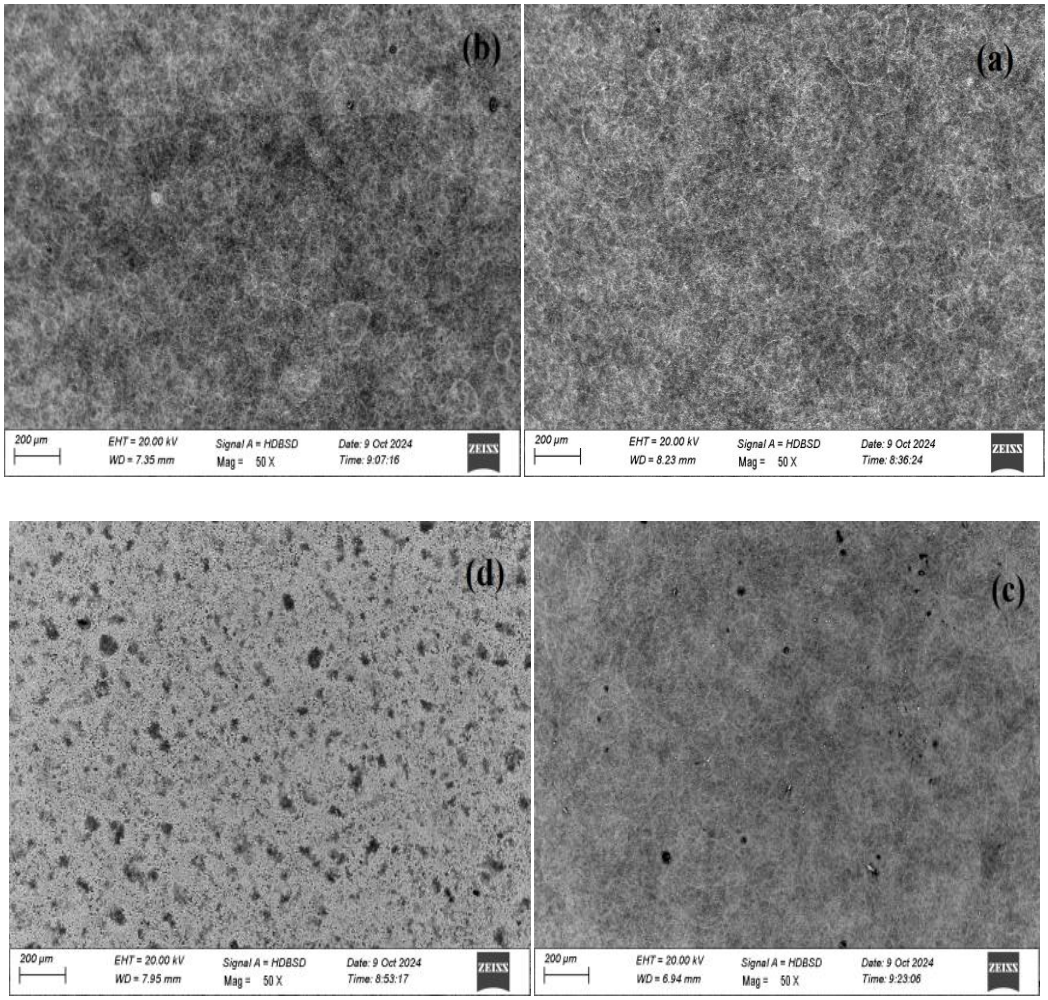

*Fig*IV.*3. SEM of Co_3O_4layers prepared at different concentrations (a): 0.025 M, (b): 0.05M, (c): 0.075 M and (c): 0.1 M.*

Figure IV. 3(a)-(d) presents high-resolution SEM images of Co3O4layers fabricated at 450°C using various concentrations. At low concentrations, the resulting layers densely cover whole the surface, forming a network of overgrown crystallites due to nucleation (see Fig.IV. 3(b) - (c)). Additionally, the films exhibit randomly distributed protrusions and bubbles. This suggests that gas phase formation occurred during the growth of the layer, leading to the formation of bubbles onto the surface. At the highest concentration (0.1 M), the layer is formed by the coalescence of grains of various shapes and sizes[16].

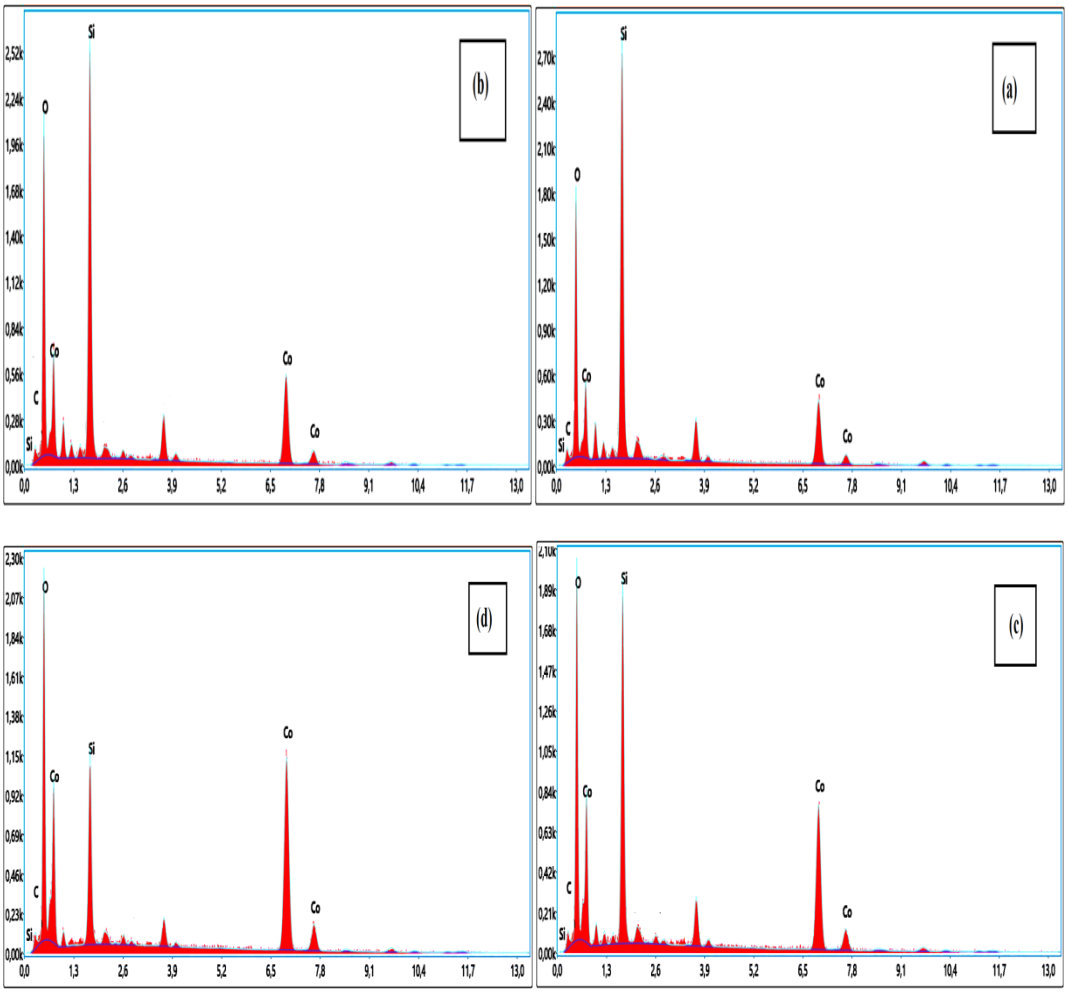

*Fig*IV.*4. EDS micrographs of Co_3O_4 layers prepared at various concentrations (a): 0.025 M, (b): 0.05 M, (c): 0.075 M and (c): 0.1 M.*

EDS spectra of Co_3O_4 films in Figure IV. 4(a-d) prove the presence of the predictable elements Co and O. Weight and atomic percent of elements present are listed in TableIV.8. Due to the glass substrate, the atomic percent of Si is high[17]. It is important to note that the lower (Co/O) ratio observed in the films indicates an excess of oxygen in the layers.

Additionally, the presence of some oxygen and silicon is an unusual occurrence in spray deposition, which is attributed to the SiO_2 in the substrate[18].

Figure 4 displays the Co_3O_4 films' EDS compositional analysis. This spectrum affirms the presence of the elements Co and O in the Co_3O_4 layers fabricated with different solution concentrations. Contamination of the glass substrate may be the cause of the appearance of silicon and carbon peaks, respectively. The increase in its atomic percentage causes the cobalt content to

increase as the molar concentration rises, while the chemisorbed oxygen from the ambient air may be the cause of the rise in the oxygen content [15].

Table IV. *8. Elementary analysis of Co_3O_4layers.*

Precursor Concentration(mol/l)	CO(at%)	O(at%)	C (at%)	Si(at%)	(CO/O)
0.025	8.12	52.24	5.21	22.19	**0.155**
0.05	10.03	54.90	3.85	19.93	**0.1826**
0.075	15	54.67	4.56	16.6	**0.274**
0.1	15.5	61.27	4.52	11.54	**0.253**

IV.2.4.FTIRAnalysis

The functional group characteristics and purity of the synthesized metal oxide nanoparticles were determined by FTIR spectroscopy.

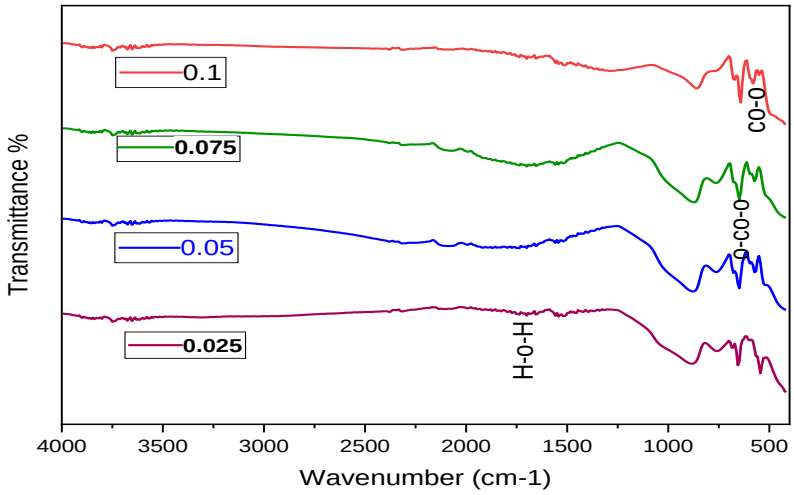

*Fig*IV.*5. Transmittance spectra of $Co_3O_4$for different concentration.*

From Figure.5,major sharp band observed at 574.01cm^{-1} which ascribe the symmetric stretch to Co-O[19-21] and at 648.55 cm^{-1} to O-Co-O[22], These two dips 574.01cm^{-1} and648.55 $cm^{-1}$are closely related to the optical vibrational modes of Co_3O_4[23-25]. Hence, the existence of some CoO impurities in the Co_3O_4layerscan be not neglected. Dip at 1546.03 $cm^{-1}$was the symmetrical stretching due to the presence of C–O and 1575.5 cm^{-1}corresponds to C=O [26]

(surface adsorbed CO_2). While the bridging vibration of the O–Co–O and Co–O–Co functions is the responsible for the peaks at 872.19 and 760.37 cm^{-1}, respectively[27] .The broadbands at 3300cm^{-1} are related to O-H stretch. The weak IR bands at 1653 and 1619.7cm^{-1} accounted as asymmetric and symmetric stretch of H-O-H due to the adsorption of humidity. These OH and H-O-H humidity bands are noticed when the sample pellets are exposed to an air environment, resulting from the stretch and vibration of water molecules[28, 29].

IV.2.5.Optical Properties

The variance of optical transmittance with wavelength (λ) in the range of 300-900 nm is utilized to define the optical characteristics of Co_3O_4 layers, including their transmission, absorption coefficient, and bandgap energy. The substrates' transmission is measured and deducted whereas the film-substrate combination is examined.

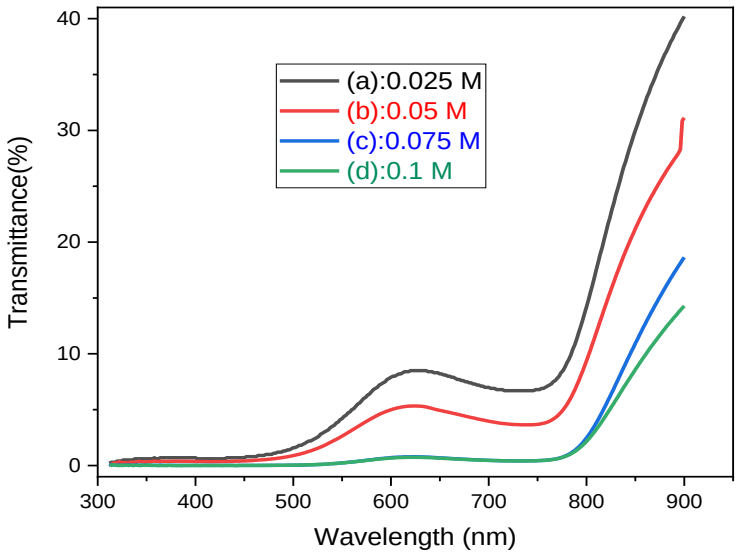

*Fig*IV.*6. indicates the transmittance spectra obtained for Co3O4for various molar concentration.*

Figure IV.*6* displays the optical transmission plots of Co_3O_4layers that were fabricated at a substrate temperature of 450 °C. The data indicates that optical transmission improves as the precursor content decreases. The mean optical transmittance of the fabricated layer is approximately 40% in the visible and near-infrared regions.

The absorption coefficient (α) can be estimated from the transmittance and reflectance spectra by the use the following relationship [30]:

$$\alpha = \frac{1}{d}\ln\left(\frac{(1-R)^2}{T}\right) \qquad (IV.11)$$

Wherein: the film thickness is d, T transmittance, and R reflectance.

The studied films have an absorption coefficient (α) that obeys the relationship given above for high photon energies (hν)[9, 30, 31].

Increased absorbance is the result of higher cobalt concentrations, particularly in the near-infrared and visible spectrums. The reason is that cobalt ions absorb more light, which leads to intra-band and inter-band transitions. As a result, when the concentration of cobalt increases, the transmittance of the film drops.

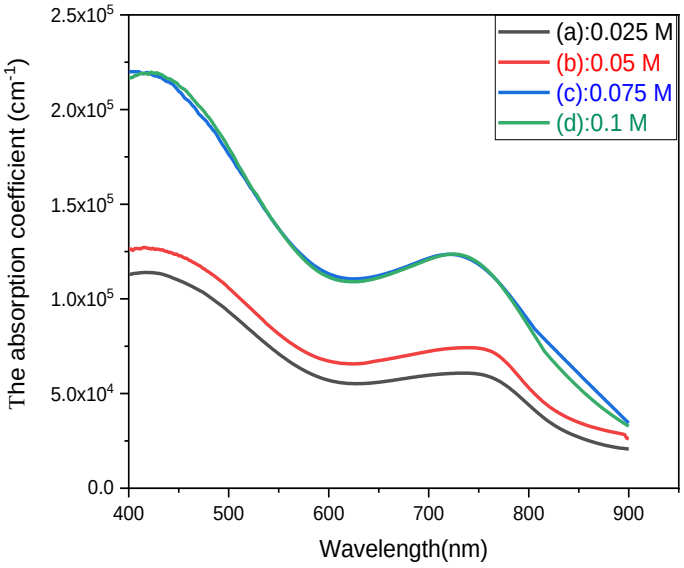

*Fig*IV.*7. The absorption coefficient versus the wavelength.*

In Figure 7, two sharp and distinct absorption edges in the visible spectrum can be observed. This is an indication that the absorption bandgap transitions in Co_3O_4layers are of the direct type. According to the band theory of matter, the relation between the absorption factor and the energy of the incidence light (hν) near the absorption limit of semiconducting materials is described by Tauc relationship[30, 32]:

$$\alpha h\nu = A\left(h\nu - E_g\right)^n \qquad (IV.12)$$

In the equation, A represents a constant, E_g denotes the energy of the band gap, and n is a constant that takes on different values depending on the type of transition: 0.5 for allowed direct

transitions, 2 for allowed indirect transitions, 1.5 for forbidden direct transitions, and 3 for forbidden indirect transitions. The plots of $(\alpha h\nu)^2$ versus $(h\nu)$ for Co_3O_4layers that were prepared at 450°C and various concentration (c=0.1;c=0.075;c=0.05;c=0.025mol/l)are illustrated in Fig. IV. 8.

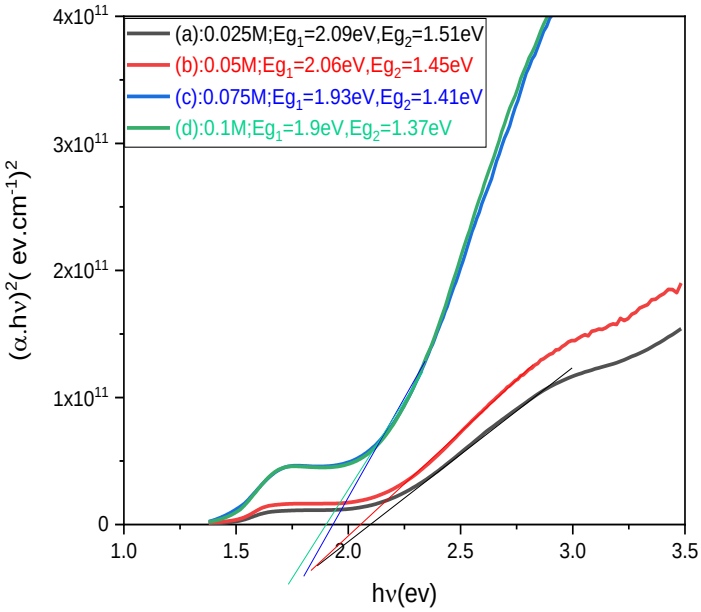

FigIV.8. $(\alpha h\nu)^2$ versus energy $(h\nu)$ for different molar concentration.

Two straight lines were observed in Figure 8, which indicates that two direct bandgap values of cobalt oxide exist, which is consistent with the literature [33]. The bandgaps (Eg) of the fabricated layers are in the domain of 1.37-1.51 eV for the region of the lower energy side and 1.94-2.09 eV for the region of the higher energy side. These values agree with the reported band structure of Co_3O_4[34, 35].It is also noted that the value of the bandgap (Eg) slightly varies with the concentration of the precursor. These observed bandgap values align with those reported by other research groups[26, 36]. The high band gap of Co_3O_4 layers suggests their potential use as absorber layers in solar cells. This project reports a higher bandgap of 1.94-2.09 eV compared to the previously reported values [37, 38]. This slight variation may be assigned to the varying quality of the Co_3O_4 films as the concentration of the solution changes. As the solution concentration increases, the bandgap energy (Eg) shows minor changes. The variation in density with the change of concentration is responsible for this small shift in band gap energy. The Burstein-Moss effect is primarily responsible for the shift of the absorption edge that occurs with rising concentration[39, 40].In semiconductors, it has been demonstrated that the absorption edge shifts to shorter wavelengths as carrier concentration rises[41]. This broadening of the bandgap can also associate with a lowering in the tail width. It is observed that the Eg values decrease as the solution molarity

increases. The decrease of the bandgap can be correlated with the decreasing tendency of the strain for which the inter-atomic spacing of semiconductors effects the energy gap when the solution concentration increases (thickness of the layer increases)[42],considers that the reduction of the bandgap can be linked to the decreasing trend of the strain for which the inter-atomic spacing of semiconductors effects the energy gap. Moreover, the decrease in the band gap, due to the raise in carrier concentration, is explained by the growth in crystallite size resulting from high precursor concentrations[2, 44, 45].

IV.2.6.Electrical Characteristics

Using the four-probe electrical method, the electrical resistivity and conductivity of Co_3O_4 films were determined. The following formula [7] is used to measure the resistivity of Co_3O_4layers:

$$\rho = R.\frac{A}{d} \quad (IV.13)$$

Where ρprepresents resistivity, R is resistance, A denotes cross-sectional area, and d signifies the inter-probe distance.

The conductivity (σ) is calculated using the following equation:

$$\sigma = \frac{1}{\rho} \quad (IV.14)$$

Table IV.9 presents the values of square resistance (R_{sh}), resistivity (ρ), and conductivity (σ) obtained using the four-point process under specified conditions as follows.

Square plate. Insertion size: 76.1 mm. Edge exclusion: 20 mm. 4 dots. Used current: 2.5312 mA.

Table IV. 9. Resistivity and Conductivity of Co_3O_4layers for different concentration.

Molar concentration(mole/l)	R_{SHEET}(ohm)	d(cm)	ρ(ohm.cm)	$\sigma(ohm.cm)^{-1}$
0.025	5.81E+06	1.03E-05	5.96E+01	1.68E-02
0.05	1.09E+05	4.27E-05	4.66E+00	2.15E-01
0.075	5.53E+04	4.46E-05	2.47E+00	4.05E-01
0.1	6.44E+04	5.37E-05	3.46E+00	2.89E-01

It is evident from the values listed in Table 9 that the conductivity rises as the concentration (0.025, 0.05, 0,075 and 0.1 M) increases. Since the spaces between crystals will be smaller when the crystals are larger, the increase in conductivity value can be explained by the crystallites' size increasing as the concentration rises. Full bonds exist amongst the atoms at this level, which promotes the decrease of many imperfections that act as traps for free charges. These outcomes closely match the values that the researcher discovered [20]. The conductivity then decreases to the value at a solution concentration of 0,075M(σ =2.89*10^{-01} $(\Omega.cm)^{-1}$). Electrical conductivity decreases as concentration increases, primarily due to increased disorder in the material[22, 23]. This disorder creates more potential obstacles, attributed to grain boundary segregation. These findings align with the results found from both X-ray diffraction (DRX) and Energy Dispersive Spectroscopy (EDS), as illustrated in FigureIV.9.

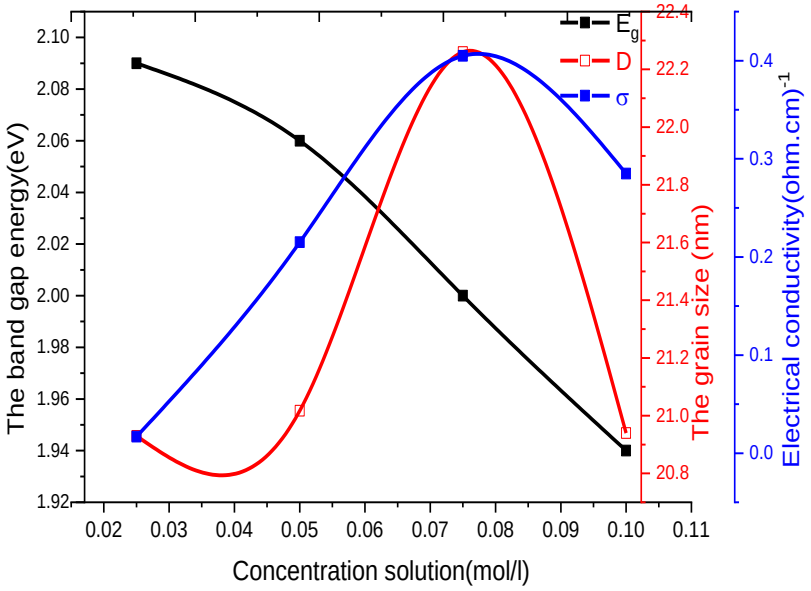

FigIV.9.Optical gap, Grain size, and Conductivity versus the concentration.

IV.3. Conclusion

The impact of molar concentration on the structural, morphological, optical, and electrical characteristics of Co_3O_4 layers deposited on glass substrates by a home-built pneumatic spray pyrolysis system is studied.X-ray diffraction indicates a polycrystalline nature for all the layers, with a preferential growth orientation along the (111) plane, as the solution concentration changes

from 0.025 to 0.1 mol/l.The crystallite sizes of the layers were found to increase from 20.93 to 22.26 nm, resulting in an increase in crystallinity. The SEM micrographs clearly show the formation of sub-micron crystallites distributed more or less uniformly over the surface. Although the films are well recovered, there are some holes indicating porosity.A spin-orbit splitting of the valence band is suggested by the results of the optical analysis, which revealed two linear regions with two different band gap energy values. In the lower energy region, the band gap energy values varied from 1.37 eV to 1.51 eV, while in the higher energy region they varied from 1.94 eV to 2.09 eV. The increase in carrier concentration (holes) is the primary cause of the deposited thin films' electrical conductivity, which rises from $1.68*10^{-02}$ to $4.05*10^{-01}$ $(\Omega.\ cm)^{-1}$ with solution concentration. Ultimately, the current study made it abundantly evident that molarity is a crucial factor that has a big impact on the physical characteristics of Co_3O_4 films. These characteristics show that Co_3O_4 films, particularly those deposited at concentrations of 0.10 mol/l, are a potential material for use as an absorber layer in gas sensing and solar applications.

References

[1] A. Abdelkrim, S. Rahmane, K. Nabila, A. Hafida, O. Abdelouahab, Polycrystalline SnO 2 thin films grown at different substrate temperature by pneumatic spray, Journal of Materials Science: Materials in Electronics 28 (2017) 4772-4779.

[2] Leaf-nosed bat, Encyclopædia Britannica, Encyclopædia Britannica Online, 2009.

[3] R. Avila-Flores, R.A. Medellin, Ecological, taxonomic, and physiological correlates of cave use by mexican bats, J. Mammal. 85 (2004) 675-687.

[4] A. Abdelkrim, S. Rahmane, O. Abdelouahab, N. Abdelmalek, G. Brahim, Effect of solution concentration on the structural, optical and electrical properties of SnO2 thin films prepared by spray pyrolysis, Optik 127 (2016) 2653-2658.

[5] Z.N. Kayani, F. Saleemi, I. Batool, Effect of calcination temperature on the properties of ZnO nanoparticles, Applied Physics A 119 (2015) 713-720.

[6] S. Brinkløv, E.K. Kalko, A. Surlykke, Intense echolocation calls from twowhispering'bats, Artibeus jamaicensis and Macrophyllum macrophyllum (Phyllostomidae), J. Exp. Biol. 212 (2009) 11-20.

[7] A. Gahtar, A. Benali, S. Benramache, C. Zaouche, Effect of annealing time on the structural, morphological, optical and electrical properties of NiS thin films, Chalcogenide Letters 19 (2022).

[8] M. Pan, F. Lu, Y. Zhu, G. Huang, J. Yin, F. Huang, G. Chen, Z. Chen, Thermodynamic, exergoeconomic and multi-objective optimization analysis of new ORC and heat pump system for waste heat recovery in waste-to-energy combined heat and power plant, Energy Conversion and Management 222 (2020) 113200.

[9] M. Salavati-Niasari, A. Khansari, F. Davar, Synthesis and characterization of cobalt oxide nanoparticles by thermal treatment process, Inorganica Chimica Acta 362 (2009) 4937-4942.

[10] C. AnChiu, W. Xian, C.F. Moss, Flying in silence: Echolocating bats cease vocalizing to avoid sonar jamming, Proc. Natl. Acad. Sci. U. S. A. 105 (2008) 13116-13121.

[11] S. Marouf, A. Beniaiche, H. Guessas, A. Azizi, Morphological, structural and optical properties of ZnO thin films deposited by dip coating method, Materials Research 20 (2016) 88-95.

[12] T. Singam, N.B. Marsi, A.H.B. Abdul Rashid, S.H.B. Nasir, S.A.B. Ibrahim, M.N.B. Roslan, N.A.B. Huzaisham, M.H.B. Mohd Fodzi, A review on characteristics and potential applications of henna leaves (Lawsonia inermis), Journal of Computational and Theoretical Nanoscience 17 (2020) 603-612.

[13] A. Gahtar, C. Zaouche, A. Maouane, A. Ammari, L. Dahbi, Substrate Temperature Effect on the Structural, Optical and Morphological Proprties of Cobalt Sulfide Thin Films Deposited Using Spray Pyrolisis, Annals of West University of Timisoara-Physics.

[14] M. Manickam, V. Ponnuswamy, C. Sankar, R. Suresh, Cobalt oxide thin films prepared by NSP technique: Impact of molar concentration on the structural, optical, morphological and electrical properties, Optik 127 (2016) 5278-5284.

[15] C.R. Dhas, R. Venkatesh, R. Sivakumar, A.M.E. Raj, C. Sanjeeviraja, Effect of solution molarity on optical dispersion energy parameters and electrochromic performance of Co3O4 films, Optical Materials 72 (2017) 717-729.

[16] A. Louardi, A. Rmili, F. Ouachtari, A. Bouaoud, B. Elidrissi, H. Erguig, Characterization of cobalt oxide thin films prepared by a facile spray pyrolysis technique using perfume atomizer, Journal of Alloys and Compounds 509 (2011) 9183-9189.

[17] R. Mariappan, V. Ponnuswamy, M. Ragavendar, Influence of molar concentration on the physical properties of nebulizer-sprayed ZnO thin films for ammonia gas sensor, Materials science in semiconductor processing 16 (2013) 1328-1335.

[18] T.A.-H. Abbas, L.H. Slewa, H.A. Khizir, S.A. Kakil, Synthesis of cobalt oxide (Co 3 O 4) thin films by electrostatic spray pyrolysis technique (ESP), Journal of Materials Science: Materials in Electronics 28 (2017) 1951-1957.

[19] J. Feng, H.C. Zeng, Size-controlled growth of Co3O4 nanocubes, Chemistry of materials 15 (2003) 2829-2835.

[20] G. Rathika, V. Suba, D.S. Lakshmi, R. Rani, Exploring the Biosynthesized Metal Nanoparticles for their Catalytic Degradation of Toxic Water Wastes and Antimicrobial Potential, Journal of Inorganic and Organometallic Polymers and Materials 32 (2022) 3153-3169.

[21] K. Bali, A. Beggas, A. Gahtar, The effect of substrate temperature on the structural, morphological, optical and electrical properties of CO3O4 thin films, Studies in Engineering and Exact Sciences 5 (2024) e12882-e12882.

[22] S.-H. Wu, D.-H. Chen, Synthesis and characterization of nickel nanoparticles by hydrazine reduction in ethylene glycol, Journal of Colloid and Interface Science 259 (2003) 282-286.

[23] P. Nkeng, J.-F. Koenig, J. Gautier, P. Chartier, G. Poillerat, Enhancement of surface areas of Co3O4 and NiCo2O4 electrocatalysts prepared by spray pyrolysis, Journal of Electroanalytical Chemistry 402 (1996) 81-89.

[24] S.R. Ahmed, P. Kofinas, Magnetic properties and morphology of block copolymer-cobalt oxide nanocomposites, Journal of magnetism and magnetic materials 288 (2005) 219-223.

[25] M. Pudukudy, Z. Yaakob, Sol-gel synthesis, characterisation, and photocatalytic activity of porous spinel Co 3 O 4 nanosheets, Chemical Papers 68 (2014) 1087-1096.

[26] S. Alias, A. Ismail, A. Mohamad, Effect of pH on ZnO nanoparticle properties synthesized by sol–gel centrifugation, Journal of Alloys and Compounds 499 (2010) 231-237.

[27] A.M. Amanulla, S.J. Shahina, R. Sundaram, C.M. Magdalane, K. Kaviyarasu, D. Letsholathebe, S. Mohamed, J. Kennedy, M. Maaza, Antibacterial, magnetic, optical and humidity sensor studies of β-CoMoO4-Co3O4 nanocomposites and its synthesis and characterization, Journal of Photochemistry and Photobiology B: Biology 183 (2018) 233-241.

[28] S. Haq, F. Abbasi, M.B. Ali, A. Hedfi, A. Mezni, W. Rehman, M. Waseem, A.R. Khan, H. Shaheen, Green synthesis of cobalt oxide nanoparticles and the effect of annealing temperature on their physiochemical and biological properties, Materials Research Express 8 (2021) 075009.

[29] R.M. Obodo, S.M. Mbam, D.C. Iwueke, M. Ramzan, R. Ijeh, I. Ahmad, M. Maaza, F.I. Ezema, Annealing optimization of graphitized Co3O4@ CuO@ NiO composite electrodes for supercapacitor applications, Energy Storage 4 (2022) e347.

[30] A. Gahtar, S. Benramache, B. Benhaoua, F. Chabane, Preparation of transparent conducting ZnO: Al films on glass substrates by ultrasonic spray technique, Journal of Semiconductors 34 (2013) 073002.

[31] J. Pal, P. Chauhan, Study of physical properties of cobalt oxide (Co3O4) nanocrystals, Materials characterization 61 (2010) 575-579.

[32] D. Souad, S. Benramache, A. Ammari, A. Gahtar, Effect of substrate temperature on the structural, optical, electrical, and morphological properties of zinc oxide thin films, Iranian Journal of Physics Research 22 (2022) 185-191.

[33] A. Gulino, G. Fiorito, I. Fragalà, Deposition of thin films of cobalt oxides by MOCVD, Journal of Materials Chemistry 13 (2003) 861-865.

[34] T. Maruyama, T. Nakai, Cobalt oxide thin films prepared by chemical vapor deposition from cobalt (II) acetate, Solar energy materials 23 (1991) 25-29.

[35] D. Barreca, C. Massignan, S. Daolio, M. Fabrizio, C. Piccirillo, L. Armelao, E. Tondello, Composition and microstructure of cobalt oxide thin films obtained from a novel cobalt (II) precursor by chemical vapor deposition, Chemistry of Materials 13 (2001) 588-593.

[36] L. Kadam, P. Patil, Thickness-dependent properties of sprayed cobalt oxide thin films, Materials chemistry and physics 68 (2001) 225-232.

[37] A. Gulino, P. Dapporto, P. Rossi, I. Fragalà, A novel self-generating liquid MOCVD precursor for Co3O4 thin films, Chemistry of materials 15 (2003) 3748-3752.

[38] K.J. Kim, Y.R. Park, Optical investigation of charge-transfer transitions in spinel Co3O4, Solid State Communications 127 (2003) 25-28.

[39] E. Burstein, Anomalous optical absorption limit in InSb, Physical review 93 (1954) 632.

[40] T. Moss, The interpretation of the properties of indium antimonide, Proceedings of the Physical Society. Section B 67 (1954) 775.

[41] G. Lee, Y. Yamamoto, M. Kourogi, M. Ohtsu, Blue shift in room temperature photoluminescence from photo-chemical vapor deposited ZnO films, Thin Solid Films 386 (2001) 117-120.

[42] M. Dutta, S. Mridha, D. Basak, Effect of sol concentration on the properties of ZnO thin films prepared by sol–gel technique, Applied Surface Science 254 (2008) 2743-2747.

[43] G.M. Allen, Bats: biology, behavior, and folklore, Dover Publications, Mineola, N.Y., 2004.

[44] Z.Y. Alami, M. Salem, M. Gaidi, J. Elkhamkhami, Effect of Zn concentration on structural and optical proprieties of ZnO thin films deposited by spray pyrolysis, Adv. Energy Int. J 2 (2015) 11-24.

[45] A. Agbogu, A. Ekwealor, F. Ezema, INFLUENCE OF PRECURSOR CONCENTRATION ON STRUCTURAL AND OPTICAL PROPERTIES OF CoxOy THIN FILMS, Digest Journal of Nanomaterials and Biostructures 9 (2014) 1289-1296.

CONCLUSIONS AND SUGGESTIONS FOR FUTURE WORK

Conclusions

The objective of the present study was to investigate on the deposition and characterization of thin layers of cobalt oxide (Co_3O_4) produced using the pneumatic spray technique.

A system has been developed for the deposition of thin layers of Co_3O_4 using the pneumatic spray method. This method entails the transportation of a solution via a compressor onto a heated surface with a controlled temperature. A series of film depositions have been conducted, with varying parameters employed to achieve the desired outcome. The parameters that must be taken into consideration are the concentration of the precursor, which ranges from 0.025 to 0.1 mol/L; the substrate temperature, which varies from 250°C to 400°C; and other relevant factors. This methodological framework enables a comprehensive investigation into the impact of these variables on various parameters, including growth kinetics, optical properties, structural characteristics, and electrical behavior. A comprehensive evaluation of the results from the various characterizations, in conjunction with subsequent discussions, has yielded the following conclusions:

The X-ray diffraction analysis of the developed samples shows that the films are polycrystalline with a spinel-like structure of Co_3O_4. A detailed examination of the films reveals multiple growth directions. The most intense peaks correspond to the orientations (311) and (111), which are observed at angles of approximately 19° and 37°, respectively. Additionally, there is a noticeable shift in the intensity of the diffraction peaks based on the deposition parameters.

The crystallite size is calculated using the Debye-Scherrer formula, varying from 14 to 16.4 nm for Co_3O_4 films deposited at different temperatures, and from 20.9 to 22.23 nm for Co3O4 films deposited at varying molarities.

The morphological study revealed that the surface morphology of the films was almost homogeneous and well covered without holes or cracks. Optical characterization over a range of 300 to 2500 nm suggests that the films are generally absorbent in the UV-Visible and NIR range, a shift to blue (Blue shift) is remarkable at the absorption limit of

Co_3O_4 with the increase in substrate temperature and to the red (Red shift) for the increase in molarity.

In addition, the transmittance spectra show that there are two fundamental absorption fronts in the visible region. This indicates that there are two gaps and the transitions of absorption band in thin layers of Co_3O_4 are direct, which is due to the possibility of degeneration of the valence band. The electrical characteristics of Co_3O_4 thin films show that conductivity increases in the range from 3.28 10^{-4} to 1.29 $(\Omega\ cm)^{-1}$ for different temperatures studied, and 1.68 10^{-2} to 4.05 10^{-1} $(\Omega \bullet cm)^{-1}$ for the different studied molarities.

Finally, the different perspectives that can be envisaged for the continuation of this work are:

Some additional measurements could still be carried out on the Co_3O_4 layers deposited during this thesis work:

•Hall-effect resistivity measurements, this technique also measures resistivity but mainly allows to determine the density and mobility of carriers in films.

It is then possible to link the structural and electrical properties.

•The determination of cobalt atom concentration in Co_3O_4 layers by other techniques than EDX, including RBS or SIMS measurements to better see the effect of cobalt content.

ABSTRACT

Abstract

The study focuses on the deposition and characterization of thin layers of cobalt oxide (Co_3O_4) developed using the pneumatic spray technique. A system was developed for the deposition of materials using a compressor on a heated surface, with the precursor concentration and substrate temperature being variables that were varied. The X-ray diffraction analysis revealed polycrystalline films with a spinel-like structure, exhibiting multiple growth directions. The size of crystallites exhibited a direct correlation with both temperature and molarity. The surface morphology exhibited homogeneity and comprehensive coverage. A thorough examination of the films' optical properties revealed their capacity for absorption across the UV-Visible and NIR spectrums. Transmittance spectra revealed two fundamental absorption fronts in the visible region, indicating potential degeneration of the valence band. Electrical characteristics exhibited increased conductivity.

Keywords: Co_3O_4 thin films, Spray-Paralysis, Surface Morphology, Optical and Electrical Properties.

ملخص

تركز الدراسة على ترسيب وتوصيف الطبقات الرقيقة من أكسيد الكوبالت (Co_3O_4) باستخدام تقنية الرش الحراري. طور الباحثون نظامًا للإيداع باستخدام ضاغط على سطح مسخن، مع تغيير تركيز المادة السابقة ودرجة حرارة الركيزة. كشفت تحليل حيود الأشعة السينية عن أفلام متعددة البلورات ذات بنية تشبه السبينل، مع اتجاهات نمو متعددة. حجم البلورات الصغيرة اختلف مع درجة الحرارة والتركيز. كانت مورفولوجيا السطح متجانسة ومغطاة بشكل جيد.كما أظهرت الخصائص البصرية أن الأفلام كانت عموما ماصة في نطاق الأشعة فوق البنفسجية-المرئية والأشعة تحت الحمراء القريبة. كشفت طيفيات النفاذية عن جبهتين أساسيتين للامتصاص في المنطقة المرئية، مما يشير إلى احتمال انحلال نطاق التكافؤ. وقد أظهرت الخصائص الكهربائية زيادة في الموصلية.

الكلمات المفتاحية: أفلام رقيقة منCo_3O_4,الرش الحراري، التركيب السطحي، الخصائص البصرية، الخصائص الكهربائية.

APPENDIX

I- JCPDS card used (#2120-074-01 and #1657-074-01).

I-1. JCPDS card # 2120-074-01used

Name and formula

Reference code: 2120-074-01

Compound name: Cobalt Oxide

Chemical formula: Co_3O_4

Crystallographic parameters

Crystal system: Cubic
Space group: Fd-3m
Space group number: 227

a:(°A) 8.0840
b (°A): 8.0840
c (°A): 8.0840
Alpha (°): 90.0000
Beta (°): 90.0000
Gamma (°): 90.0000

Calculated density (g/cm^3): 6.05
Volume of cell (10^6 pm^3): 528.30
Z: 8.00

RIR: 4.37

References

Primary reference: *Calculated from ICSD using POWD-12*(1997) ,*++*
Structure: Smith, W.L., Hobson, A.D ,*.Acta Crystallogr., Sec. B* , (1973) ,362 ,**29**

Peak list

I [%]	2Theta[deg]	d [A]	h	k	l	No.
21.8	18.999	4.66730	1	1	1	1
34.8	31.270	2.85813	0	2	2	2
100.0	36.846	2.43742	1	1	3	3

9.6	38.548	2.33365	2	2	2	4
19.2	44.810	2.02100	0	0	4	5
0.1	49.082	1.85460	1	3	3	6
7.5	55.655	1.65014	2	2	4	7
30.2	59.356	1.55577	1	1	5	8
30.8	65.235	1.42906	0	4	4	9
1.3	68.627	1.36645	1	3	5	10
0.1	69.741	1.34733	2	4	4	11
1.9	74.120	1.27819	0	2	6	12
6.0	77.341	1.23280	3	3	5	13
3.4	78.405	1.21871	2	2	6	14
1.5	82.626	1.16682	4	4	4	15
0.8	85.763	1.13199	1	5	5	16

Stick Pattern

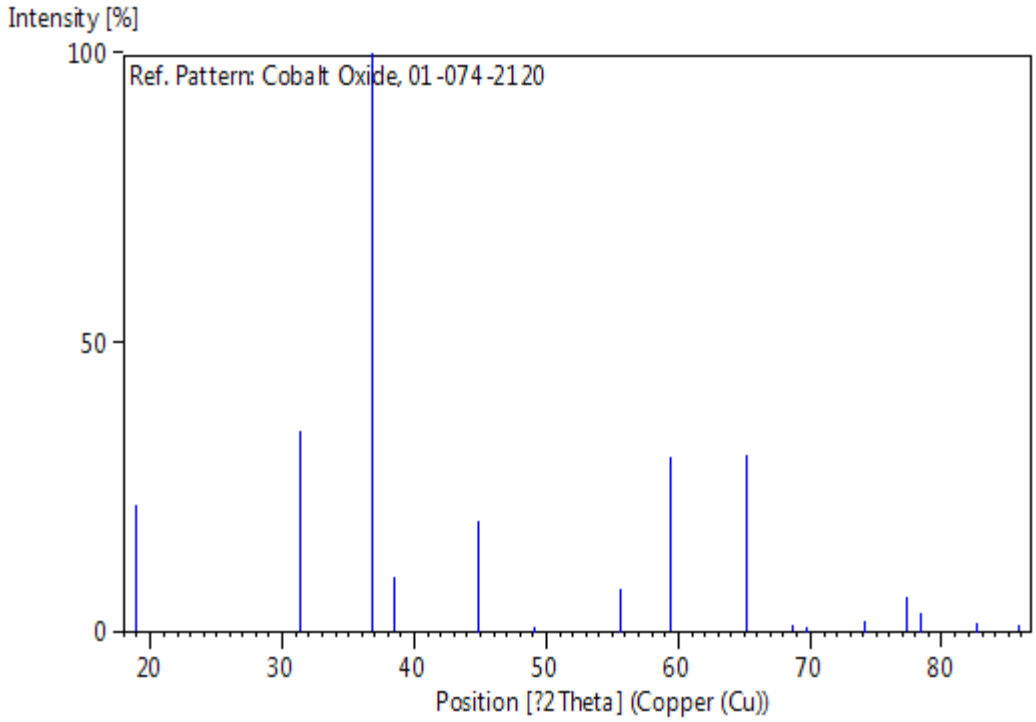

II-1. JCPDS card # 1657-074-01used.

Name and formula

Reference code: 1657-074-01

Compound name: Cobalt Oxide
Chemical formula: Co_3O_4

Crystallographic parameters

Crystal system: Cubic

Space group:	Fd-3m
Space group number:	227
a (°A):	8.0650
b (°A) :	8.0650
c (°A) :	8.0650
Alpha (°):	90.0000
Beta (°):	90.0000
Gamma (°):	90.0000
Calculated density (g/cm^3):	6.10
Volume of cell (10^6 pm^3):	524.58
Z:	8.00
RIR:	4.68

References

Primary reference: *Calculated from ICSD using POWD-12*(1997) ,*++*
Structure: Roth, W.L ,*.J. Phys. Chem. Solids*(1964) ,1 ,**25** ,

Peak list

I [%]	2Theta[deg]	d [A]	h	k	l	No.
17.1	19.045	4.65633	1	1	1	1
32.3	31.346	2.85141	0	2	2	2
100.0	36.936	2.43169	1	1	3	3
8.9	38.642	2.32817	2	2	2	4
20.0	44.921	2.01625	0	0	4	5
0.1	49.205	1.85024	1	3	3	6
8.1	55.797	1.64626	2	2	4	7
30.6	59.510	1.55211	1	1	5	8
34.5	65.408	1.42570	0	4	4	9
1.2	68.812	1.36323	1	3	5	10
0.1	69.929	1.34417	2	4	4	11
2.4	74.323	1.27519	0	2	6	12
6.7	77.557	1.22990	3	3	5	13
3.4	78.626	1.21584	2	2	6	14
1.9	82.863	1.16408	4	4	4	15
0.7	86.014	1.12933	1	5	5	16

Stick Pattern

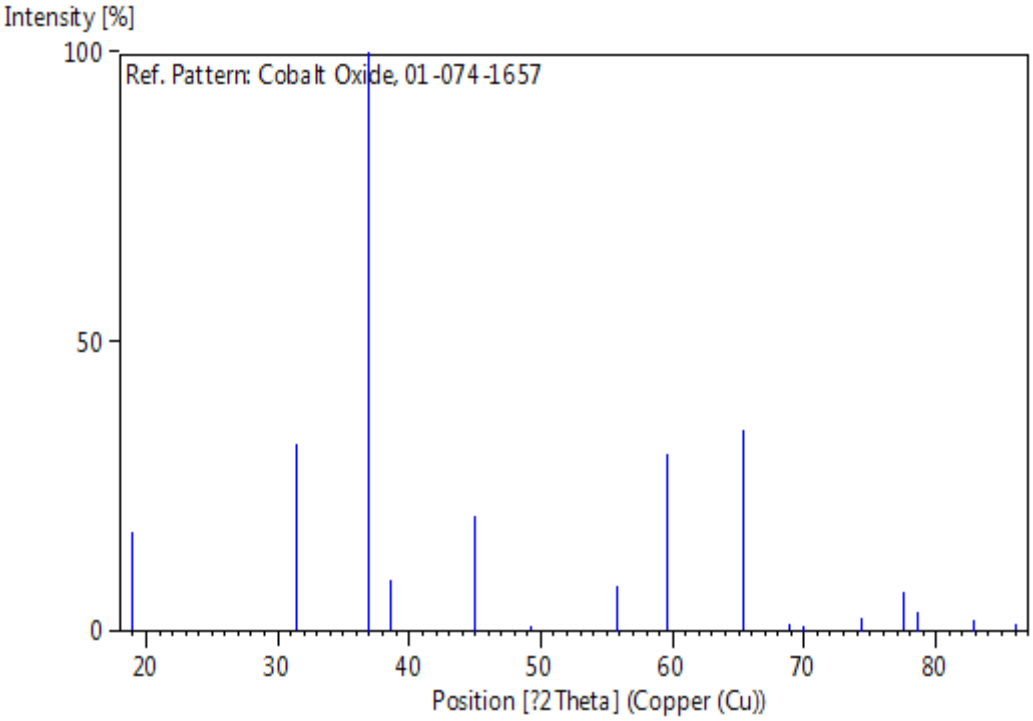
Intensity [%]
100
50
0
Ref. Pattern: Cobalt Oxide, 01-074-1657
20
30
40
50
60
70
80
Position [?2Theta] (Copper (Cu))